

2011

Tuning Bifunctional Surface Redox-Acid Sites for Enhanced Catalytic Performance

Kevin Doura
Lehigh University

Follow this and additional works at: <http://preserve.lehigh.edu/etd>

Recommended Citation

Doura, Kevin, "Tuning Bifunctional Surface Redox-Acid Sites for Enhanced Catalytic Performance" (2011). *Theses and Dissertations*. Paper 1039.

This Dissertation is brought to you for free and open access by Lehigh Preserve. It has been accepted for inclusion in Theses and Dissertations by an authorized administrator of Lehigh Preserve. For more information, please contact preserve@lehigh.edu.

Tuning Bifunctional Surface Redox-Acid Sites for Enhanced Catalytic Performance

by

Kevin Doura

Presented to the Graduate and Research Committee
Of Lehigh University
in Candidacy for the Degree of

Doctor of Philosophy

In

Chemical Engineering

Lehigh University

May 2011

Copyright

Copyright by Kevin Doura

2011

CERTIFICATE OF APPROVAL

Approved and recommended for acceptance as a dissertation in partial fulfillment for the degree of Doctor of Philosophy

Acceptance Date

Professor Israel E. Wachs
Lehigh University
Dissertation Advisor and Committee Chair

Committee members:

Professor Hugo S. Caram
Lehigh University

Professor Mark Snyder
Lehigh University

Dr. Jose´ G. Santiesteban
ExxonMobil

ACKNOWLEDGEMENTS

I would like to thank my advisor, Prof. Israel Wachs, for accepting me as a student into his group. I would also like to thank him for his guidance and mentoring over the years. You have opened up my eyes and exposed me to some of the most exciting research imaginable. Deciding to come to Lehigh to work with you is one of the best decisions I have ever made in my life. You have truly changed my life and I am forever grateful.

I would like to also thank my committee members for their guidance, Prof. Mark Snyder, Prof. Hugo Caram, and Dr. Jose´ Santiesteban.

I would like to thank all my colleagues that I have worked with over the years who have helped me get to this point; I certainly could not have done this alone. I would like to thank Dr. Elizabeth Ross-Medgardeen for mentoring me when I came into the group. I would also like to thank Prof. Jih-Mirn Jehng for his invaluable help in the lab every summer and fruitful discussions. I would like to give a very special thanks to Prof. Tavakoli for allowing me to conduct experiments in his lab whenever I needed to. I would also like to thank all my lab mates, Chip Roberts, Chris Keturakis, Julie Molinari, Peter Phivilay, Dr. Michael Ford, Dr. Kamalakanta Routray, and Soe Lwin.

I would like to thank my parents and brother for their continued support, guidance, and unconditional love over the years. I hope that I have been able to live up to your expectations and make you proud.

Finally I would like to thank my wife, Sharon. I believe that we share this Ph.D degree because without your encouragement to go forward with this endeavor, without your help in making sure I have what I need every single week for the past 5 years, and without your continued love and support, I would have never been able to do this. It took so much sacrifice to get to this point and I will forever be indebted to you. I dedicate this dissertation to you my love.

TABLE OF CONTENTS

ACKNOWLEDGEMENTS	iv
LIST OF TABLES	vii
LIST OF FIGURES	viii
ABSTRACT.....	1
CHAPTER 1: Tuning Catalytic Active Sites	6
1. Introductory Remarks	6
2 Synopsis.....	8
3. Tuning Surface Redox Sites.....	10
4. Tuning Surface Acid Sites.....	20
5. Tuning Bifunctional Redox-Acid Sites.....	25
6. Conclusion.....	28
7. Outline of Research.....	29
CHAPTER 2: Resolving the Contributions of Surface Lewis and Brønsted Acid Sites during SCR of NO _x with NH ₃ by Model Supported V ₂ O ₅ - WO ₃ /TiO ₂ /SiO ₂ Catalysts: An <i>Operando</i> TP-IR Spectroscopic Investigation.....	55
Abstract.....	55
1. Introduction.....	56
2. Experimental.....	63
3. Results.....	69
4. Discussion.....	74
5. Conclusion.....	82

CHAPTER 3: Fundamental Mechanistic Insights into the Selective Oxidation of CH ₃ OH to H ₂ C(OCH ₃) ₂ over Bifunctional Supported V ₂ O ₅ -WO ₃ /TiO ₂ /SiO ₂ Catalysts.....	108
Abstract.....	108
1. Introduction.....	109
2. Experimental.....	110
3. Results.....	115
4. Discussion.....	125
5. Conclusion.....	132
 CHAPTER 4: Catalyst by Design: Tuning the Selective Oxidation of CH ₃ OH to H ₂ C(OCH ₃) ₂ over Supported V ₂ O ₅ -WO ₃ /TiO ₂ /SiO ₂ with TiO ₂ Nanoligands.....	152
Abstract.....	152
1. Introduction.....	154
2. Experimental.....	156
3. Results.....	160
4. Discussion.....	164
5. Conclusion.....	170
 CHAPTER 5: Conclusions and Proposed Future Studies	191
1. Molecular and Electronic Structures of SiO ₂ -Supported VO _x , WO _x and TiO _x Phases.....	191
2. Selective Catalytic Reduction (SCR) of NO _x with NH ₃	192
3. Selective Oxidation of Methanol to Dimethoxymethane.....	194
4. Future Studies.....	195
 CURRICULUM VITAE.....	197

LIST OF TABLES

Table 4.S1. Selectivity of bifunctional redox-acidic catalysts at 150°C [V=V₂O₅, W=WO₃, TiSi = TiO₂/SiO₂].

Table 4.S2. Selectivity of bifunctional redox-acidic catalysts at 180°C [V=V₂O₅, W=WO₃, TiSi = TiO₂/SiO₂].

Table 4.S3. Selectivity of bifunctional redox-acidic catalysts at 190°C [V=V₂O₅, W=WO₃, TiSi = TiO₂/SiO₂].

Table 4.S4. Selectivity of bifunctional redox-acidic catalysts at 200°C [V=V₂O₅, W=WO₃, TiSi = TiO₂/SiO₂].

Table 4.S5. Selectivity of bifunctional redox-acidic catalysts at 230°C [V=V₂O₅, W=WO₃, TiSi = TiO₂/SiO₂].

LIST OF FIGURES

CHAPTER 1

Figure 1.1. Dehydration of n-butanol via “concerted mechanism

Figure 1.2. Initial step of Knoevenagel condensation of benzaldehyde

Figure 1.3. The silica surface as a macroscopic ligand providing a range of acid-base distances for bifunctional cooperativity

Figure 1.4. Ion-pair mechanism of catalysis by amine-functionalized silica for the production of β -nitro alcohol product in the Henry reaction

Figure 1.5. Bilayered metal oxide catalysts with the active metal oxide species (green triangle), M_1O_x , self assembled to M_2O_x , that is anchored to an inert surface

Figure 1.6. Model of interacting additives (phosphorous) with the surface vanadium oxide species on titania

Figure 1.7. EXAFS analysis shows that the Ti(IV)-centered active site in the epoxidation catalyst (Ti/SiO₂) is a tripodally attached titanol group (left), which is akin to a titanosilsesquioxane species (right)

Figure 18. A vanadyl active site: (a) grafted on to MCM-41 (left), (b) surrounded by nearby surface methyl groups (center), and (c) in a vanadium-rich AMMO microporous solid

Figure 1.9. SEM images of the MCM-41 and Ta-MCM-41 catalysts

Figure 10. Molecular structure of the grafted Mn complexes

Figure 1.11. Polyoxometallate (POM) vanadium tungstate ($H_{3+x}PW_{12-x}V_xO_{40}$ with $x = 0-3$) Keggin NPs (a) VO_x into the Keggin structure (b) $VO_x/H_3PW_{12}O_{40}$ on the surface of the Keggin catalyst

Figure 1.12. Representative HR-TEM images of TiO₂/SiO₂ containing [A] 12 wt% TiO₂ and [B] 30 wt% TiO₂ with circles highlighting the crystalline TiO₂(anatase) NPs [C] nanoscale raftlike TiO₂ domains on the SiO₂ support, exhibiting fringe structures that are consistent with [100], [110], and [111] projections of the anatase phase

Figure 1.13. Structure of the phosphor-tungstic Wells-Dawson heteropolyoxo-anion $P_2W_{18}O_{62}^{-6}$. W: tungsten, P: phosphorous and O: oxygen atoms

Figure 1.14. Proposed Catalytic Active Sites Present in Supported WO_3/ZrO_2 Catalysts. Surface WO_x Species Represents Monotungstate and Polytungstate Surface $O=W(-O)_4$ Species, with the latter predominating above low surface WO_x coverage

Figure 1.15. In $M^{II}M^{III}$ AlPO-36 ($M=Co, Mn$), the framework M^{III} ions are the redox-active centers (A_1), whereas the $M^{II}OH$ ions that have ionizable O-H bonds are the Brønsted (B_1) acid sites. Mg^{II} ions in the framework also have neighboring ionizable OH ions (the B_2 sites). Right: In M^{III} AlPO-18 all the framework M^{III} ions are again redox active centers: there are no Co^{II} (or Mn^{II}) framework sites. Mg^{II} framework ions again have neighboring (B_2) Brønsted sites

CHAPTER 2

Figure 2.1: *In situ* Raman spectrum (532 nm) of the dehydrated supported 1% V_2O_5 -5% WO_3 / 30% TiO_2 /SiO₂ catalyst in the [A] 200-1200 cm^{-1} region that is dominated by $TiO_2(A)$ bands and [B]700-1200 cm^{-1} region that is dominated by the WO_x and VO_x vibrations.

Figure 2.2: TOP: Time-resolved MS spectrum of gas phase NH_3 and BOTTOM: Time-resolved IR intensity of the surface NH_3 (1610 cm^{-1}) and NH_4^+ (1450 cm^{-1}) reaction intermediates during steady-state SCR of NO/NH_3 reaction.

Figure 3: MS signal profiles for the ammonia isotopic substitution on 1% V_2O_5 -5% WO_3 /30% TiO_2 /SiO₂ sample. Reaction temperature 250°C. MS Analysis of NH_3 (17), ND_3 (20), NO (30), O_2 (32), N_2 (28), H_2O , (18), D_2O (20) species. In the region indicated above, the reaction has been followed by IR spectra of the surface recorded in the rapid scan mode.

Figure 2.4: Evolution of the integrated bands for ammonia (green) and ammonium (red) species during the $NH_3 + NO + O_2 \rightarrow ND_3 + NO + O_2$ substitution at 250°C. The chosen integration limits are 1622-1594 cm^{-1} for adsorbed ammonia and 1481-1382 cm^{-1} for ammonium ion.

Figure 2.5: Evolution of the integrated bands for ammonia (green) and ammonium (red) species during the $ND_3 + NO + O_2 \rightarrow NH_3 + NO + O_2$ substitution at 250°C. The chosen integration limits are 1622-1594 cm^{-1} for adsorbed ammonia and 1481-1382 cm^{-1} for ammonium ion.

Figure 2.6: *In situ* FT-IR spectra of NH_3 adsorption at 150°C and temperature

programmed surface reaction from 150°C to 400°C at 5°C/min in the presence of flowing NO/O₂.

Figure 2.7: TOP: MS spectrum of gas phase SCR products (N₂, H₂O, NO) and BOTTOM: IR intensity of surface NH₃ (1610 cm⁻¹) and NH₄⁺ (1450 cm⁻¹) reaction intermediates during temperature programmed surface reaction in flowing NO/O₂.

Figure 2.8: MS signal profiles for the NO transient SCR experiments on 1% V₂O₅-5% WO₃/30% TiO₂/SiO₂ sample. Reaction temperature 250°C. MS analysis of NH₃, N₂, NO_x species during removal and re-introduction of NO reacting agent: 1st: 350 ppm NH₃ + 5% O₂ + 350ppm NO (steady state, 30s scan); 2nd: 350ppm NH₃ + 5% O₂; 3rd: 350ppm NH₃ + 5% O₂ + 350ppm NO; 4th: 350ppm NH₃+5% O₂; 5th: 350ppm NH₃+5% O₂ + 350ppm NO; 6th: 350ppm NH₃ + 5% O₂; 7th: 350ppm NH₃ + 5% O₂ + 350ppm NO; 8th: 350ppm NH₃ + 5% O₂; 9th: 350ppm NH₃+5% O₂ + 125ppm NO.

Figure 2.9: Evolution of the integrated bands for surface NH₃* (green-dotted) and NH₄⁺* (red) species under the NH₃ + NO + O₂ flow during intermittent NO supply at 250°C. The chosen integration limits are 1621-1590 cm⁻¹ for adsorbed ammonia and 1470-1386 cm⁻¹ for ammonium ion. Zoomed in common scale.

Figure 2.10: Schematic of the dehydrated supported 1% V₂O₅-5% WO₃/30% TiO₂ catalyst that corresponds to the *in situ* Raman spectra in Figure 1.

SUPPLEMENTAL FIGURE CAPTIONS

2.S1: Dehydrated FT-IR spectrum of the supported 1% V₂O₅-5% WO₃/30% TiO₂/SiO₂ catalyst in the OH stretching region in flowing O₂/Ar.

S2: Evolution of the integrated bands for surface NH₃* (green-dotted) and NH₄⁺* (red) species under the NH₃ + NO + O₂ flow during intermittent NO supply at 250°C. The chosen integration limits are 1621-1590 cm⁻¹ for adsorbed ammonia and 1470-1386 cm⁻¹ for ammonium ion. Full scale shown.

2.S3: MS signal profiles at 350°C for the ammonia isotopic substitution on 1% V₂O₅-5% WO₃/30% TiO₂/SiO₂ sample. Reaction temperature 350°C. MS Analysis of NH₃ (17), ND₃ (20), NO (30), O₂ (32), N₂ (28), H₂O, (18), D₂O (20) species. In the region indicated above, the reaction has been followed by IR spectra of the surface recorded in the rapid scan mode.

2.S4: Evolution of the integrated bands for ammonia (green) and ammonium (red) species during isotopic substitution at 350°C. The chosen integration limits are 1622-1594 cm⁻¹ for adsorbed ammonia and 1481-1382 cm⁻¹ for ammonium ion.

2.S5: Evolution of the integrated bands for ammonia (green) and ammonium (red) species during the NH₃ + NO + O₂ → ND₃ + NO + O₂ substitution at 350°C. The

chosen integration limits are 1622-1594 cm^{-1} for adsorbed ammonia and 1481-1382 cm^{-1} for ammonium ion.

2.S6: Evolution of the integrated bands for ammonia (green) and ammonium (red) species during the $\text{ND}_3 + \text{NO} + \text{O}_2 \rightarrow \text{NH}_3 + \text{NO} + \text{O}_2$ substitution at 350°C. The chosen integration limits are 1622-1594 cm^{-1} for adsorbed ammonia and 1481-1382 cm^{-1} for ammonium ion.

2.S7: IR bands associated to NH_4^{+*} (1424 cm^{-1}) and NH_3^* (1607 cm^{-1}) disappearing during $\text{NH}_3 + \text{NO} + \text{O}_2 \rightarrow \text{ND}_3 + \text{NO} + \text{O}_2$ substitution at 350°C.

2.S8: MS signal profiles for the ammonia isotopic substitution on 1% V_2O_5 -5% WO_3 /30% TiO_2 /SiO₂ sample. Reaction temperature 150°C. MS Analysis of NH_3 (17), ND_3 (20), NO (30), O_2 (32), N_2 (28), H_2O , (18), D_2O (20) species. In the region indicated above, the reaction has been followed by IR spectra of the surface recorded in the rapid scan mode.

2.S9: Evolution of the integrated bands for ammonia (green) and ammonium (red) species during the $\text{NH}_3 + \text{NO} + \text{O}_2 \rightarrow \text{ND}_3 + \text{NO} + \text{O}_2$ substitution at 150°C. The chosen integration limits are 1622-1594 cm^{-1} for adsorbed ammonia and 1481-1382 cm^{-1} for ammonium ion.

2.S10: Evolution of the integrated bands for ammonia (green) and ammonium (red) species during the $\text{ND}_3 + \text{NO} + \text{O}_2 \rightarrow \text{NH}_3 + \text{NO} + \text{O}_2$ substitution at 150°C. The chosen integration limits are 1622-1594 cm^{-1} for adsorbed ammonia and 1481-1382 cm^{-1} for ammonium ion.

CHAPTER 3

Figure 3.1. *In situ* Raman spectrum (532 nm) of the dehydrated supported 1% V_2O_5 -5% WO_3 /40% TiO_2 /SiO₂ catalyst in [A] 200-1200 cm^{-1} region that is dominated by TiO_2 (A) bands and [B] 700-1200 cm^{-1} region that is dominated by the WO_x and VO_x vibrations.

Figure 3.2. *In situ* Raman spectrum (532 nm) of the dehydrated 12% TiO_2 /SiO₂ supported catalysts [A] 2% V_2O_5 -5% WO_3 /12% TiO_2 /SiO₂ catalyst [B] 0.5% V_2O_5 -5% WO_3 /12% TiO_2 /SiO₂ catalyst [C] 1% V_2O_5 -3% WO_3 /12% TiO_2 /SiO₂ catalyst [D] 1% V_2O_5 -1% WO_3 /12% TiO_2 /SiO₂ catalyst in the 900-1200 cm^{-1} region that is dominated by the WO_x and VO_x vibrations.

Figure 3.3. *In Situ* Raman spectra during methanol chemisorption at 100°C on the supported 1% V_2O_5 -5% WO_3 /40% TiO_2 /SiO₂ catalyst in the 700-1200 cm^{-1} region .

Figure 3.4. *In Situ* IR spectra during methanol chemisorption at 100°C on the supported 1% V₂O₅-5% WO₃/40% TiO₂/SiO₂ catalyst

Figure 3.5. Methanol-TPSR spectra where CH₃OH is initially chemisorbed and the TPSR experiment is conducted in flowing O₂/He with the supported 1% V₂O₅-5% WO₃/40% TiO₂/SiO₂ catalyst

Figure 3.6. Methanol-TPSR spectra where CH₃OH is initially chemisorbed and the TPSR experiment is conducted in flowing CH₃OH/O₂/He with the supported 1% V₂O₅-5% WO₃/40% TiO₂/SiO₂ catalyst

Figure 3.7. Methanol -TPSR spectra during CH₃OH/CH₃OH-TPSR and CD₃OD/CD₃OD-TPSR over the supported 1% V₂O₅-5% WO₃/40% TiO₂/SiO₂ catalyst

Figure 3.8. Methanol -TPSR spectra during CH₃¹⁶OH/CH₃¹⁶OH-TPSR and CH₃¹⁸OH/CH₃¹⁸OH -TPSR over supported 1% V₂O₅-5% WO₃/40% TiO₂/SiO₂ catalyst

Figure 3.9. Methanol -TPSR spectra in the presence and absence of gas phase oxygen over the supported 1% V₂O₅-5% WO₃/40% TiO₂/SiO₂ catalyst

Figure 3.10. Methanol-TPSR spectra over the supported 1% V₂O₅-5% WO₃/12% TiO₂/SiO₂, 1% V₂O₅-5% WO₃/30% TiO₂/SiO₂, and 1% V₂O₅-5% WO₃/40% TiO₂/SiO₂ catalysts

Figure 3.11. Methanol-TPSR spectra over the supported 2% V₂O₅-5% WO₃/12% TiO₂/SiO₂, 1% V₂O₅-5% WO₃/12% TiO₂/SiO₂, and 0.5% V₂O₅-5% WO₃/12% TiO₂/SiO₂ catalysts

Figure 3.12. Methanol-TPSR spectra over the supported 1% V₂O₅-5% WO₃/12% TiO₂/SiO₂, 1% V₂O₅-3% WO₃/12% TiO₂/SiO₂, and 1% V₂O₅-1% WO₃/12% TiO₂/SiO₂ catalysts

Figure 3.13. Methanol-TPSR spectra where CH₃OH is initially chemisorbed and the TPSR experiment is conducted in flowing CD₃OD/O₂/He with the supported 1% V₂O₅-5% WO₃/40% TiO₂/SiO₂ catalyst

Figure 3.14. *In Situ* TP-IR spectra during methanol-TPSR where CH₃OH was initially chemisorbed at 100°C and the temperature programmed reaction was

conducted with flowing CD₃OD/O₂/He over the supported 1%V₂O₅-5%WO₃/40%TiO₂/SiO₂ catalyst (A) 1800-3700 cm⁻¹ region and (B) 1100-2100 cm⁻¹ region with zoomed in inset for the 1400-1550 cm⁻¹ region.

SUPPLEMENTAL FIGURE CAPTIONS

3.S1. Comparison of HCHO/CH₃OH-TPSR and DCDO/CD₃OD-TPSR spectra over the supported 1%V₂O₅-5%WO₃/40%TiO₂/SiO₂ catalyst

CHAPTER 4

Figure 4.1. Dehydrated Raman (532 nm) spectra of bifunctional redox-acid supported V₂O₅-WO₃/TiO₂/SiO₂ catalysts

Figure 4.2. [A] BF-STEM image of TiO₂(anatase) rafts and [B] HAADF of atomically dispersed W atoms. Note the superposition of the surface W atoms in B on the TiO₂(anatase) rafts in A.

Figure 4.3. Aberration Corrected STEM-EELS of supported 5% V₂O₅/30% TiO₂/SiO₂ [A] V edge [B] Ti edge [C] superposition of the V edge and Ti edge

Figure 4.4. DMM selectivity of bifunctional supported V₂O₅-WO₃/TiO₂/SiO₂ catalysts as a function of VO₄/WO₅ ratio, titania domain size and reaction temperature [V= V₂O₅, W=WO₃, TiSi = TiO₂/SiO₂].

Figure 4.5. DMM selectivity and TOF_{DMM} during methanol oxidation at 150°C as a function of titania domain size

Figure 4.6. DMM selectivity and TOF_{DMM} during methanol oxidation at 190°C as a function of titania domain size

Figure 4.7. DMM selectivity and TOF_{DMM} during methanol oxidation at 230°C as a function of titania domain size

Figure 4.8. Dependence of kinetics for methanol oxidation to DMM on the gas phase CH₃OH partial pressure at 190°C for the supported 1%V₂O₅-5%WO₃/40%TiO₂/SiO₂ catalyst

Figure 4.9. Dependence of kinetics for methanol oxidation to DMM on the gas phase molecular O₂ partial pressure at 190°C for the supported 1%V₂O₅-5%WO₃/40%TiO₂/SiO₂ catalyst

Figure 4.10. Schematic of titania nanoligand structures on the SiO₂ support

Figure 4.11. Molecular design of bifunctional redox-acid catalysts by self-assembly of surface VO_x and WO_x species on titania nanoligand domains.

ABSTRACT

Although previous studies have extensively focused on single component acidic (VO_x) or redox (WO_x) catalytic active sites supported on nano- TiO_2 domains for methanol oxidation to formaldehyde (redox sites) or dimethyl ether (acidic sites), respectively, no investigation has yet explored the influence of the oxide substrate dimension, in the critical ~ 0.5 -10 nm region, upon the resultant catalytic properties of heterogeneous catalysts with bifunctional supported metal oxide catalytic active sites. As such, a unique nanotechnology research opportunity currently exists to investigate and explore the fundamental science of tuning the electronic and molecular structures of bifunctional supported metal oxide catalytic active sites with nanostructured oxide substrate domains for enhanced catalytic performance. Consequently, the main research objectives of this research program will be (1) the rational design of bifunctional supported metal oxide catalyst containing redox and acid sites (2) developing next generation bifunctional supported metal oxides catalysts for enhanced performance by molecularly tuning the catalytic active sites and (3) understanding the fundamental catalysis science of complex bi- and tri-molecular reactions (NO/NH_3 -SCR and methanol oxidation to dimethoxymethane) requiring dual redox-acid functionalities. In accomplishing these objectives, emphasis will be placed on the relationships between the molecular/electronic structures of the catalytic active sites and the corresponding catalytic activity/selectivity for the targeted reactions.

A model supported V_2O_5 - WO_3 / TiO_2 / SiO_2 catalyst was used to study the selective catalytic reduction of NO_x with NH_3 to N_2 and H_2O . The objective of this investigation is to molecularly design fundamental experiments that would be able to resolve this long standing debate on the contributions of surface NH_3^* on Lewis acid sites and surface NH_4^{+*} on Brønsted acid sites during the SCR NO/NH_3 reaction over supported V_2O_5 - WO_3 / TiO_2 catalysts. The approach undertaken in the current investigation involves time-resolved *in situ* FT-IR spectroscopy of the surface NH_3^* and NH_4^{+*} species under reaction conditions with simultaneous IR/MS analysis of the gas phase products (referred to as *operando* spectroscopy). Model supported 1% V_2O_5 -5% WO_3 / TiO_2 / SiO_2 catalysts were investigated under steady-state and temperature programmed reaction conditions with the aid of transient isotopic labeling of ammonia to obtain fundamental mechanistic insights into the SCR NO/NH_3 reaction. These unprecedented, designed experiments have provided the molecular level insights that have finally resolved the long standing debate in the literature and have definitively demonstrated that although both acid sites participate in the SCR reaction it is the surface Brønsted acid sites that are the dominant catalytic active sites during the $NO-NH_3$ SCR reaction over supported V_2O_5 - WO_3 / TiO_2 / SiO_2 catalysts.

The selective oxidation of methanol to dimethoxymethane (DMM) was also investigated over the model bifunctional supported V_2O_5 - WO_3 / TiO_2 / SiO_2 catalyst, where VO_x and WO_x were molecularly dispersed and self-assembled onto 5-9 nm

TiO₂(anatase) nanoparticles that in turn were anchored on the relatively inert silica support. The molecular structures of the supported metal oxide catalytic active sites were determined to be mono-oxo surface VO₄ and WO₅ species with *in situ* Raman spectroscopy. Complementary *in situ* FT-IR spectroscopy revealed that surface CH₃O* species are the most abundant reactive intermediates (mari) during DMM formation. The catalytic surface chemistry was probed with CH₃OH-Temperature Programmed Surface Reaction (TPSR) spectroscopy whereby a monolayer of CH₃O* was reacted with gas phase isotopically labeled methanol (CD₃OD or CH₃¹⁸OH) and revealed that C-H bond breaking of surface CH₃O* species on the redox surface VO₄ sites is the rate-determining-step (rds) in DMM formation. The molecularly designed catalyst provided a “green” one step synthetic route for the synthesis of DMM, whereby toxic HCHO is generated *in situ* from the catalytic active VO₄ sites and synergistically coupled with surface CH₃O* species on the surface WO₅ sites to produce DMM.

DMM has recently been investigated for its potential benefit as an oxygenated additive in diesel fuel because of its ability to suppress soot formation and the objective was to molecularly design a supported V₂O₅-WO₃/TiO₂/SiO₂ catalyst whereby methanol could be selectively oxidized to give DMM by changing the titania domain size and tuning the relative catalytic contributions of the redox VO₄ and acid WO₅ sites. It was found that the local electron density of oxide nanoligand supports allows for tuning of the specific activity of the supported

surface redox and acid catalytic active sites. In the low temperature regime (150-190°C), the selectivity to DMM is highest due to a high concentration of surface CH_3O^* species, essentially monolayer surface methoxy coverage, that can efficiently further react with the HCHO produced on the redox surface VO_4 sites by coupling HCHO with the surface methoxy species on the acid surface WO_5 sites to produce DMM.. In the high temperature regime (200-230°C), the concentration of surface CH_3O^* species is significantly below monolayer coverage and the probability for coupling reacting between HCHO and surface methoxy species is significantly diminished, consequently, the DMM selectivity decreases and the HCHO selectivity increases. Steady-state and CH_3OH -TPSR kinetic measurements also reveal that the formation of DMM from methanol oxidation proceeds via a Mars-van Krevelen mechanism involving surface lattice oxygen from the catalyst, which is reflected in the zero-order dependence on the partial pressure of gas phase molecular O_2 . At high methanol partial pressures where the catalyst surface is saturated with surface methoxy species, the DMM reaction kinetics also approaches zero-order kinetics because the surface is saturated with surface methoxy species in the low temperature regime. At high temperatures or low methanol partial pressures, the DMM reaction kinetics approaches first-order, indicative of C-H bond breaking to form HCHO. This study demonstrated that the ability to molecularly engineer the catalytic active sites at the nanoscale requires fundamental understanding of the synthesis-structure-property relationships of supported metal

oxide catalysts that enables their rational design involving complex, multisite and multistep reactions such as the selective oxidation of methanol to DMM.

Chapter 1

Tuning Catalytic Active Sites

1. Introductory Remarks

The ability to design and control a catalyst on a molecular level for a given reaction is an often sought goal in the field of catalysis. The complexity of a heterogeneous catalyst however, makes this a challenging objective to achieve. The molecular design of a catalyst requires the assistance of detailed spectroscopic characterization in order to elucidate the nature of the catalytic active site. Once the catalyst has been thoroughly investigated using molecular/atomic techniques under ambient, dehydrated as well as reaction conditions, will a fundamental structure-performance understanding be established that will facilitate rational catalyst design of next generation tunable catalytic surface structures.

For many applications, a catalyst is typically designed with the specific intent to catalyze one particular type of reaction (e.g., an acidic reaction, a basic reaction, or a redox reaction). The starting molecule, however, may go through multiple reaction pathways and reaction intermediates before arriving at the final product. This tortuous path in going from the starting molecule to the desired final product can be economically expensive, as multiple reactors may be required to facilitate the desired chemical transformations. Bifunctional or multifunctional catalysis is an attractive solution, whereby 2 or more types of active sites are

present on the same catalytic surface that are able to synergistically catalyze different reaction pathways towards the desired reaction product. A major thrust in the area of bifunctional catalytic studies to date has been in the area of acid-base catalysis [1-15]. Acid-base reactions represent an important class of reactions, and the ability to create catalyst for this multifunctional purpose has received much attention.

Bifunctional pathways have been proposed to proceed via a concerted or sequential process [1]. Concerted bifunctional pathways require that sites co-exist within molecular distances, whereas non-concerted or sequential bifunctional pathways avoid this requirement and occur even when the required sites are located farther apart. In sequential processes, sites interact via the formation and migration of gas phase and surface species [1]. The dehydration of 1-butanol on Na-doped alumina is an example of a reaction proposed to proceed via a concerted mechanism [6]. In this reaction, the interaction of the acidic and basic sites is thought to interact simultaneously at different positions of the same molecule, and share one catalytic function together, as shown in Figure 1. Bifunctional catalytic reactions can also occur simultaneously or successively. The simultaneous interaction can occur when different catalytic active sites interact with different substrate molecules simultaneously but independently, typically seen in Tishchenko reactions. This is illustrated in Figure 2, where one molecule of benzaldehyde interacts with a basic O^{2-} site of CaO to form the intermediate (A), while another

molecule of benzaldehyde interacts with a Lewis acid site, Ca^{+2} , to form another intermediate (B) [6]. Intermediates (A) and (B) go on to react with each other to eventually form the final product. Recent progress by Bass et al [5] demonstrated the ability to effectively design an acid-base catalyst whereby the idea is to have the acid and base groups at optimal distances for cooperativity, as displayed in Figure 3, where a silica surface is used as a macroscopic ligand providing a range of acid-base distances for bifunctional cooperativity. The idea was effectively implemented using an amine functionalized silica surface for the production of β -nitro alcohol as shown in Figure 4 [5].

2. Synopsis

The methods used in the field of heterogeneous catalysis to tune catalytic active sites have been demonstrated through (1) surface coverage (2) oxide support (3) additives (4) spatial constraints/accessibility to the active site and (5) atomic manipulation.

Surface coverage (1) has been recognized to have two affects, first the structure of the active site (isolated, polymeric, crystalline) can influence the reactivity [16-19]. Second, the nature of acidity (Brønsted vs Lewis) can be controlled by the surface density of the surface metal oxide species [20]. In addition to the structure affecting the catalytic reactivity, catalyst preparation conditions, such as calcination temperature [21], can influence which active surface structure is formed. Most often however, the oxide support (2), specifically the M-

O-Support bond is the catalytic active site. As such, varying the oxide support (Si, Al, Ti, Zr) can have a significant effect (factor of $\sim 10^3$) on the catalytic activity [16,19,22]. The specific oxide support also controls the number of active sites and activity per site which are specific to a particular oxide support. The oxide support can also influence the dispersion of the active oxide phase, which can affect the reactivity [22]. Alternatively, when considering the support as a ligand, the advent of bilayered catalysts ($M_1O_x/M_2O_x/SiO_2$), as shown in Figure 5, whereby M_1O_x is anchored to M_2O_x (in the 0.1 -10 nm range) and grafted to an inert silica surface, can alter the electronic properties of the resulting catalytic material and ultimately the reactivity [23]. Additives (3) can be interacting or non-interact with the active site. For interacting additives, it can have a positive or negative effect on the resulting catalytic activity/selectivity [24]. Additives can block potential unwanted sites that produce side reactions or they can be detrimental to the catalyst by poisoning the catalytic active site, as shown in Figure 6. Spatial constraints (4) can determine the stability of reactants specifically within zeolite channels where the location of active sites can strongly influence reactivity. As such, researchers attempt to rationally position active sites within specific channel locations [25] or at optimal distances to increase their accessibility. Finally atomic manipulation (5) of well defined Keggin structures provides readily tunable properties whereby an atom can be replaced by a different atom within the structure to alter the resulting catalytic properties [26].

As summarized, there are numerous ways in which catalysis researchers have been tuning catalytic active sites. This review will highlight some of the important advances made in the field of heterogeneous catalysis regarding tuning catalytic active sites, of which fall within one of the five major categories described, with pertinent examples related to mono-functional surface redox and acid sites, and bifunctional redox-acidic metal oxide heterogeneous catalysts.

3. Tuning Surface Redox Sites

Redox catalysis constitutes one of the most extensively examined areas of catalysis both industrially and academically. While there has been much work in the area of redox catalysis, little has been done in the area of molecular catalyst design and the ability to tune redox catalytic active sites for targeted chemical transformations.

Initial attempts to controlling catalytic active sites came from researchers attempting to heterogenize homogenous catalysts in the attempts to design uniform single site catalysts. The idea was to graft organometallic complexes onto high surface area mesoporous materials. Significant progress has been made in this area and continues to be an active area of research. It was shown by Thomas [28, 29] that tripodally attached titanol groups to silica, as shown in Figure 7, which are analogous to titanosilsesquixane species, can be engineered as uniform active sites for the epoxidation of alkenes. The enhanced performance was attributed to the accessibility of the modified Ti^{IV} active center. It was similarly shown [28] that a

boost in catalytic performance could be achieved by enhancing the hydrophobicity of the immediate vicinity of a vanadyl active site. This was achieved by grafting pendant methyl groups on an MCM-41 catalyst in the vicinity of the active site, which was found to significantly enhance the catalytic performance in the epoxidation of cyclohexene, as shown in Figure 8. This enhancement was suggested to be the result of facilitation of the approach of the reactant to the catalytic active site. While the approach of grafting highly active complexes onto a support has received much attention the limitation with this technology has been the recyclability of the catalyst [27].

An alternative approach well developed by Wachs *et al.* [16-19,22] for tuning the catalytic active site was to vary the MoO_x surface structure when supported on a second metal oxide substrate. Though the affect of the supported MoO_x structure ($\sim 10^1$) is not as great as the affect due to the specific oxide support ($\sim 10^3$), as will be described later, it is still of critical importance. In fact, the phenomena of surface structure affects on reactivity have been investigated for multiple metal oxide species other than MoO_x (V₂O₅, CrO₃, Re₂O₇). The reactivity of the metal oxide surface structures have been probed by the methanol oxidation reaction, due to its sensitivity to the nature of the surface sites present. As such, the affect of isolated, polymerized, or crystalline species can be readily discriminated. In general, a slight increase in turn over number (TON) has been reported with increasing surface coverage from isolated to polymerized species, where as bulk

crystalline species are typically less active than their corresponding surface species [16]. This phenomenon has been well documented with $\text{MoO}_3/\text{SiO}_2$, where the surface molybdenum oxide coverage on silica is the only relevant factor that determines the catalytic properties during methanol oxidation [18]. As such, the catalytic activity decreases with increasing surface molybdenum coverage, due to the extent of aggregation increasing (into crystalline $\beta\text{-MoO}_3$) with the surface molybdenum coverage.

The idea of varying surface density to affect catalytic properties has become more widely applied with more examples now found in the literature which in principal tunes the catalytic properties by varying surface metal oxide density, which affects the surface polymer/monomer ratio. An interesting example comes from J-M. Jehng *et al.* [30] in the study of tantalum modified mesoporous silicalite (MCM-41) catalysts, which in affect may be considered a dual redox-acid catalyst system. Bulk Ta_2O_5 has been found to only possess acid sites, as determined from methanol oxidation experiments. However, the researchers were able to molecularly disperse TaO_x species on the MCM-41 support and control the various surface structures formed. As shown in Figure 9, at low Ta concentrations, the MCM-41 surface starts to become rough and form nanoscale particles with increasing Ta concentration. As such, Ta atoms are predominately incorporated into the MCM-41 frame structure at low Ta concentration (below 3% Ta), and forms an isolated TaO_4 species on the Ta-MCM-41 surface with further increasing

Ta concentration. Specifically, three types of tantalum oxide species coexist on Ta-MCM-41 catalysts as a function tantalum oxide surface coverage: an isolated TaO_4 species in the MCM-41 framework, an isolated surface TaO_4 species on the MCM-41 external surface, and bulk Ta_2O_5 in (and on) the Ta-MCM-41 catalysts. Their results nicely showed that TaO_x incorporated into the MCM-41 framework results in a higher activity than that for the dispersed TaO_4 species on the MCM-41 surface, which results in the decrease of methanol reactivity with increasing tantalum oxide loading. Gao *et al.* [31] also came to a similar conclusion when investigating the structure-reactivity properties of Nb-MCM-41 catalysts. It was found that under dehydrated conditions, Nb cations in both Nb-MCM-41 and supported 1% $\text{Nb}_2\text{O}_5/\text{SiO}_2$ are predominantly composed of isolated NbO_4 units, while Nb cations in the supported $\text{Nb}_2\text{O}_5/\text{SiO}_2$ catalysts possess polymerized NbO_x species and/or bulk Nb_2O_5 with increasing tantalum oxide loadings. The isolated NbO_4 species in Nb-MCM-41 and 1% $\text{Nb}_2\text{O}_5/\text{SiO}_2$ exclusively behave as catalytic active redox sites for methanol oxidation. At higher niobia loadings, the polymeric surface NbO_x species and Nb_2O_5 nanoparticles (NPs) also coexisted and resulted in the production of dimethyl ether (DME) that forms on catalytic surface acid sites. In addition, the overall reactivity (TOFs) for the supported $\text{Nb}_2\text{O}_5/\text{SiO}_2$ catalyst systems decreased dramatically with increasing niobia loading, revealing that isolated surface NbO_4 species on silica are more active than polymeric surface niobia species and Nb_2O_5 NPs.

Similar to the ideas that Thomas [28,29] presented regarding organometallic complexes, Saikia *et al.* [32] investigated the selective oxidation properties of Mn complexes, shown in Figure 10, grafted onto SBA-15. By carefully controlling the complex, manganese complexes of 5,10,15,20-tetraphenylporphyrin (Mn(TPP)Cl) were carefully grafted onto SBA-15 and functionalized with propyl-amine, -thiol and –sulfonic acid groups. The various supported complexes were probed using the selective oxidation of R-(+)-limonene to endo-1,2-epoxide as a test reaction. It was concluded that the nature of the support as well as the ligand play a crucial role in controlling the redox behavior, molecular electronic structure and the catalytic activity of the supported Mn complexes.

3. 1 Tuning Surface VO_x Redox Sites

More recently, Nakka *et al.* [33] investigated the oxidation and dehydration of methanol over mixed metal oxide polyoxometallate (POM) vanadium tungstate ($H_{3+x}PW_{12-x}V_xO_{40}$ with $x = 0-3$) Keggin NPs. The ability to tune the $H_3PW_{12}O_{40}$ Keggin was made possible by the introduction of VO_x sites. Surface VO_x sites on TPA decrease the TOF_{acid} kinetics by ~100-fold from site blocking and titration of acidic surface hydroxyls. Incorporation of VO_x into the TPA Keggin does not affect the TOF_{acid} kinetics for TPAV1 ($H_4PW_{11}V_1O_{40}$), which has only a minimal amount of surface VO_x sites. The methanol oxidation to formaldehyde kinetics (TOF_{redox}) over $H_4PW_{11}V_1O_{40}$ is comparable to that for the more active vanadium oxide catalysts (V_2O_5/CeO_2). The TOF_{redox} kinetics for the supported

$\text{VO}_x/\text{H}_3\text{PW}_{12}\text{O}_{40}$ Keggin catalyst is comparable to that of the least active supported vanadium oxide catalyst ($\text{V}_2\text{O}_5/\text{SiO}_2$). As such, tuning the complex Keggin structure by careful placing of the catalytic active VO_x sites was achieved by incorporating it into either the primary Keggin structure and/or the secondary surface structure of the Keggin unit, as shown in Figure 11a-b. The findings highlight the complexity of Keggin POMs and shed light on the surface and bulk metal oxide structures present for POMs under realistic reaction conditions.

As described above, the conventional way of tuning catalytic active sites has been to vary the domain size of the active site. A novel approach that has been undertaken and well developed over the past decade to molecularly control and tune the active site has been the control of the underlying oxide support dimensions [34-42]. The novel catalytic materials were electronically, molecularly and chemically characterized with the most advanced state-of-the-art molecular level in situ microscopic and spectroscopic techniques, and under different reaction conditions, to determine their fundamental electronic/molecular structure-activity/selectivity relationships. It is well documented that the nature of the active metal oxide component-support interaction has a pronounced effect on the catalytic performance, and is many times the most significant factor among the different catalyst variables. This enhancement can be the result of charge transfer and/or formation of unique catalytic active sites that form at the interface from structural and electronic modifications. The catalytic enhancement is usually the result of

charge transfer between the metal oxide active component and the underlying oxide support ligand [43-50]. Such a charge transfer can modify the electron density of nano-sized metal oxide catalytic active sites with consequent catalytic performance modification. The electron density of nanostructured metal oxide clusters is known to be dependent on the metal oxide domain size, with the local electron density increasing for smaller dimensions and the electrons becoming more delocalized for larger dimensions [51]. Consequently, nanostructured support substrates exhibit variable electron density that can be shared with the supported catalytic active metal oxide components [52]. This suggests that catalytic active sites that require electrons (i.e. redox VO_x) should ultimately be enhanced as electron delocalization is increased [43,44].

As detailed by Wachs [34] a number of detailed studies have focused on tailoring the electronic and molecular structures of oxide nanoligands and their resulting impact on the catalytic performance of molecularly engineered supported metal oxide catalytic active sites. A series of model supported catalysts were molecularly engineered to allow for variation of the catalytic active sites and oxide nanoligands. Molecularly controlled synthesis of the nanoligand domains was achieved by means of incipient wetness impregnation into SiO_2 . The underlying nanoligand dimensions (isolated and polymeric surface species as well as 2D raft-like domains and 3D nanoparticles) and resulting electronic structure, molecular structure, nanoligand composition (TiO_2 [23, 35,36,39-42], ZrO_2 [37,39,41,42],

Al₂O₃ [38,39,41,42]) and the catalytic active site (redox VO_x) were controlled to tune the catalytic activity/selectivity. The methanol oxidation reaction was used to probe the chemical reactivity of these multilayered catalysts. The results indicate that TOF values increased by a factor of ~20 in replacing V-O-Si bonds with V-O-S bonds (where S = Ti, Zr, or Al), which clearly demonstrates the influence of the support cation electronegativity on the reactivity of the bridging V-O-S bond.

Recent work by Ross-Medgardeen *et al.* [23] took an in depth look at the titania nanoligand domain size influence on the catalytic activity of redox surface VO_x sites. Variable metal oxide domain sizes were synthesized by impregnating a relatively inert and high surface area amorphous SiO₂ support (15-30 nm) with Ti-isopropoxide dissolved in isopropanol, dried, and then calcined at 500 °C in air to form TiO₂ domains dispersed on SiO₂. The presence of the SiO₂ matrix was critical in controlling the agglomeration of the nanostructured TiO₂ domains.

The structures of a series of supported TiO₂/SiO₂ samples were examined with transmission electron microscopy (aberration corrected HR-TEM) imaging, as shown in Figure 12, *in situ* Raman, and *in situ* UV-Vis spectroscopy characterization studies. Raman spectroscopy provided molecular structural information and UV-Vis provided the complementary electronic structural details about the SiO₂-supported titania phase. Raman and UV-Vis spectroscopy revealed that the 1% TiO₂/SiO₂ sample consists of isolated surface TiO₄ species and the 12% TiO₂/SiO₂ sample consists of polymeric surface TiO₅ species. The local

coordination of the surface TiO_x species were obtained by *in situ* XANES measurements. Bright field images and selected area electron diffraction patterns showed no obvious signs of TiO_2 crystallites and EDS analysis confirmed the presence of surface Ti atoms for the 12% $\text{TiO}_2/\text{SiO}_2$. A 20 wt% $\text{TiO}_2/\text{SiO}_2$ sample was synthesized and found to contain 2-4 nm crystalline TiO_2 NPs as well as coexisting surface TiO_x species. Higher titania contents (>20% TiO_2) gave rise to larger TiO_2 NPs (3-5 nm for 30% and 5-9 nm for 40% $\text{TiO}_2/\text{SiO}_2$) that also completely consumed the surface TiO_x layer due to the greater affinity of surface TiO_x for TiO_2 NPs over the relatively inert SiO_2 support. Raman spectroscopy and selected area electron diffraction studies indicated that the TiO_2 NPs possessed the anatase structure. Additionally, the 3-5 nm NPs present in 30% $\text{TiO}_2/\text{SiO}_2$ sample were found to uniquely be present as thin 2D rafts of $\text{TiO}_2(\text{anatase})$.

The electronic structures of the novel supported $\text{TiO}_2/\text{SiO}_2$ samples were examined with *in situ* UV-Vis spectroscopy, a characterization technique that provides information about the local electron density of the supported titania phase. The edge energy, or E_g values, for the different supported TiO_2 domains increased continuously as the TiO_x domain size became smaller, which is evidence for the well-known quantum confinement effect. Larger edge energy values correspond to higher local electron density and less electron delocalization (less reducible oxide).

The nature of the dehydrated supported vanadia phase on the $\text{TiO}_2/\text{SiO}_2$ support was determined with *in situ* Raman spectroscopy. The researchers were

able to molecularly disperse surface VO_x species without forming V_2O_5 NPs (confirmed with a single Raman band at $\sim 1031\text{ cm}^{-1}$ and absence of the crystalline V_2O_5 Raman band at $\sim 994\text{ cm}^{-1}$) on the $\text{TiO}_2/\text{SiO}_2$ support. For the dehydrated supported $\text{V}_2\text{O}_5/\text{SiO}_2$ catalyst, the Raman band of the mono-oxo surface VO_4 species vibrates at $\sim 1036\text{-}1040\text{ cm}^{-1}$. For the dehydrated supported $\text{V}_2\text{O}_5/\text{TiO}_2$ catalyst, the mono-oxo surface VO_4 species band appears at $\sim 1031\text{ cm}^{-1}$. The surface VO_4 species, always possess the mono-oxo $\text{V}=\text{O}$ structure and does not change coordination with different support ligands. There is a slight shift, however, in the terminal $\text{V}=\text{O}$ vibration when it is coordinated to different oxide support ligands. The Raman band of the terminal $\text{V}=\text{O}$ vibration at $\sim 1031\text{ cm}^{-1}$ reflects the preferential coordination of the surface VO_4 species to the supported titania phase over the silica support. The researchers further confirmed this finding using $\text{CH}_3\text{OH-IR}$ that demonstrated the preferential anchoring of the surface VO_4 species on the titania sites since Ti-OCH_3 vibrations were never detected reflecting that the Ti sites are always covered by the surface VO_x species. Thus, the catalytic active surface VO_4 species were discovered to preferentially anchor or self-assemble at the surface titania sites.

The surface chemistry of the surface VO_4 species on the titania nanoligands was chemically probed with CH_3OH oxidation to HCHO and H_2O , which only takes place on surface redox catalytic active sites. Formation of CH_3OCH_3 from catalytic active acid sites was not observed, which reflects the dominance of the

redox nature of the surface VO_4 species. The first-order reaction rate constants for breaking of the C-H bond of the surface CH_3O^* intermediates were determined with CH_3OH -TPSR and compared with the E_g values of the titania nanoligands as a function of the titania content in the catalysts. The monotonic decrease in k_{rds} with decreasing titania domain size was found to vary inversely to the increasing E_g value of the titania nanoligands. Similar trends were also obtained for steady-state methanol oxidative dehydrogenation to formaldehyde over the supported $\text{VO}_x/\text{TiO}_2/\text{SiO}_2$ catalysts as a function of the titania nanoligand domain size. These findings reveal that lower E_g values, possessing greater electron delocalization, correspond to enhanced redox activity of surface VO_4 catalytic active sites.

4. Tuning Surface Acid Sites

There has been a major research thrust to develop new and improved solid acid catalysts to avoid the environmental emissions and corrosiveness associated with liquid acid catalysts [55-70]. A particularly promising set of solid acid catalysts that are being intensely investigated and shows great promise due to its readily tunable properties are Wells-Dawson heteropoly-compounds, as shown in Figure 13. Wells-Dawson heteropoly-anions possess the formula $[(X^{n+})_2M_{18}O_{62}]^{(16-2n)-}$ where X^{n+} represents a central atom surrounded by a cage of M addenda atoms, such as tungsten(VI), molybdenum(VI) or a mixture of elements, each of them composing MO_6 (M-oxygen) octahedral units. An example of their unique properties is demonstrated with the catalytic acylation and alkylation of iso-

butylene with Wells-Dawson phosphor-tungstic acid $H_6P_2W_{18}O_{62}$ POM, in liquid phase or gas phase reactions either as bulk or silica-supported catalysts [68]. It was shown that the alkylation/acylation of iso-butylene with methanol produces MTBE, and that the rate of reaction is influenced by the methanol partial pressure due to the absorption of methanol inside of the bulk of the Keggin POM. Though the Wells-Dawson acid strength is lower compared to Keggin-type acids, its ability to absorb larger amounts of methanol was attributed to the higher activity for this particular reaction [68].

4. 1 Tuning Surface WO_x Redox Sites

Another class of solid acid catalysts receiving major attention is supported tungsten oxide catalysts [57-59] due to their applicability to the petroleum, chemical and pollution control industries. Recent in depth studies by E.I. Ross-Medgaarden *et al.* [40] investigating a series of supported $WO_3/ZrO_x(OH)_{4-2x}$ catalysts (WZrOH) provided a new model for the origin of the enhanced solid acidity of supported WZrOH catalysts, as shown in Figure 14. By applying cutting edge characterization techniques (HR-TEM, Raman and UV-vis spectroscopy as well as XRD and XPS) the researchers were able to conclude that the supported WZrOH catalyst system attains monolayer coverage at ~ 5 W-atoms/nm². In the sub-monolayer region, dehydrated surface WO_x species and some Zr-stabilized distorted WO_3 NPs were found to be present. By molecularly controlling the catalyst tungsten oxide structures, *in situ* UV-vis and Raman revealed that surface

WO_x species could rapidly become polymerized with surface coverage and surface polytungstates become the dominant species at modest surface coverage. Above the monolayer region, the supported WZrOH catalysts were found to possess the surface polytungstate monolayer; distorted Zr-WO₃ NPs and ordered crystalline WO₃ NPs, with their relative concentrations varying as: crystalline WO₃ NPs > Zr-stabilized distorted WO₃ NPs > surface polytungstate species. The combined characterization and methanol dehydration experiments revealed that the distorted Zr-WO₃ NPs are the catalytic active sites for the supported WZrOH catalysts, and their maximum concentration corresponds to ~6-7 W-atoms/nm², which is just above monolayer coverage. These new concepts developed by Ross-Medgaarden *et al.* [40] were expanded upon by Soutanidis *et al.* [21] relating the surface density of WO_x/ZrO₂ to the catalytic activity for n-pentane isomerization. These catalytic results demonstrated that 5.2 W/nm² produced the maximum activity in pentane isomerization, which was found to be just above surface WO_x monolayer coverage and the onset of Zr-WO_x clusters. The calcination temperature was determined to be a critical factor, with calcinations conditions at 973 K favoring sub-nm Zr-WO_x clusters.

More recent studies by Ross-Medgaarden *et al.* [23] and Lee *et al.* [41,42] shed light on the design and synthesis of nanoligand-supported metal oxide complexes that are supported on relatively inert high-surface area silica supports. Covering the spectrum of domain sizes (0.5-10 nm), compositions (ZrO₂ [41,42]),

TiO₂ [23,41,42], Al₂O₃ [41,42]), and catalytic active site composition (WO_x), they developed a fundamental understanding of nanoligand effects in heterogeneous supported catalysts. Prior to these studies, no investigation had systematically examined the influence of the oxide substrate nanostructure in the critical 0.5-10 nm range for the acidic WO_x catalytic active component-support interaction upon the resultant electronic structures, molecular structures and catalytic properties. Ultimately, the foundation of their ground breaking research lies in the fundamental principles of thermodynamics. The reason being is that the thermodynamic driving force is lowering of the system surface free energy (replacing higher free energy surface Ti-OH bonds with lower surface free energy terminal W=O bonds) and the kinetics are facilitated by surface diffusion of the metal oxides (related to the modest WO₃ Tammann temperature of ~873 K [71-73]). Thus, both location and structure of surface WO_x species were controlled by the metal oxide nanoligands.

The studies by Ross-Medgardeen *et al.* [23] entailed synthesizing variable metal oxide domain sizes by impregnating a relatively inert and high surface area amorphous SiO₂ support (15-30 nm) with Ti-isopropoxide dissolved in isopropanol, dried, and then calcined at 500 °C in air to form TiO₂ domains dispersed on SiO₂. The presence of the SiO₂ matrix was critical in controlling the agglomeration of the nanostructured TiO₂ domains. The nature of the deposited tungsten oxide phase on the TiO₂/SiO₂ support was determined with *in situ* Raman spectroscopy, and revealed that crystalline WO₃ NPs were not present (absence of

strong bands at 804, 710 and 270 cm^{-1}) and, consequently, that the active tungsten oxide was 100% dispersed as surface WO_x species on the $\text{TiO}_2/\text{SiO}_2$ support (Raman bands in the $\sim 1000 \text{ cm}^{-1}$ range). For dehydrated WO_3/SiO_2 , the Raman W=O vibration occurs at $\sim 980 \text{ cm}^{-1}$, characteristic of dioxo (O=W=O) WO_4 species, with a weaker vibration at $\sim 1020 \text{ cm}^{-1}$, associated with monoxo (W=O) WO_5 species. The Raman spectra for all of the synthesized dehydrated supported $\text{WO}_x/\text{TiO}_2/\text{SiO}_2$ catalysts in the study were dominated by the monoxo W=O vibration at $\sim 1020 \text{ cm}^{-1}$, which is characteristic of the preferential coordination of the surface tungsten oxide species to the titania nanoligands.

The catalytic results for CH_3OH dehydration reaction over the supported $\text{WO}_3/\text{TiO}_2/\text{SiO}_2$ catalysts were demonstrated to be 100% selective towards CH_3OCH_3 formation, reflecting the catalytic dominance of the acidic surface WO_x sites in these catalysts. The first-order reaction rate constants for scission of the C-O bond on the supported $\text{WO}_3/\text{TiO}_2/\text{SiO}_2$ catalysts were determined with CH_3OH -temperature programmed surface reaction (TPSR) spectroscopy and compared with the corresponding titania E_g values as a function of the catalyst titania content. It was concluded that higher E_g values of the titania nanoligand, corresponding to less electron delocalization, enhanced the acidic activity of the surface WO_5 catalytic active sites.

The experimental findings clearly demonstrated that the catalytic active surface WO_x species migrate and preferentially coordinate to the TiO_2 domains

during heat treatment and transform from dioxo WO_4 to monoxo WO_5 surface species. As a result, it was concluded that varying the local electron density of oxide nanoligand supports indeed allows tuning the catalytic activity of acidic surface metal oxide catalytic active sites.

5. Tuning Bifunctional Redox-Acid Sites

While significant advances over the past two decades have been made in tuning individual redox or acidic catalytic active sites as described above, far less progress has been made in the ability to manipulate, control, and tune bifunctional redox-acidic catalytic active sites. The lack of advancement on this front stems from the inherent difficulty in being able to molecularly control multiple surface sites on the nanometer and even atomic level. There are however a number of reactions requiring this dual functionality (hydroxylation of phenol to hydroquinone and catechol [74], methanol oxidation to dimethoxymethane [65-71], cyclohexanone to ϵ -caprolactam [82,83], selective catalytic reduction of NO_x to benign N_2 and H_2O [84,85,94], propane oxidation to acrylic acid [86,87], propane ammoxidation to acrylonitrile [88,89], butane oxidation to maleic anhydride [90], isobutene oxidation to methyl tert-butyl ether [91]). As such, there exists a unique opportunity to make significant advances in this relatively unexplored field.

Recent work by J.M. Thomas *et al.* [82, 83] demonstrated an environmentally friendly one step process to produce ϵ -caprolactam, a precursor of nylon-6 that is finding increasing importance in the automobile industry. The

current manufacturing process of ϵ -caprolactam is a two step process, starting with the oxidant that forms the intermediate cyclohexanone oxime is hydroxylamine sulfate, and ammonia is used to neutralize the acid. Aqueous H_2O_2 is subsequently used with a solid redox catalyst, a titanosilicate TS-1 to ammoxidize the ketone. In addition, this process produces large quantities of environmentally undesirable ammonium sulfate as a by-product. With the design of a bifunctional AlPO-5 catalyst, the researchers were able to create redox active centers into the catalysts, as shown in Figure 15, whereby hydroxylamine (NH_2OH) is readily formed *in situ* inside the pores from NH_3 and O_2 at the redox sites. Hydroxylamine was then found to convert cyclohexanone into cyclohexanone oxime both inside and outside the pores of the catalyst. Likewise, at the Brønsted acid sites cyclohexanone oxime isomerizes to ϵ -caprolactam inside the pores of the catalyst. The ability to molecularly perform both steps on one catalyst allowed for the development of a benign single step, solvent free, low temperature synthesis of ϵ -caprolactam without generating ammonium sulfate as a by-product.

Another industrially relevant process is the oxidative dehydrogenation (ODH) of propane to propene. Dimitratos *et al.* [92] investigated this reaction using polyoxometallates, which are readily tunable for redox-acidic reactions. Using a $\text{CS}_{2.5}\text{H}_{1.5}\text{PV}_1\text{Mo}_{11}\text{O}_{40}$ Keggin POM, the researchers were able to tune the intrinsic catalytic properties by introducing redox elements (Co^{II} , Fe^{III} , Ga^{III} , Ni^{II} , Sb^{III} , or Zn^{II}) in a 1:1 atomic ratio to vanadium. The presence of these substituted

cations allowed for high selectivity to propene at relatively low temperatures (300-400°C) while keeping the heteropolyacid salt stable under catalytic reaction conditions.

An elegant display of catalytic surface manipulation was demonstrated by X. Wang and Wachs [93], whereby surface acidic, basic, redox, mixed redox-acidic and mixed redox-basic active sites were carefully designed and probed with methanol oxidation. With the use of Raman spectroscopy, the researchers were able to determine the exact locations of surface methoxy intermediates on the mixed oxide catalyst surfaces during methanol oxidation. The formation of dimethoxymethane (DMM) was found to require the presence of dual surface redox (VO_x) and Lewis acid (Al_2O_3) sites. The molecularly designed catalyst (15% $\text{V}_2\text{O}_5/\text{Al}_2\text{O}_3$) was found to selectively convert methanol to DMM at reaction temperatures of 180-190°C where the concentration of surface CH_3O^* was very close to monolayer coverage. Their results demonstrated that it is possible to determine the specific surface site requirements for each reaction pathway for methanol oxidation to products and that the desired selectivity characteristics can be tuned by the design of the catalytically active surface sites.

The synthesis of DMM has been receiving much attention due to its potential as a diesel fuel additive. As such, the synthesis of DMM was also investigated by H. Liu *et al.* [75] on unsupported and SiO_2 -supported POM Keggin $[\text{H}_{3+n}\text{PV}_n\text{Mo}_{12-n}\text{O}_{40}$ ($n = 0-4$)]. The current two step process to produce

DMM requires methanol oxidation to formaldehyde (HCHO) over a redox catalyst followed by condensation of HCHO with additional methanol over a solid acid catalyst. By using tunable bifunctional Keggin clusters, the researchers were able to selectively produce DMM in one step. The ratio of redox and Brønsted acids was varied by controlled thermal dehydroxylation of the Keggin clusters. By supporting the Keggin clusters on SiO₂, the accessibility of acid and redox sites increased along with the rate of methanol conversion to DMM. Atomic manipulation of the Keggin clusters, whereby some Mo atoms were replaced by vanadium was found to increase the rate and selectivity of DMM production. Ultimately, the researchers were able to demonstrate that by the rational design of catalytic active sites, high DMM selectivity's could be achieved from methanol or dimethyl ether in a single reaction step.

6. Conclusions

The quest to molecularly engineer catalysts for a given application has long been sought after by researchers. Not until the recent technological advancements with atomic characterization tools and molecular spectroscopies has the field of catalysis begun to open up to the possibilities of active site manipulation. New complex catalysts such as Keggin structures and polyoxometalates are becoming better understood and show tremendous promise with tunable redox and/or acidic active sites. Their low thermal and structural stability (~300°C) however, remains a challenge for their wider industrial use. Similarly, the major advancements made

over the past decade with molecularly engineered bilayered catalysts, has pushed nanotechnology to the forefronts and advanced the knowledge of atomic level materials chemistry.

Bifunctional catalysis provides many unique opportunities to perform multiple catalytic steps on one surface, and its industrial relevance is sure to be of major importance in the near future. Due to the inherent complexity of multiple active surface sites and multiple reaction steps occurring at various atomic positions, the advancement of tuning bifunctional catalytic active sites is still in its infancy. As such, much opportunity exists in this area and is destined to be a major research thrust going forward.

7. Outline of Research

Although previous studies have extensively focused on single component acidic (WO_x) or redox (VO_x) catalytic active sites supported on nano- TiO_2 domains for methanol oxidation to formaldehyde (redox sites) or dimethyl ether (acidic sites), no investigation has systematically examined the influence of the oxide substrate dimension, in the critical $\sim 0.5\text{-}10$ nm region, upon the resultant catalytic properties of active bifunctional catalysts. As such, a unique nanotechnology research opportunity currently exists to investigate and explore the fundamental science of tuning the electronic and molecular structures of bifunctional supported catalytic active sites for enhanced catalytic performance with nanostructured oxide substrate domains. Thus, the main research objectives of this study are (1) the

rational design of bifunctional catalytic materials (2) developing next generation bifunctional metal oxides catalysts for enhanced performance by molecularly tuning their catalytic active sites (3) understanding the fundamental catalysis of complex reactions (NO/NH₃-SCR and methanol oxidation to dimethoxymethane) requiring dual redox-acid functionalities. In accomplishing this objective, relationships between the molecular structures and catalytic activity/selectivity will be established. The general scheme for the present research is outlined as follows:

Chapter 1: Tuning Catalytic Active Sites

This chapter introduces the concepts of rational catalyst design of metal oxides throughout the heterogeneous catalysis literature and establishes the foundation for the subsequent research.

Chapter 2: Resolving the Contributions of Surface Lewis and Brønsted Acid Sites during NO_x/NH₃ SCR by Model Supported V₂O₅-WO₃/TiO₂/SiO₂ Catalysts: An Operando TP-IR Spectroscopic Investigation

This chapter addresses a 30-year old issue that has been a source of confusion in the catalysis literature up until now. The state-of-the-art spectroscopic experiments employed have provided new insights and clarity to this unresolved problem.

Chapter 3: Fundamental Mechanistic Insights into the Selective Oxidation of CH₃OH to H₂C(OCH₃)₂ over Bifunctional Supported V₂O₅-WO₃/TiO₂/SiO₂ Catalysts

This chapter critically investigates the mechanism of methanol oxidation to dimethoxymethane over a supported bifunctional catalyst with dual redox-acid catalytic active sites. The mechanism has been investigated using cutting edge in situ molecular spectroscopies with corresponding steady state experiments to investigate the reaction kinetics.

Chapter 4: Catalyst by Design: Tuning the Selective Oxidation of CH₃OH to H₂C(OCH₃)₂ over Supported V₂O₅-WO₃/TiO₂/SiO₂ with TiO₂ Nanoligands

This chapter expands upon the ideas presented in Chapter 3, and details the rational design of a series of metal oxide catalysts that are molecularly designed with bifunctional redox-acidic catalytic active sites. The ability to tune the multiple active sites with TiO₂ nanoligands has been demonstrated by selectively oxidizing methanol to dimethoxymethane.

Chapter 5: Conclusions and Proposed Future Studies

References

1. E. Iglesia, D.G. Barton, J.A. Biscardi, M.J.L. Gines, S.L. Soled, *Catal. Today* **38** (1997) 339
2. J.J. Spivey, M.R.Gogate, J.R. Zoeller, R.D. Colberg, *Ind. Eng. Chem. Res.* **36** (1997) 4600
3. K. Tanabe, W.F. Holderich, *Appl. Catal. A: General* **181** (1999) 399
4. J.D. Bass, S.L. Anderson, A. Katz, *Angew.Chem.Int.Ed.* **42** (2003) 5219
5. J.D. Bass, A. Solovyov, A.J. Pascall, A. Katz, *J. Am. Chem. Soc.* **128** (2006) 3737
6. T. Setoyama, *Catal. Today* **116** (2006) 250
7. S. Delsarte, M. Florea, F. Mauge, P. Grange, *Catal. Today* **116** (2006) 216
8. K. Ebitani, K. Motokura, K. Mori, T. Mizugaki, K. Kaneda, *J. Org. Chem* **71** (2006) 5440
9. R. Zeidan, M.E. Davis, *J. Catal.* **247** (2007) 379
10. G. Jiang, L. Zhang, Z. Zhao, X. Zhou, A. Duan, C. Xu, J. Gao, *Appl. Catal. A: General* **340** (2008) 176
11. K. Motokura, M. Tada, Y. Iwasawa, *Catal. Today* **147** (2009) 203
12. K. Motokura, N. Viswanadham, G. M. Dhar, Y. Iwasawa, *Catal. Today* **141** (2009) 19
13. A. El Kadib, K. Molvinger, M. Bousmina, D. Brunel, *Org. Lett.*, **12** (2010) 948

14. R. Arrigo, M. Havecker, S. Wrabetz, R. Blume, M. Lerch, J. McGregor, E.P.J. Parrott, J.A. Zeitler, L.F. Gladden, A. Knop-Gericke, R. Schlögl, D. S. Su, *J. Am. Chem. Soc.* **132** (2010) 9616
15. N. Kondamudi, S. K. Mohapatra, M. Misra, *Appl. Catal. A: General* **393** (2011) 36
16. I.E. Wachs, G. Deo, D.S. Kim, M.A. Vuurman, H. Hu, *Studies in Surface Science and Catalysis* **75** (1993) 543
17. I.E. Wachs, G. Deo, M.A. Vuurman, H. Hu, D.S. Kim, J.-M. Jehng, *J. Mol. Catal.* **82** (1993) 443
18. M.A. Banares, H. Hu, I.E. Wachs, *J. Catal.* **150** (1994) 407
19. H. Hu, I.E. Wachs, *J. Phys. Chem.* **99** (1995) 10911
20. I.E. Wachs, *Colloids and Surfaces* **105** (1995) 143
21. N. Soultanidis, W. Zhou, A.C. Psarras, A.J. Gonzalez, E.F. Lliopoulou, C.J. Kiely, I.E. Wachs, M.S. Wong, *J. Am. Chem. Soc.* **132** (2010) 13462
22. D.S. Kim, I.E. Wachs, K. Segawa, *J. Catal.* **146** (1994) 268
23. E.I. Ross-Medgaarden, I.E. Wachs, W.V. Knowles, A. Burrows, C.J. Kiely, M.S. Wong, *J. Am. Chem. Soc.* **131** (2009) 680
24. G. Deo, I.E. Wachs, *J. Catal.* **146** (1994) 335
25. R. Gounder, E. Iglesia, *J. Am. Chem. Soc.* **131** (2009) 1958
26. F. Cavani, *Catal. Today* **41**(1998) 73
27. A.P. Wight and M.E. Davis, *Chem. Rev.* **102** (2002) 3589

28. J.M. Thomas, *J. Mol. Catal. A: Chemical* **146** (1999) 77
29. J.M. Thomas, *Angew. Chem. Int. Ed.* **38** (1999) 3588
30. J-M. Jehng, W-C. Tung, C-H. Huang, I.E. Wachs, *Microporous and Mesoporous Mat.* **99** (2007) 299
31. X. Gao, I.E. Wachs, M.S. Wong, J.Y. Ying, *J. Catal.* **203** (2001) 18
32. L. Saikia, D. Srinivas, *Catal. Today* **141** (2009) 66
33. L. L. Nakka, J.E. Molinari, I.E. Wachs, *J. Am. Chem. Soc.* **131** (2009) 15544
34. I.E. Wachs, *Catal. Today* **100** (2005) 79
35. X. Gao, S.R. Bare, J.L.G. Fierro, M.A. Banares, I.E. Wachs, *J. Phys. Chem. B* **102** (1998) 5653
36. X. Gao, S.R. Bare, J.L.G. Fierro, I.E. Wachs, *J. Phys. Chem. B* **103** (1999) 618
37. X. Gao, J.L.G. Fierro, I.E. Wachs, *Langmuir* **15** (1999) 3169
38. X. Gao, I.E. Wachs, *J. Catal.* **192** (2000) 18
39. X. Gao, I.E. Wachs, *Topics Catal.* **18** (2002) 243
40. E.I. Ross-Medgaarden, W.V. Knowles, T. Kim, M.S. Wong, W.Zhou, C.J. Kiely, I.E. Wachs, *J. Catal.* **256** (2008) 108
41. E. L. Lee, I.E. Wachs, *J. Catal.* **258** (2008) 103
42. E. L. Lee, I.E. Wachs, *J. Phys. Chem. C.* **112** (2008) 20418

43. M. Boudart, *Kinetics of Catalytic Processes*. Princeton: Princeton University Press, 1984.
44. G. C. Bond and D. T. Thompson, *Catal. Rev.-Sci. Eng.* **41** (1999) 319
45. Q. Fu, H. Saltsburg, and M. Flytzani-Stephanopoulos, *Science* **301** (2003) 935
46. R. J. Davis, *Science* **301** (2003) 926
47. M. Jacoby, *Chem. & Eng. News*, Aug. 30 2004.
48. G. Deo and I. E. Wachs, *J. Catal.* **129** (1991) 307
49. A. Khodakov, B. Olthof, A. T. Bell, and E. Iglesia, *J. Catal.* **181** (1999) 205
50. J. Macht, C. D. Baertsch, M. May-Lozano, S. L. Soled, Y. Wong, and E. Iglesia, *J. Catal.* **227** (2004) 479
51. R.S. Weber, *J. Catal.* **151** (1995) 470
52. M. Fernandez-Garcia, A. Martinez-Arias, J. C. Hanson, and J. A. Rodriguez, *Chem. Rev.* **104** (2004) 4063
53. H. Liu, P. Cheung, and E. Iglesia, *J. Catal.* **217** (2003) 222
54. M. S. Chen and D. W. Goodman, *Science* **306** (2004) 252
55. R.A. Van Santen, *Chem. Eng. Science* **50** (1995) 4027
56. T. Okuhara, *Catal. Today* **73** (2002) 167
57. J. Macht, C.D. Baertsch, M. May-Lozano, S.L. Soled, Y. Wang, E. Iglesia, *J. Catal.* **227** (2004) 479
58. I.E. Wachs, T. Kim, E.I. Ross, *Catal. Today* **116** (2006) 162

59. T. Kim, A. Burrows, C.J. Kiely, I.E. Wachs, *J. Catal.* **246** (2007) 370
60. H. Benaissa, P.N. Davey, Y.Z. Khimyak, I.V. Kozhevnikov, *J. Catal.* **253** (2008) 244
61. H. Benaissa, P.N. Davey, E.F. Kozhevnikova, I.V. Kozhevnikov, *Appl. Catal. A: General* **351** (2008) 88
62. J.Fang, F. Wang, K. Qian, H. Bao, Z. Jiang, W. Huang, *J. Phys. Chem. C.* **112** (2008) 18150
63. A. Corma, V. Martinez-Soria, E. Schnoefeld, *J. Catal* **192** (2000) 163
64. B.C. Gagea, Y. Lorgouilloux, Y. Altintas, P.A. Jacobs, J.A. Martens, *J. Catal.* **265** (2009) 99
65. K. Shimizu, S.Kontani, S. Yamada, G. Takahashi, T. Nishiyama, A. Satsuma, *Appl. Catal. A: General* **380** (2010) 33
66. V. Crocella, G. Cerrato, G. Magnacca, C. Morterra, F. Cavani, S. Cocchi, S. Passeri, D. Scagliarini, C. Flego, C. Perego, *J. Catal.* **270** (2010) 125
67. S. Van de Vyver, J. Geboers, P.A. Jacobs, B.F. Sels *ChemCatChem* **3** (2011) 82
68. L. E. Briand, G. T. Baronetti, H.J. Thomas, *Appl. Catal. A: General* **256** (2003) 37
69. F.T. Sejidov, Y. Mansoori, N. Goodarzi, *J. Mol. Catal. A: Chem.* **240** (2005) 186

70. R. Weingarten, G.A. Tompsett, W.C. Conner Jr., G.W. Huber, *J. Catal* **279** (2011) 174
71. H. Knözinger and E. Taglauer, "Toward Supported Oxide Catalysts via Solid-Solid Wetting," *Catalysis* **10**, 1-40 (1993).
72. H. Knözinger and E. Taglauer, "Spreading and Wetting," in *Handbook of Heterogeneous Catalysis*, edited by G. Ertl, H. Knözinger, and J. Weitkamp. Weinheim: Wiley-VCH, 1997.
73. H. Knözinger and E. Taglauer, "Spreading and Wetting," in *Preparation of Solid Catalysts*, edited by G. Ertl, H. Knözinger, and J. Weitkamp. Weinheim: Wiley-VCH, 1999.
74. K.M. Parida, S. Mallick, *J. Mol. Catal. A: Chemical* **279** (2008) 104
75. H. Liu, E. Iglesia, *J. Phys. Chem. B* **107** (2003) 10840
76. Q. Sun, D. Fang, S. Wang, J. Shen, A. Auroux, *Appl. Catal. A: General* **327** (2007) 218
77. Q. Zhang, Y. Tan, C. Yang, Y. Han, *J. Mol. Catal. A: Chemical* **263** (2007) 149
78. Q. Sun , Y. Fu, J. Liu, A. Auroux, J. Shen, *Appl. Catal. A: General* **334** (2008) 26
79. H. Zhao, S. Bennici, J. Shen, A. Auroux, *Appl. Catal. A: General* **356** (2009) 121
80. H. Zhao, S. Bennici, J. Shen, A. Auroux, *J. Catal.* **272** (2010) 176

81. X. Lu, Z. Qin, M. Dong, H. Zhu, G. Wang, Y. Zhao, W. Fan, J. Wang, *Fuel* (2011) doi: 10.1016/j.fuel.2011.01.007
82. J.M. Thomas, R. Raja, D.W. Lewis, *Angew. Chem. Int. Ed.* **44** (2005) 6456
83. J.M. Thomas, R. Raja, *Proc. Natl. Acad. Sci.* **102** (2005) 13732
84. I.E. Wachs, G. Deo, B.M. Weckhuysen, A. Andreini, M.A. Vuurman, M. de Boer, M.D. Amiridis, *J. Catal.* **161** (1996) 211
85. M.D. Amiridis, I.E. Wachs, G. Deo, J.M. Jehng, D.S. Kim, *J. Catal.* **161** (1996) 247
86. M. Baca, M. Aouine, J.L. Dubois, J.M.M. Millet, *J. Catal.* **233** (2005) 234
87. R. Lopez-Medina, H. Golinska, M. Ziolek, M.O. Guerrero-Perez, M.A. Banares, *Catal. Today* **158** (2010) 139
88. M.O. Guerrero-Perez, M.V. Martinez-Huerta, J.L.G. Fierro, M.A. Banares, *Appl. Catal. A: General* **298** (2006) 1
89. M. O. Guerrero-Perez, T. Kim, M.A. Banares, I.E. Wachs, *J. Phys. Chem. C* **112** (2008) 16858
90. I.E. Wachs, J-M. Jehng, G. Deo, B.M. Weckhuysen, V.V. Guliants, J.B. Benziger, S. Sundaresan, *J. Catal.* **170** (1997) 75
91. R. Van Grieken, G. Ovejero, D.P. Serrano, M.A. Uguina, J. Melero, *Ind. Eng. Chem. Res* **37** (1998) 4215
92. N. Dimitratos, J.C. Vadrine, *Catal. Today* **81** (2003) 561
93. X. Wang, I.E. Wachs, *Catal. Today* **96** (2004) 211

94. M.D. Amiridis, R.V. Duevel, I.E. Wachs, *App. Catal. B: Env.* **20** (1999)

111

FIGURES

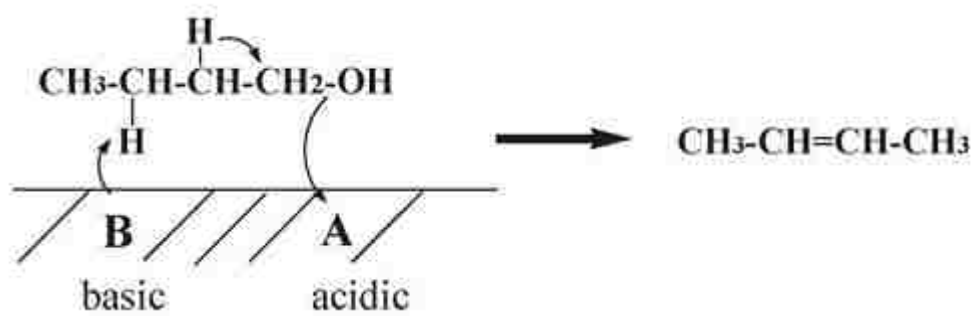


Figure 1.1. Dehydration of n-butanol via “concerted mechanism [6].

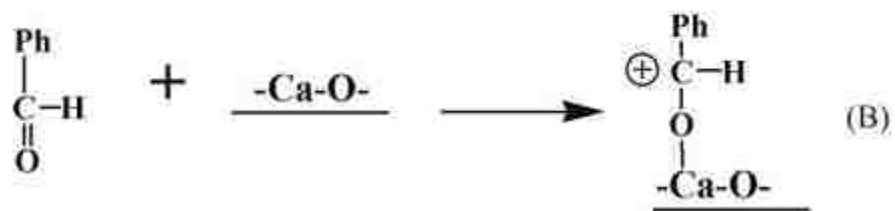
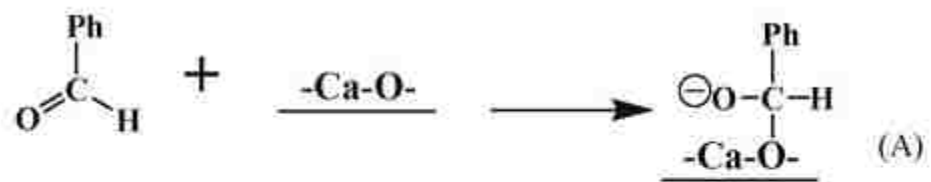


Figure 1.2. Initial step of Knoevenagel condensation of benzaldehyde [6].

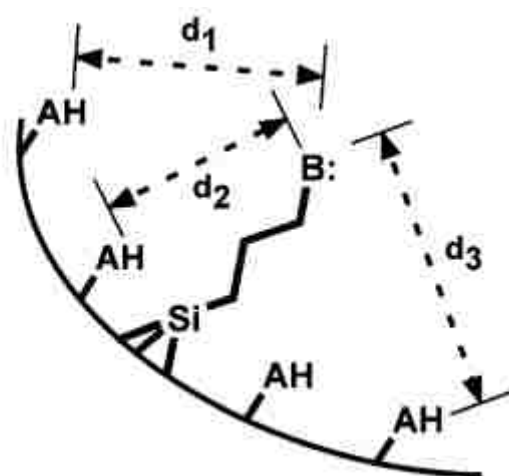


Figure 1.3. The silica surface as a macroscopic ligand providing a range of acid-base distances for bifunctional cooperativity [5].

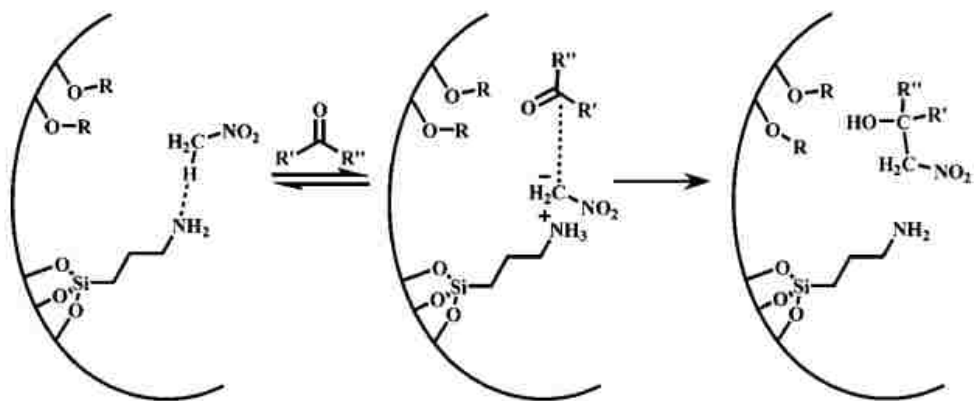


Figure 1.4. Ion-pair mechanism of catalysis by amine-functionalized silica for the production of β -nitro alcohol product in the Henry reaction [5].

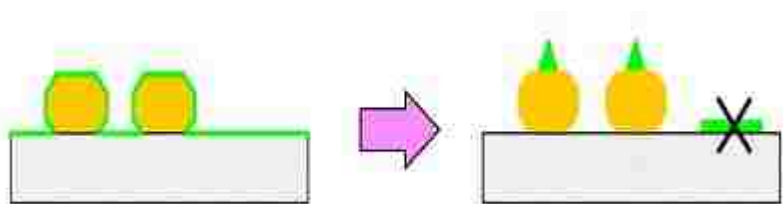


Figure 1.5. Bilayered metal oxide catalysts with the active metal oxide species (green triangle), M_1O_x , self assembled to M_2O_x , that is anchored to an inert surface [23].

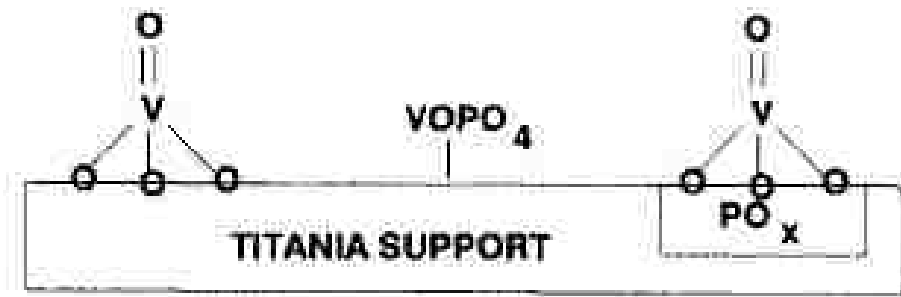


Figure 1.6. Model of interacting additives (phosphorous) with the surface vanadium oxide species on titania [24].

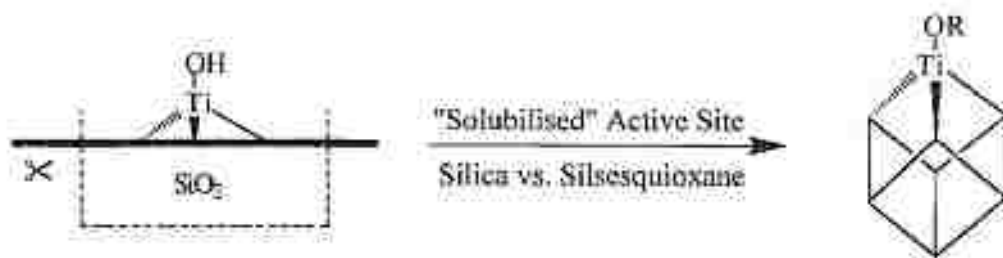


Figure 1.7. EXAFS analysis shows that the Ti(IV)-centered active site in the epoxidation catalyst (Ti/SiO₂) is a tripodally attached titanol group (left), which is akin to a titanosilsesquioxane species (right) [28]

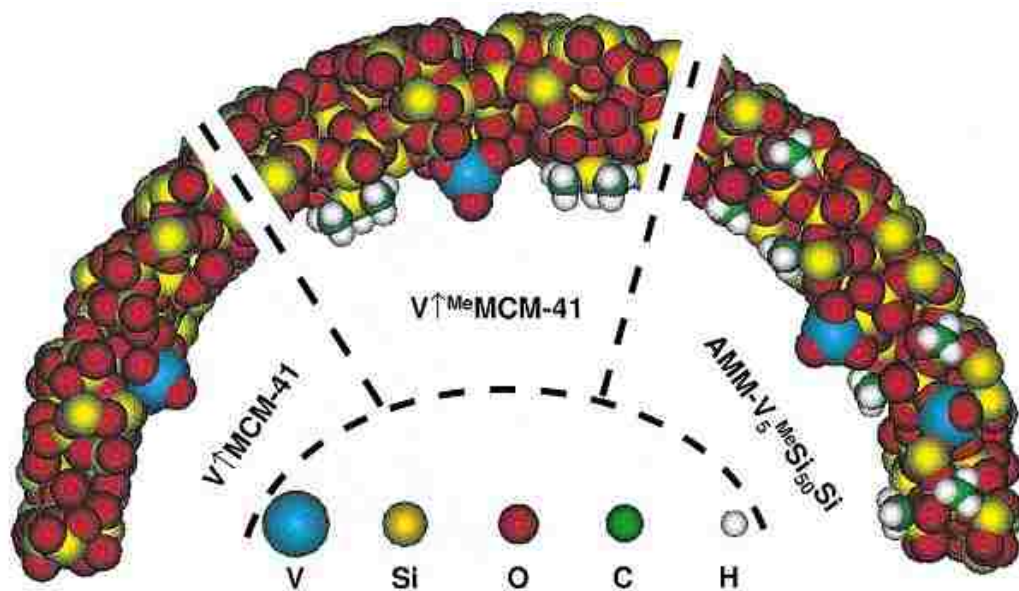


Figure 1.8. A vanadyl active site: (a) grafted on to MCM-41 (left), (b) surrounded by nearby surface methyl groups (center), and (c) in a vanadium-rich AMMO microporous solid [28]

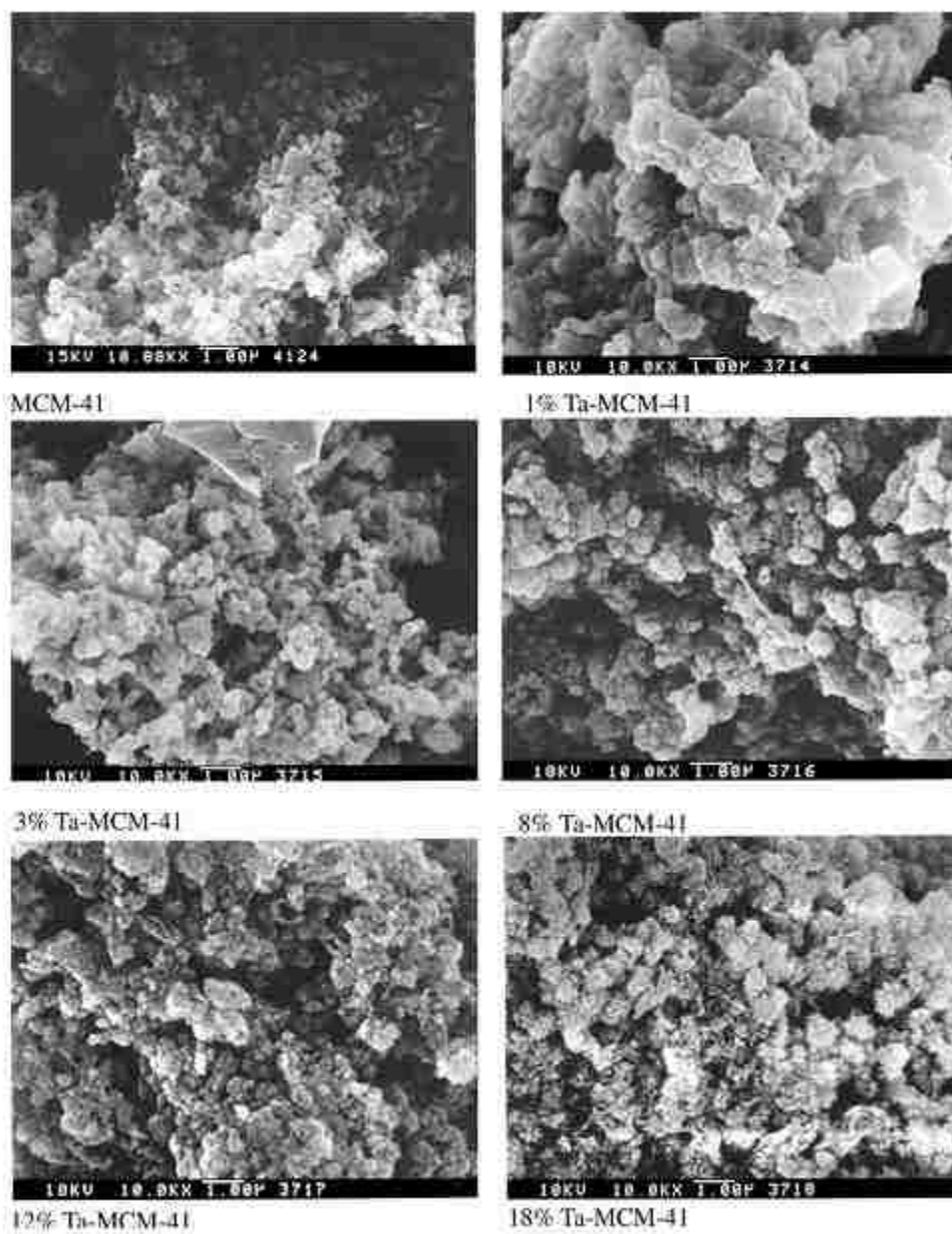


Figure 1.9. SEM images of the MCM-41 and Ta-MCM-41 catalysts [30]

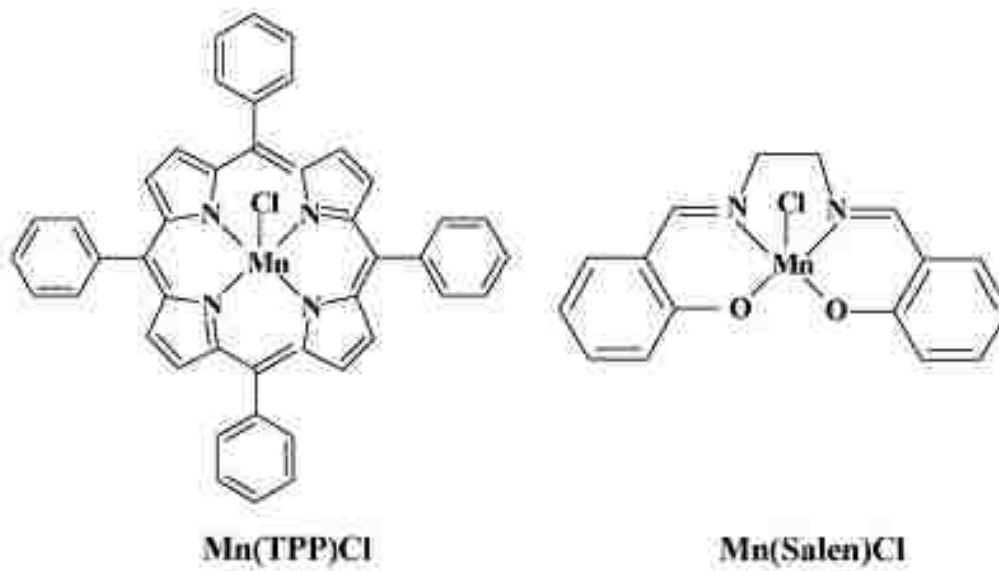


Figure 1.10. Molecular structure of the grafted Mn complexes [32]

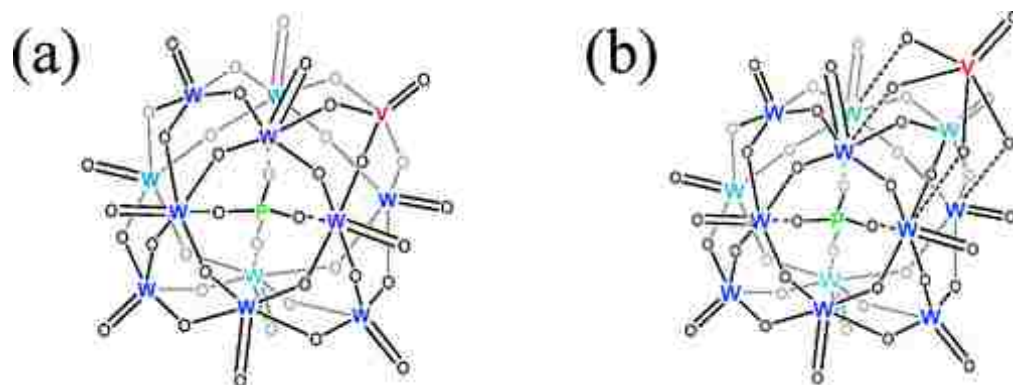


Figure 1.11. Polyoxometallate (POM) vanadium tungstate ($H_{3+x}PW_{12-x}V_xO_{40}$ with $x = 0-3$) Keggin NPs (a) VO_x into the Keggin structure (b) $VO_x/H_3PW_{12}O_{40}$ on the surface of the Keggin catalyst [33]

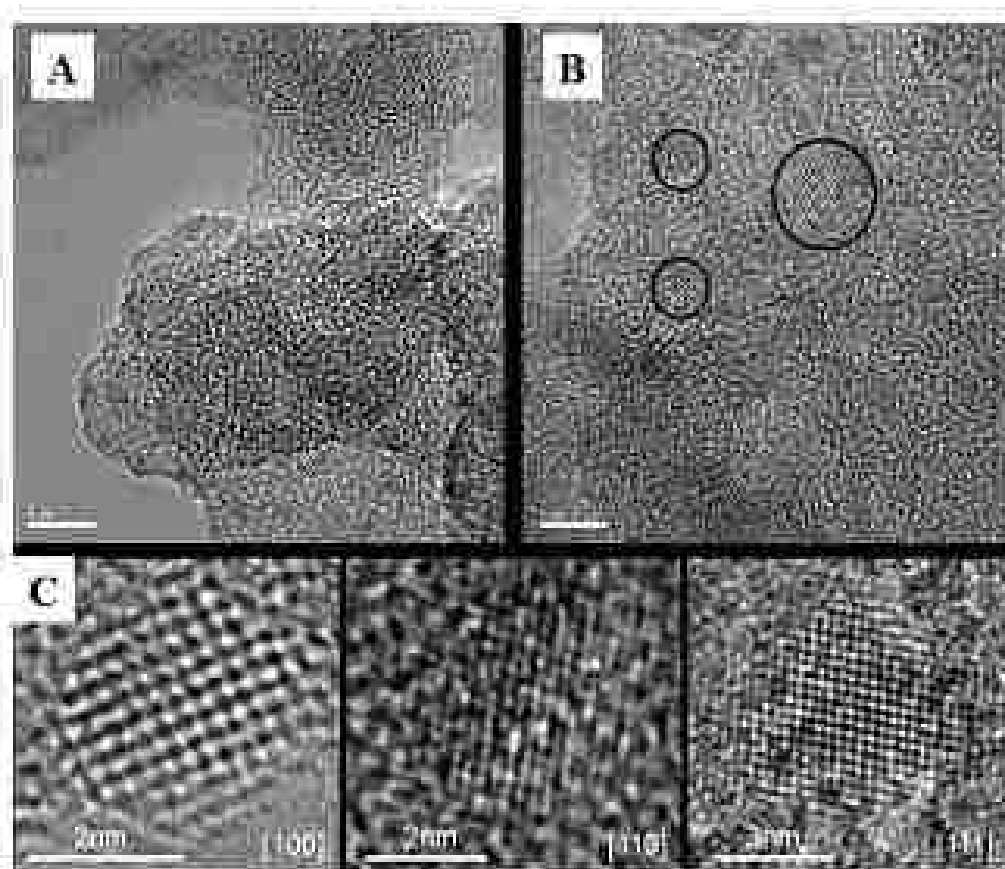


Figure 1.12. Representative HR-TEM images of $\text{TiO}_2/\text{SiO}_2$ containing [A] 12 wt% TiO_2 and [B] 30 wt% TiO_2 with circles highlighting the crystalline TiO_2 (anatase) NPs [C] nanoscale raftlike TiO_2 domains on the SiO_2 support, exhibiting fringe structures that are consistent with [100], [110], and [111] projections of the anatase phase [23].

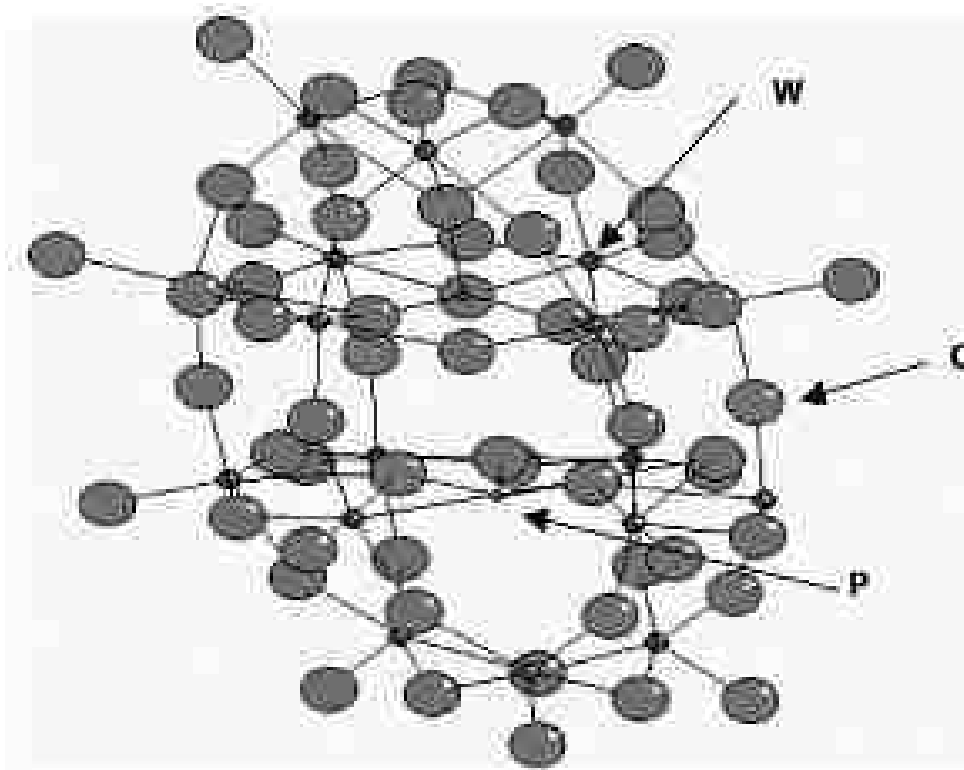


Figure 1.13. Structure of the phosphor-tungstic Wells-Dawson heteropolyoxo-anion $P_2W_{18}O_{62}^{6-}$. W: tungsten, P: phosphorous and O: oxygen atoms. [68]

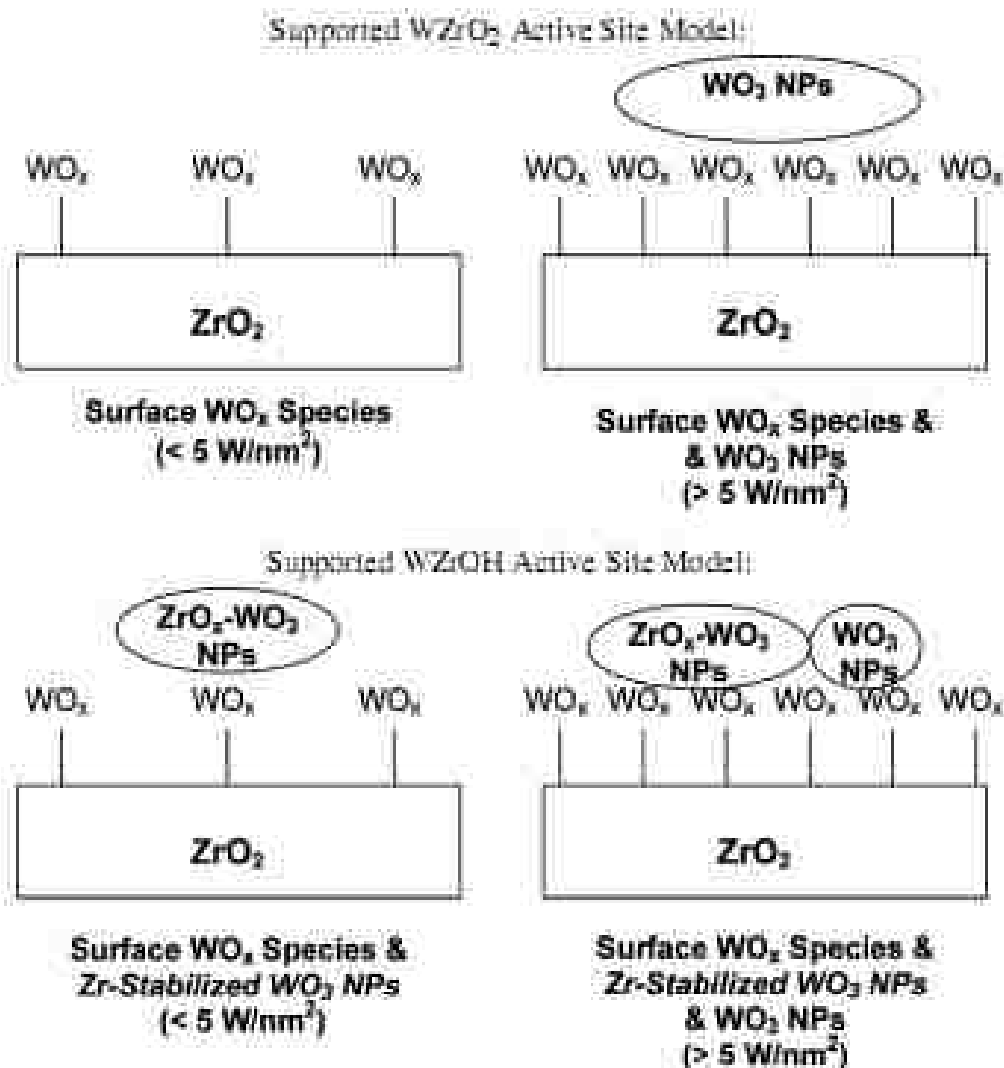


Figure 1.14. Proposed Catalytic Active Sites Present in Supported WO₃/ZrO₂ Catalysts. Surface WO_x Species Represents Monotungstate and Polytungstate Surface O=W(-O)₄ Species, with the latter predominating above low surface WO_x coverage [40].

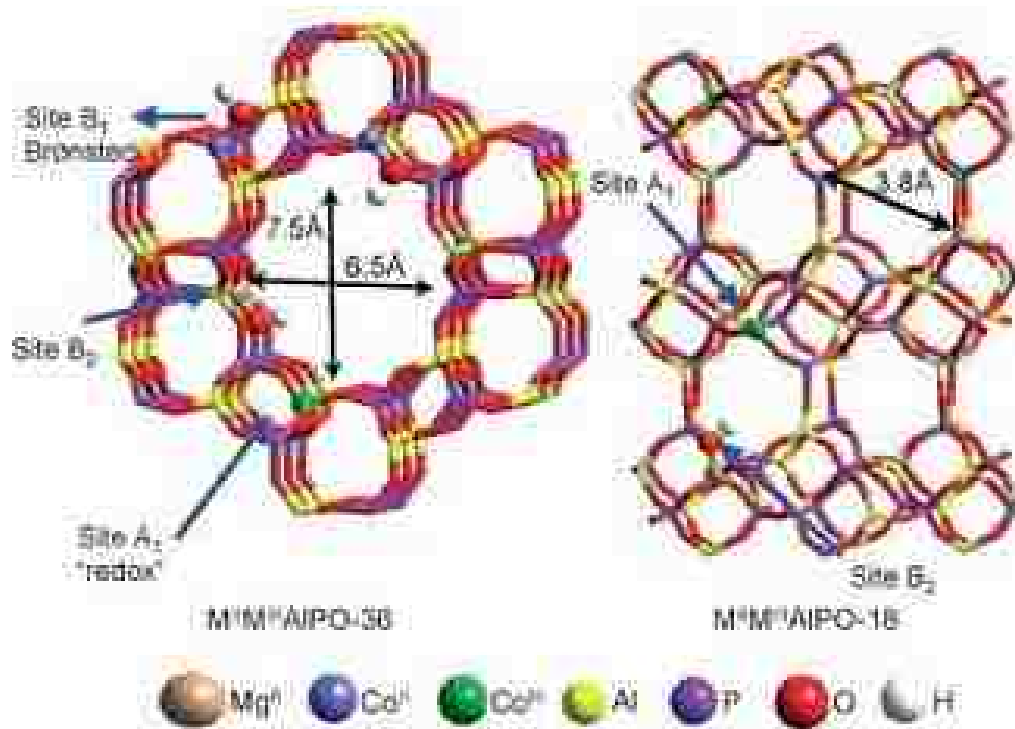


Figure 1.15. In $M^{II}M^{III} AlPO-36$ ($M=Co, Mn$), the framework M^{III} ions are the redox-active centers (A_1), whereas the $M^{II}OH$ ions that have ionizable O-H bonds are the Brønsted (B_1) acid sites. Mg^{II} ions in the framework also have neighboring ionizable OH ions (the B_2 sites). Right: In $M^{III}AlPO-18$ all the framework M^{III} ions are again redox active centers: there are no Co^{II} (or Mn^{II}) framework sites. Mg^{II} framework ions again have neighboring (B_2) Brønsted sites [82]

Chapter 2

Resolving the Contributions of Surface Lewis and Brønsted Acid Sites during SCR of NO_x with NH₃ by Model Supported V₂O₅-WO₃/TiO₂/SiO₂ Catalysts: An *Operando* TP-IR Spectroscopic Investigation

ABSTRACT

A model supported V₂O₅-WO₃/TiO₂/SiO₂ catalyst was used to study the selective catalytic reduction of NO_x with NH₃. An *operando* steady state and temperature programmed-IR spectroscopy investigation (FT-IR analysis of the surface NH₃* and NH₄⁺ species with simultaneous IR and MS analysis of the gas phase products) was used to understand the relative contributions of the surface Lewis and Brønsted acid sites under reaction conditions. The *in situ* surface and gas phase IR spectra for NH₃ chemisorption on the supported V₂O₅-WO₃/TiO₂/SiO₂ catalyst were collected during NH₃ adsorption at 150°C while simultaneously monitoring the gas phase species by mass spectrometry (MS). Subsequent surface and gas phase IR spectra were collected during the surface reaction between gas phase NO/O₂ and adsorbed NH₃ while simultaneously monitoring the gas phase species by MS during the temperature ramp to 400°C (5°C/minute). The study revealed that in the lower SCR reaction temperature regime of ~200-250°C, the surface NH₄⁺ species on Brønsted acid sites are preferentially consumed and some surface NH₃* species on Lewis acid sites are converted to surface NH₄⁺ species in the presence of

moisture. In the intermediate temperature regime of $\sim 250\text{-}320^\circ\text{C}$, both surface NH_x species are consumed in the production of N_2 . At the highest temperature regime of $\sim 350\text{-}400^\circ\text{C}$, the surface NH_3 species are predominantly responsible for N_2 formation. Steady state *operando*-IR-MS SCR experiments showed that at the low temperature regime (250°C), both surface NH_3^* and NH_4^+ react to form the SCR products. With an increase in temperature, the NH_4^+ species markedly decreased, and at the highest temperature (350°C), coordinated NH_3^* were largely responsible for the SCR activity.

The combined *operando* IR-MS spectroscopy experiments were able to distinguish between the different reactivities of the surface NH_4^+ species on Brønsted acid sites and the surface NH_3^* species on Lewis acid sites during the SCR reaction, and revealed the higher reactivity of Brønsted acid surface sites.

1. INTRODUCTION

The selective catalytic reduction (SCR) of environmentally undesirable NO_x by NH_3 to benign N_2 and H_2O represents one of the most important catalytic environmental processes introduced in the 1970s, and is recognized as the best technology for NO_x abatement from stationary sources [1]. The majority of NO_x produced from coal-fired power plants is NO (400-700 ppm) with NO_2 only constituting a trace amount (2-5 ppm) of the flue gas composition [2]. The commonly used catalyst for SCR of NO_x with NH_3 is supported $\text{V}_2\text{O}_5/\text{TiO}_2$. The vanadia content is typically kept low ($\leq 1\%$) to minimize the oxidation of SO_2 to

SO₃ and the titania support is usually in the anatase phase [2]. In addition, tungsten oxide is added in much larger amounts (5-10%) to act as both a chemical and structural promoter that accelerates the reaction rate and stabilizes the surface area, respectively [2].

Though the SCR of NO_x with NH₃ process has been studied for over 30 years, there are still fundamental questions that have not been resolved. Particularly, the basic understanding of the relative contributions of the surface Lewis and Brønsted acid sites for the SCR reaction is still being debated. It has been well documented that gas phase NH₃ chemisorbs on the surface of the supported V₂O₅-WO₃/TiO₂ catalyst to form molecular surface NH₃* on Lewis acid sites and protonated surface NH₄⁺* on Brønsted acid sites. Confusion still persists in the literature, however, about the catalytic roles of the surface NH₃* and NH₄⁺* intermediates. Some researchers claim that that protonated surface NH₄⁺* species on Brønsted acid sites [3–17, 26-29, 32, 33] are the key surface reaction intermediates responsible for reduction of the weakly adsorbed NO to produce N₂ and H₂O, while others claim that molecular surface NH₃* species on Lewis acid sites are the key surface reaction intermediates [18–25, 30] that reduce the weakly adsorbed NO.

Numerous characterization techniques have been used to investigate the NO/NH₃ SCR reaction mechanism, dating back to early reports by Takagi *et al.* [3] and Miyamoto *et al.* [4, 5, 6]. Significant advances have been made in molecular-

based spectroscopic techniques over the past four decades since these early studies that now allow for a more detailed level of characterization. In depth investigations by Topsøe *et al.* [7, 8, 10, 13-15] employing *in situ* FT-IR spectroscopy with on-line activity studies proposed that ammonia adsorption on Lewis acid sites (NH_3^*) is stronger than on Brønsted acid sites (NH_4^{+*}) and, consequently, the ammonia adsorbed on Brønsted acid sites is the active species during the SCR reaction of NO_x with NH_3 . In the studies undertaken by Chen *et al.*, [9] TGA, XPS and IR analyses after the SCR reaction, it was suggested that the SCR reaction initiates on Brønsted acid sites. This conclusion was based on the differences in XPS intensities of TiO_2 compared to $\text{SO}_4^{-2}/\text{TiO}_2$ after the SCR reaction under ambient conditions. However, only $\text{SO}_4^{-2}/\text{TiO}_2$ catalysts were investigated and not the active $\text{V}_2\text{O}_5/\text{TiO}_2$ based catalyst used industrially. Kantcheva *et al.* [11] performed NO_2 - NH_3 adsorption studies with IR spectroscopy under vacuum and demonstrated that surface NH_3^* species bound to Lewis acid sites is selectively displaced by NO_2 . While these observations are quite insightful, NO_2 constitutes a trace amount of the flue gas from stationary sources and, thus, only shed light on a small part of the issue. Wachs *et al.* [16] examined the SCR reaction of NO with NH_3 over supported vanadia catalysts and the influence of vanadia coverage, promoters (tungsten oxide, niobium oxide and sulfate species), and various oxide supports (TiO_2 , Al_2O_3 and SiO_2). Employing Raman spectroscopy, FT-IR with pyridine adsorption to probe Lewis and Brønsted acid sites, and steady-state SCR reactivity

studies with an online MS, it was concluded that surface NH_4^{+*} species on Brønsted acid sites are more active than surface NH_3^+ species during the SCR reaction. This conclusion was further supported with studies [17a] under reaction conditions in the presence and absence of H_2O and SO_2 that are also typically present in flue gas streams. Amiridis *et al* [17b] further examined the effect of multiple promoters on supported $\text{V}_2\text{O}_5/\text{TiO}_2$ catalysts and demonstrated that the SCR activity correlates with the number of Brønsted acid sites ($\text{WO}_3 > \text{MoO}_3 > \text{Nb}_2\text{O}_5 > \text{GeO}_2 > \text{V}_2\text{O}_5 > \text{Fe}_2\text{O}_3 > \text{CeO}_2 > \text{MnO}_2 > \text{SnO}_2 > \text{Ga}_2\text{O}_3 > \text{La}_2\text{O}_3 > \text{ZnO}$). In contrast, a number of researchers have proposed that surface NH_3^* species on Lewis acid sites are the active species involved in the SCR reaction of NO_x with NH_3 . Ramis *et al.* [18, 21] and Busca *et al.* [22, 25] utilized FT-IR spectroscopy in vacuum to investigate the thermal stability when NH_3 was adsorbed at room temperature and observed the FT-IR spectral changes upon increasing the temperature to 250°C . Their results led them to conclude that surface ammonium ions (NH_4^{+*}) formed by ammonia protonation over Brønsted acid sites are much less stable than molecularly coordinated surface ammonia (NH_3^*). Likewise, Lietti *et al.* [19, 20] applied FT-IR spectroscopy in vacuum over a titania-supported vanadia catalyst to examine the reactivity of adsorbed ammonia with NO, by reacting NO with adsorbed NH_3 at room temperature and increasing the temperature to 250°C , and noted a progressive decrease of surface NH_3^* species (1600 and $1300\text{--}1100\text{ cm}^{-1}$) while surface NH_4^{+*} species (1450 cm^{-1}) first grew and then decreased

slowly. Based on these observations, it was concluded that molecular surface NH_3^* bound to Lewis acid sites are the active species during the SCR reaction. More recent studies by Parvulescu *et al.* [24] (involving adsorbing NH_3 at room temperature for 30 minutes, increasing the temperature under helium flow and recording the corresponding *in situ* FT-IR spectra at 100, 250 and 300°C) concluded that NH_3 adsorbs on both Brønsted and Lewis sites and that at high temperatures (300°C) there is almost complete disappearance of the surface NH_4^{+*} species while those associated with surface NH_3^* species were still present. These studies, however, were conducted at conditions very far from actual SCR conditions and their findings needed to be extrapolated in order to infer what the contributions of the surface ammonia species would be under actual SCR reaction conditions.

Kinetic studies on the NH_3 -SCR process over supported $\text{V}_2\text{O}_5/\text{TiO}_2$ catalysts have also been widely studied in order to build a mechanistic and kinetic understanding. Topsøe *et al.* [14] were able to convincingly demonstrate a catalytic cycle consisting of the adsorption and activation of ammonia on a Brønsted acid site, the reaction of the surface NH_4^{+*} species with gaseous or weakly adsorbed NO, and the reoxidation of the active surface vanadia site by gaseous molecular O_2 . Amiridis *et al.* [17] corroborated the conclusions by Topsøe *et al.* by providing insightful kinetic conclusions under industrially relevant conditions, looking at the effect of promoters, H_2O and SO_2 . Using *in situ* Raman

and IR spectroscopy, H₂O was found to competitively adsorb on vanadia sites with ammonia and, thus, decrease the SCR turnover frequency. Dumesic *et al.* [15] provided supporting evidence of this conclusion in a separate study. The effect of SO₂ however, was found to have the opposite effect [17], and in the presence of H₂O increased the SCR rate, by increasing the number of available sites for the adsorption and activation of ammonia.

A number of theoretical studies have more recently been undertaken to gain a better fundamental understanding of the SCR NO/NH₃ reaction over bulk V₂O₅, where the quantum chemical computations have been performed largely using density functional theory (DFT). Experimental results have suggested that the V₂O₅ (010) surface is the most active surface during NO-NH₃ SCR and, as such, has been predominantly used as the catalytic surface of choice to investigate the SCR reaction by theoreticians. These theoretical studies, however, have not resolved the issues surrounding the SCR NO/NH₃ reaction because they employed different structures for the catalytic active sites and computational methods. The V₂O₅ (010) surface has been modeled numerous ways (V₂O₉H cluster [26, 27], periodic slab of the bulk V₂O₅ (010) surface [28], V₄O₁₆H₁₂ cluster [29], V₂O₉H₈ cluster [32], and V₆O₂₀H₁₀ cluster [33]) with DFT and applying the finite cluster approximation to an infinite surface of a substrate [27]. The computational investigations with unsupported VO_x clusters concluded that ammonia adsorbed on Brønsted sites as surface NH₄^{+*} species is more energetically favored than surface

NH_3^* species to reduce adsorbed NO. Unfortunately, these simulations neglected the interaction of the surface VO_x species with the TiO_2 support that is known to be critical for the performance of the SCR NO- NH_3 reaction. In attempts to perform more accurate total energy calculations, Vittadini *et al.* [31] coupled DFT and periodic slab models to search for reaction pathways. The supported $\text{V}_2\text{O}_5/\text{TiO}_2$ catalyst was modeled assuming that the TiO_2 (anatase) support exposed the (101) surfaces and minority hydroxylated (001) surfaces onto which isolated VO_x species were grafted. The calculations found that the reaction paths involving the surface NH_4^{+*} on Brønsted acid sites and surface NH_3^* on Lewis acid sites proceed with similar energy barriers. On the contrary, Jug *et al.* [30] derived a detailed mechanism of the SCR process assuming ammonia adsorbs at a V atom as Lewis acid center and using a semi-empirical MSINDO calculation on a V_2O_7 species bound to the anatase (100) surface that is modeled by small $\text{V}_2\text{O}_7\text{H}_4\text{Ti}_{133}\text{O}_{66}(\text{H}_2\text{O})_{17}$ and large $\text{V}_2\text{O}_7\text{H}_4\text{Ti}_{132}\text{O}_{264}(\text{H}_2\text{O})_{48}$ clusters, respectively. However, the analysis by Jug *et al.* [30], was incomplete since the calculations never compared the energy barrier of ammonia adsorbing on a Brønsted acid site, but instead took the experimental conclusions of Ramis *et al.* [18] of ammonia adsorbing on a Lewis acid site as their starting point. Thus, more realistic DFT calculation studies still need to be performed for the NO- NH_3 SCR reaction.

The objective of this investigation is to design experiments that would be able to resolve this long standing debate on the contributions of surface NH_3^* on

Lewis acid sites and surface NH_4^{+*} on Brønsted acid sites during the SCR NO/NH_3 reaction over supported $\text{V}_2\text{O}_5\text{-WO}_3/\text{TiO}_2$ catalysts. The approach undertaken in the current investigation involves real-time *in situ* FT-IR spectroscopy of the surface NH_3^* and NH_4^{+*} species under reaction conditions with simultaneous IR/MS analysis of the gas phase products (referred to as *operando* spectroscopy in the recent catalysis literature [53]). Model supported 1% $\text{V}_2\text{O}_5\text{-5%WO}_3/\text{TiO}_2(\text{anatase})/\text{SiO}_2$ catalysts were investigated under steady-state, and temperature programmed reaction conditions with the aid of transient isotopic labeling of ammonia to obtain mechanistic insights into the SCR NO/NH_3 reaction. These unprecedented, designed experiments have provided the molecular level insights that have finally resolved the long standing debate in the literature about the contributions of surface Brønsted and Lewis acid sites during the NO-NH_3 SCR reaction over supported $\text{V}_2\text{O}_5\text{-WO}_3/\text{TiO}_2/\text{SiO}_2$ catalysts.

2. EXPERIMENTAL

2.1. Catalyst Synthesis

2.1.1. Preparation of Supported $\text{TiO}_2/\text{SiO}_2$ Catalysts

The synthesis procedure previously described by Ross-Medgaarden *et al.* [34] was used to prepare a 30% $\text{TiO}_2/\text{SiO}_2$ support. The silica support material, amorphous SiO_2 (Cabot, Cab-O-Sil fumed silica EH-5, S.A. $\sim 332 \text{ m}^2/\text{g}$), was employed and found to be more easily handled by an initial water pretreatment and calcination at 500°C for 4 h without changing the material properties. The

supported TiO₂/SiO₂ catalysts were prepared by the incipient-wetness impregnation of isopropanol solutions of titanium isopropoxide (Ti(O-Prⁱ)₄, Alfa Aesar, 99.999%). The silica support was initially dried for 2 h at 120°C to remove the physisorbed water prior to catalyst preparation inside a glovebox (Vacuum Atmospheres, Omni-Lab VAC 101965) under a continuously flowing N₂ (Airgas, Ultra High Purity) environment. After impregnation at room temperature, the sample was kept inside the glovebox to dry overnight under flowing N₂. The calcination of the supported TiO₂/SiO₂ sample entailed ramping at 1°C/min to 120°C in flowing N₂ for 2 h, and then subsequently followed by another 1°C/min ramp under flowing air (Airgas, Zero Grade) to 500°C for 4 h. A multi-step preparation procedure was employed to prepare the 30% TiO₂/SiO₂ support, where incremental loadings of 8 wt% TiO₂ were made for each step.

2.1.2. Preparation of Supported WO_x/TiO₂/SiO₂ Catalysts

The supported tungsten oxide catalyst were prepared by the incipient-wetness impregnation of aqueous solutions of ammonium metatungstate, (NH₄)₁₀W₁₂O₄₁·5H₂O (Pfaltz & Bauer, 99.5% purity) on the 30% TiO₂/SiO₂ support. The supported 5% WO₃/30%TiO₂/SiO₂ sample was dried overnight under ambient conditions and subsequently dried in flowing air (Airgas, Zero Grade) at 120°C for 1 h and further calcined in the flowing air at 450°C for 4 h.

2.1.3. Preparation of Supported VO_x-WO_x/TiO₂/SiO₂ Catalysts

The supported vanadium oxide catalysts were prepared by the incipient-

wetness impregnation of isopropanol solutions of vanadium tri-isopropoxide ($\text{VO}[\text{CHO}(\text{CH}_3)_2]_3$, Alfa Aesar, 97%) onto the supported 5% WO_3 /30% TiO_2 /SiO₂ catalyst. The preparation was performed inside a glovebox with continuously flowing N₂ (Airgas, Ultra High Purity) and the 5% WO_3 /30% TiO_2 /SiO₂ catalyst was initially dried at 120°C to remove the physisorbed water before impregnation. After impregnation at room temperature, the samples were kept inside the glovebox under flowing N₂ overnight. The calcination of the supported 1% V₂O₅-5% WO_3 /30% TiO_2 /SiO₂ sample entailed ramping at 1°C/min to 120°C in flowing N₂ for 2 h, and then by another 1°C/min ramp under flowing air (Airgas, Zero Grade) up to 500°C for 4 h.

2.2. Catalyst Characterization

2.2.1. In Situ Raman Spectroscopy

Raman spectroscopy was employed to determine The molecular structures of the supported V₂O₅, WO_3 , TiO_2 and SiO₂ components of the supported 1% V₂O₅-5% WO_3 /30% TiO_2 /SiO₂ catalyst were determined with *in situ* Raman spectroscopy with a visible (532 nm) laser excitation on a The single stage Raman spectrometer (Horiba-Jobin Yvon, Lab Ram-HR) was r equipped with a confocal microscope (Olympus BX-30), a notch filter (Kaiser Super Notch), a Nd-YAG doubled diode pumped laser (Coherent Compass 315M-150; output power of 150 mW with sample power 10 mW), and the scattered photons were detected by a UV-sensitive liquid-N₂ cooled CCD detector (Horiba-Jobin Yvon, CCD-3000V). Laser

excitation was at 532 nm and a spectral resolution of $\sim 2 \text{ cm}^{-1}$ was obtained for the given parameters, with 900 grooves/mm grating. The Raman spectrometer was also equipped with an environmentally-controlled high-temperature cell (Harrick) that examined the catalyst samples in loose powder form ($\sim 5\text{-}10 \text{ mg}$) that allowed for control of both the catalyst temperature and gaseous composition. *In situ* Raman spectra were collected for the supported $1\% \text{V}_2\text{O}_5\text{-}5\% \text{WO}_3/30\% \text{TiO}_2/\text{SiO}_2$ catalyst under dehydrated conditions (400°C , $10\% \text{O}_2/\text{He}$). The spectral acquisition time employed was 20 scans for 20 seconds/scan for a total of $\sim 7 \text{ min/spectrum}$. System alignment was verified daily using a silica reference standard provided by Horiba-Jobin Yvon.

2.2.2. Operando IR Spectroscopy

2.2.2.1. The reactor system

The *operando* IR spectrometer system, as detailed by Sarria *et al.* [35], consists of glass lines connected to an IR reactor cell. Gases are introduced into the lines (heated at 60°C) by mass flow controllers. Two independent gas mixtures can be simultaneously produced in the system (activation and reactants flow) and then sent to the reactor cell. The system allows the analysis of the reactants and/or the reaction products by quadrupole mass spectrometry (Balzers TCP 121) and FTIR spectroscopy via a gas microcell of 0.088 cm^3 volume. The IR spectra were collected with a Nicolet Magna 750 FT-IR spectrometer equipped with MCT detectors. To ameliorate the signal/noise ratio, 64 scans at a resolution of 4 cm^{-1}

¹were collected resulting in a spectrum per second. The same time resolution is obtained in the case of the QMS analysis and the following m/e ratios were employed for the identification of the multiple gases: NH₃ (m/e = 17,15), NO (m/e = 30), O₂ (m/e = 32), H₂O (m/e = 18,17), N₂ (m/e = 28), ND₃ (m/e=20,18,17), D₂O (m/e=20), Ar (m/e=40, 20)

The IR reactor cell consists of a cylinder of stainless steel carrying a toroidal sample holder in its center, where the catalyst is placed in the form a a self-supported wafer of 10 mg cm⁻². The rest of the space is filled by KBr windows, which limit the dead volume to 0.12 cm³. The heating system guarantees a maximum temperature of 500°C on the sample, while the experiments are carried out at atmospheric pressure. Additional details are given in reference [35].

2.3. Reactivity Studies

2.3.1. Time-Resolved Selective Catalytic Reduction of NO with NH₃

The *in situ* IR spectra of catalyst surface and gas phase MS spectra were simultaneously collected in a flowing reaction environment (350 ppm NH₃ (AirLiquide, Ultra High Purity), 350 ppm NO (AirLiquide, Ultra High Purity), 5% O₂ (AirLiquide, Ultra High Purity), and the remainder Ar (AirLiquide, Ultra High Purity)) over the supported 1%V₂O₅-5%WO₃/30%TiO₂/SiO₂ catalyst at 250°C. After allowing the reaction system to reach steady-state at 250°C, the reactor cell temperature was increased to 350°C in flowing argon. After reaching 350°C, the Ar flow was replaced with the flowing reactive mixture described above. The

simultaneous analysis of the catalyst surface with FT-IR and the gas phase with MS continued throughout the entire procedure.

Isotopic time-resolved experiments were also undertaken at 150, 250 and 350°C. The experimental procedure involved first flowing the standard SCR reaction mixture as detailed above. Once steady-state was reached, the 350 ppm NH_3 within the reactant mixture was switched to 350 ppm ND_3 (1% in Ar, Euroisotop), and allowed to come to a steady state. Finally, a switch back to 350 ppm NH_3 within the mixture was made and again allowed to reach state-state. Simultaneous *in situ* IR spectra (Rapid Scan) of the catalyst surface and gas phase MS spectra were collected during the experiment.

2.3.2. Transient Selective Catalytic Reduction of NO with NH₃

The *in situ* IR spectra of the surface ammonia species during NH_3 chemisorption on the supported 1% V_2O_5 -5% WO_3 /30% TiO_2 /SiO₂ catalyst were collected at 150°C while simultaneously also monitoring the gas phase molecules with a mass spectrometer. Subsequently, *in situ* IR spectra of the catalyst surface and the gas phase with MS were collected during the surface reaction between flowing gas phase NO/O₂ and adsorbed NH_3 during the temperature ramp to 400°C (5°C/minute).

Transient experiments were performed whereby a reactant mixture (350 ppm NH_3 + 350 ppm NO + 5% O₂) was sent to the 1% V_2O_5 -5% WO_3 /30% TiO_2 /SiO₂ catalyst at 250°C for 20 minutes. Within the 20 minute

period, NO was removed from the reactant mixture and reintroduced back into the reactant mixture periodically. The pulsing of NO in and out of the reactant mixture occurred 9 times throughout the 20 minute time interval. Corresponding gas phase data was collected with a MS concurrently while rapid scan FT-IR spectra were being collected of the surface intermediates.

3. Results

3.1. Characteristics of the Model Supported VO_x - WO_x /TiO₂/SiO₂ Catalyst

3.1.1. In Situ Raman Spectroscopy

The *in situ* Raman spectrum of the dehydrated supported 1% V₂O₅-5% WO₃/30% TiO₂/SiO₂ catalyst is presented in Figure 1. The Raman spectrum in the 200-1200 cm⁻¹ region is dominated by the bands of crystalline TiO₂(anatase) at 144, 400, 520 and 643 cm⁻¹ in Figure 1a [38] and the Raman bands associated with crystalline TiO₂(rutile) (142, 445, and 610 cm⁻¹) and crystalline TiO₂(brookite) (242, 320, 363, and 407 cm⁻¹) are not present in Figure 1a [34, 38]. Molecular structural information about the deposited tungsten and vanadium oxide components in the dehydrated supported 1% V₂O₅-5% WO₃/30% TiO₂/SiO₂ catalyst is also contained Figure 1 and is zoomed in for the 700-1200 cm⁻¹ region of Figure 1b. The *in situ* Raman spectrum in Figure 1b reveal that neither crystalline WO₃ (strong bands at 804, 710 and 270 cm⁻¹) [51] or crystalline V₂O₅ (strong band at 995, 690 and 525 cm⁻¹) [52] nanoparticles (NPs) are present in this catalyst. Consequently, both the tungsten oxide and vanadium oxide components are 100%

dispersed as surface WO_x and VO_x species on the 30% $\text{TiO}_2/\text{SiO}_2$ support [36,37]. Complementary information can be appreciated from the dehydrated FT-IR spectrum (Figure S1) in the hydroxyl region. A clear band is evident at 3740 cm^{-1} related to Si-OH [23] in addition to a shoulder at $\sim 3660\text{ cm}^{-1}$ assigned to Ti-OH [13]. The lack of distinct peaks at 3718 , 3669 , and 3644 cm^{-1} indicate the titration of the Ti-OH with vanadia and tungsten surface species, which is agreement with the Raman spectroscopy findings. Similar observations were noted by Topsøe et al [13] for various loadings of $\text{V}_2\text{O}_5/\text{TiO}_2$ catalysts.

3.2. Operando FT-IR Spectroscopy

3.2.1. Time-Resolved SCR of NO/NH₃

The time-resolved *operando* IR-MS spectroscopy SCR NO-NH₃ findings under reaction conditions (350 ppm NH₃, 350 ppm NO; 5% O₂ and Ar balance) are presented in Figure 2. The top portion of Figure 2 contains the gas phase concentration of NH₃ and the bottom portion tracks the relative abundance of molecularly coordinated NH₃* ($\sim 1610\text{ cm}^{-1}$) and protonated NH₄⁺* ($\sim 1420\text{ cm}^{-1}$) on the surface of the model supported 1% V_2O_5 -5% WO_3 /30% $\text{TiO}_2/\text{SiO}_2$ catalyst. As the flowing reactive gas mixture is introduced into the reaction cell at 250°C, the gas phase NH₃ concentration decreases indicating that gas phase NH₃ is chemisorbing on the catalysts surface. This is directly confirmed by the appearance of surface NH₃* and NH₄⁺* species in the corresponding IR spectrum and their IR intensity are plotted in Figure 2. Thus, both surface NH₃* and NH₄⁺ are present on

the catalyst surface during steady-state reaction at 250°C. Upon replacing the reactive mixture flow with an inert Ar flow and raising the reactor temperature to 350°C, the concentration of both surface NH_3^* and NH_4^{+*} species decreases. The concentration of the surface NH_4^{+*} species on Brønsted acid sites, however, markedly decreases while the concentration of surface NH_3^* species on Lewis acid sites only modestly decreases. Replacing the Ar flow with that of the reactive mixture at 350°C, increases the conversion of NH_3 by a factor of 3-4 relative to that at 250°C. The corresponding IR spectra at 350°C of the catalyst surface reveals that at this higher reaction temperature, the concentration of surface NH_4^{+*} species dramatically decreases and the concentration of surface NH_3^* species remains about the same as for the SCR reaction at 250°C.

3.2.2 Isotopic *Time-Resolved SCR of NO-ND₃*

To further probe the contributions of surface NH_3^* on Lewis acid sites and NH_4^{+*} on Brønsted acid sites in the SCR reaction, the gas phase reductant, NH_3 , was switched to isotopically labeled ND_3 in the SCR reaction mixture (350 ppm NH_3 or ND_3 , 350 ppm NO ; 5% O_2 and Ar balance) at 250°C. The gas phase species are tracked with an on-line MS shown in Figure 3 and the surface species are tracked with rapid scan FT-IR spectroscopy during the steady-state isotopic switch during the SCR reaction. The MS signals for the gaseous N_2 product and the gaseous O_2 and NO reactants are constant indicating that steady-state reaction conditions were maintained during the isotopic switch experiments. Due to the

overlapping MS signals, the change in gas phase ND_3 can be difficult to discern. For instance, the overlapping signal with the carrier gas, Ar, prohibits any ND_3 spectral features to be noticed. However, the overlapping signal with NH_3 and H_2O reveals a gradual decrease in their signals after the isotopic switch, indicative of ND_3 consumption. Further evidence is realized in the change in reference level before and after the switch. When switching back to NH_3 from ND_3 , the signal returns to its original reference level. The surface NH_3^* and NH_4^{+*} species are also concurrently tracked with FT-IR spectroscopy as shown in Figure 4. The ammonia isotopic switch reveals that the concentration of surface NH_4^{+*} species decreases more rapidly than the surface NH_3^* species when gas phase NH_3 is replaced with gas phase ND_3 . Upon switching from gaseous ND_3 to gaseous NH_3 , there is a quick decrease in the concentration of the surface NH_3^* and NH_4^{+*} species and they return to their initial reference levels as shown in Figure 5, but the surface NH_3^* species increases at a faster rate compared to the surface NH_4^{+*} species.

3.2.3. Temperature Programmed SCR of NO-NH₃

Chemisorption of ammonia at 150°C on the supported $1\% \text{V}_2\text{O}_5$ - $5\% \text{WO}_3/30\% \text{TiO}_2/\text{SiO}_2$ catalyst gives rise to IR peaks characteristic of both surface NH_3^* species (~ 1610 , 1293 , and 3100 - 3500 cm^{-1}) [22] bound to Lewis acid sites and surface NH_4^+ species (~ 1420 and 2600 - 3000 cm^{-1}) [22] coordinated to Brønsted acid sites, as shown in Figure 6. The concentration of surface NH_3^* (1610 cm^{-1}) and NH_4^{+*} (1425 cm^{-1}) were tracked during TP-IR-MS spectroscopy

while flowing NO, O₂ and Ar over the catalyst. The corresponding gas phase molecules (N₂, H₂O and NO) were simultaneously monitored with an online MS, which is displayed in the top portion of Figure 7. After initially saturating the catalyst surface with chemisorbed ammonia, the catalyst was kept under Ar flow to remove any physically adsorbed ammonia, and the temperature was subsequently ramped at 5°C/min under flowing NO/O₂/Ar. The weak NH stretching vibrations for ammonium coordinated to Brønsted acid sites (2600-3200 cm⁻¹) and ammonia coordinated to Lewis acid sites (3100-3500 cm⁻¹) disappear by ~300°C. The *operando* TP-IR-MS spectroscopy experiment revealed that both adsorbed surface NH₃* and NH₄⁺* are consumed by reaction with gas phase NO on the model supported 1% V₂O₅-5% WO₃/30% TiO₂/SiO₂ catalyst to produce N₂ (T_p~250 and 392°C, respectively). At 300°C, new IR bands begin to appear at ~1946 cm⁻¹, characteristic of an overtone band of the terminal V=O of the surface VO_x species [14], and at ~1822 cm⁻¹, attributed to surface nitrosyl species (vNO) [25,50] (see Figure 6). As shown in Figure 7, between 220 and 320°C the surface NH₄⁺* species are predominantly consumed whereas the surface NH₃* species concentration only moderately decreases. Interestingly, the concentration of surface NH₄⁺* species initially slightly increases at ~240°C by the transformation of some surface NH₃* species to surface NH₄⁺* species due to the presence of moisture from the simultaneous SCR reaction at this temperature. Both types of surface ammonia species are continuously consumed with temperature between

~250-320°C. Above 350°C temperature range, only surface NH_3^* species remain and are, thus, responsible for N_2 formation from the SCR reaction in this temperature range.

3.2.4. Transient NO Pulsing During NH_3 -SCR

The transient experiments were also performed to probe the reactivity of the surface NH_3^* and NH_4^{+*} species by pulsing NO in and out of the SCR reaction mixture. The MS signals of the gas phase molecules during the pulsing experiments are depicted in Figure 8. Corresponding information on the surface intermediates was obtained utilizing FT-IR spectroscopy in rapid scan mode (see Figure 9), which permitted the tracking of dynamical surface changes accurately on the order of milliseconds. The transient results indicate that the Brønsted acid bound surface NH_4^{+*} species are markedly affected by the NO pulses whereas the Lewis bound surface NH_3^* species shows minimal perturbation during the NO pulses.

4. DISCUSSION

4.1 *Molecular Structures and Location of the Dehydrated Surface WO_x and VO_x Active Sites*

For dehydrated supported WO_3/SiO_2 , the primary Raman $\text{W}=\text{O}$ vibration occurs at $\sim 980 \text{ cm}^{-1}$, characteristic of dioxo $(\text{O}=\text{O})_2\text{WO}_2$ surface WO_4 species [34, 40], with a weaker vibration at $\sim 1010 \text{ cm}^{-1}$, associated with mono-oxo surface $\text{O}=\text{WO}_4$ species [36, 40-44]. The Raman spectrum for the dehydrated model

supported 1% V₂O₅-5% WO₃/30% TiO₂/SiO₂ catalyst is dominated by the W=O vibration of the mono-oxo surface WO₅ species at ~1013 cm⁻¹. The position of the Raman band at ~1013 cm⁻¹ also reveals that the surface WO₅ species preferentially coordinate to TiO₂ sites rather than exposed SiO₂ sites since dehydrated supported WO₃/TiO₂ exhibits its W=O vibrations at ~1007-1016 cm⁻¹ [51].

Unlike supported WO_x species that can form either mono-oxo O=WO₄ and dioxo (O=)₂WO₂ surface species, supported VO_x species exclusively form mono-oxo O=VO₃ structures [34, 45-48]. For the dehydrated supported V₂O₅/SiO₂ and V₂O₅/TiO₂ catalysts, the Raman band of the mono-oxo surface O=VO₃ species vibrates at ~1036-1040 cm⁻¹ [45] and at ~1027-1031 cm⁻¹ [49], respectively. The appearance of the V=O vibration for the dehydrated supported 1% V₂O₅-5% WO₃/30% TiO₂/SiO₂ catalyst at ~1031 cm⁻¹ indicates that the surface O=VO₃ species also preferentially coordinate to the TiO₂ sites rather than the exposed SiO₂ sites. Previous *in situ* X-ray absorption near edge spectroscopy (XANES) results also revealed the preferential coordination of the surface VO₄ species to the exposed titania sites [34, 48]. A schematic of the supported 1% V₂O₅-5% WO₃/30% TiO₂/SiO₂ catalyst is shown in Figure 10, with surface VO₄ and WO₅ catalytic active sites shown anchored to the crystalline TiO₂(A) phase.

4.2 Role of Surface NH₃* and NH₄⁺* Reaction Intermediates during NO-NH₃ SCR

Both surface NH₃* and NH₄⁺* species are present on the model supported

V_2O_5 - WO_3 / TiO_2 / SiO_2 catalyst during SCR of NO with NH_3 under steady-state (250-350°C - see Figure 2) as well as temperature programmed conditions (150-350°C – see Figure 6). The surface NH_3^* species concentration is relatively constant at steady-state with temperature between 250 and 350°C (see Figure 2) while the surface NH_4^{+*} species concentration significantly diminishes with temperature under the same reaction conditions. Furthermore, the surface NH_4^{+*} concentration also dramatically decreases between 250 and 350°C in the Ar atmosphere while the surface NH_3^* concentration decreases only mildly under the same conditions. These steady-state *operando* IR-MS spectroscopy measurements demonstrate that the surface NH_4^{+*} species on the Brønsted acid sites are more reactive than the surface NH_3^* species on Lewis acid sites during the NO- NH_3 SCR reaction over supported V_2O_5 - WO_3 / TiO_2 / SiO_2 catalysts. .

The conclusion that the surface NH_4^{+*} species on Brønsted acid sites is more reactive than the surface NH_3^* species on Lewis acid sites is further supported by the steady-state isotopic transient kinetic experiments where the NH_3 reactant is switched to the ND_3 reactant (see Figure 4). During the $NH_3 \rightarrow ND_3$ isotopic switch, the surface NH_4^{+*} concentration decreases more rapidly than that of the surface NH_3^* concentration reflecting the greater consumption rate of the surface NH_4^{+*} species relative to the surface NH_3^* species during the NO- NH_3 SCR reaction. During the $ND_3 \rightarrow NH_3$ isotopic switch (see Figure 5), repopulation of the surface NH_4^{+*} species is slightly more sluggish than the repopulation of the

surface NH_3^* species because of the greater consumption rate of the surface NH_4^{+*} species than the surface NH_3^* species by the NO-NH₃ SCR reaction. Thus, the steady-state transient isotopic kinetic experiments are also in agreement with the conclusion that the surface NH_4^{+*} species on Brønsted acid sites are more reactive than the surface NH_3^* species on Lewis acid sites during NO-NH₃ SCR over the supported V₂O₅-WO₃/TiO₂/SiO₂ catalyst.

The transient NO pulsing experiments into the NH₃/Ar reaction mixture provides additional insights into the relative reactivity of the surface NH_4^{+*} and NH_3^* intermediates during the NO-NH₃ SCR reaction. In the presence of gas phase NO reactant, the surface NH_4^{+*} concentration markedly increases while the surface NH_3^* concentration is relatively unaffected (see Figures 10 and S1). The increase in the surface NH_4^{+*} concentration is a consequence of the conversion of surface NH_3^* to NH_4^{+*} species by the H₂O reaction product formed by the NO-NH₃ SCR reaction [18,19], which markedly decrease in the absence of gaseous NO. The insensitivity of the surface NH_3^* species on Lewis acid site and the significant perturbation of the surface NH_4^{+*} species on Brønsted acid site to the presence/absence of gaseous NO reactant further substantiates the greater reactivity of the surface NH_4^{+*} species on Brønsted acid sites during the NO-NH₃ SCR reaction over supported V₂O₅-WO₃/TiO₂/SiO₂ catalysts.

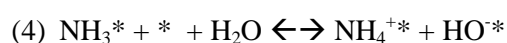
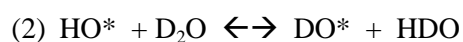
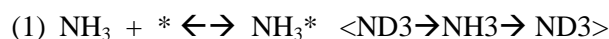
The reactivity of the surface NH_4^{+*} and NH_3^* species was also chemically probed by temperature programmed *operando* IR-MS spectroscopy (see Figures 6

and 7) where the chemisorbed ammonia species are reacted with gas phase NO while the catalyst temperature is continuously increased. The chemisorbed ammonia species react with the gaseous NO in two temperature regimes: ~295 and 390°C. At the lower temperature region, the surface NH_4^{+*} species are preferentially consumed by the SCR reaction. At the higher temperature region, only surface NH_3^* species on Lewis acid sites remain to be consumed by the SCR reaction. The temperature programmed *operando* IR-MS spectroscopy experiment reveals that both surface NH_4^{+*} and NH_3^* species are able to participate in the NO- NH_3 SCR reaction and that the surface NH_4^{+*} species on Brønsted acid sites are significantly more reactive than the surface NH_3^* species on Lewis acid sites during the NO- NH_3 SCR reaction over supported $\text{V}_2\text{O}_5\text{-WO}_3/\text{TiO}_2/\text{SiO}_2$ catalysts.

. In contrast to the results presented above, previous studies by Lietti et al [23] and Went et al [54] have concluded that the adsorption and activation of NH_3 takes places primarily on surface Lewis acid sites, whereas Topsøe et al [13,14] proposed the reaction proceeds via the activation of NH_3 on Brønsted acid sites. However, the fundamental results in this study are unique in showing that both NH_4^{+*} and NH_3^* species are active during the NO- NH_3 SCR reaction, and that each species contributes to the production of N_2 and H_2O . In accessing their individual contributions however, NH_3^* species on Lewis acid sites are found to be significantly less reactive than the NH_4^{+*} species on Brønsted acid sites.

4.3 SCR NO- NH_3 Reaction Mechanism

The in situ spectroscopic data generated in this study, which directly probed the reaction step between NO and the active ammonia species, suggest that ammonia adsorbs and is activated on an acid site (Brønsted and Lewis). Steady state, transient, and temperature programmed *operando* IR-MS spectroscopy results revealed that NH_4^{+*} species on Brønsted acid sites are more reactive than the surface NH_3^* species on Lewis acid sites, which would suggest that the conversion of NH_3^* to NH_4^{+*} could be rate the rate limiting process. These insights would suggest the following mechanistic steps:

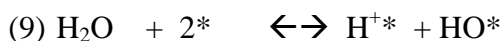
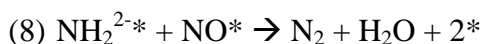
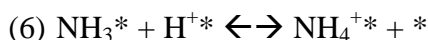
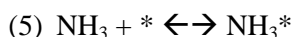


The SCR reaction mechanism has been extensively studied by numerous researchers both experimentally and theoretically using DFT. The most common mechanisms proposed are the Langmuir-Hinshelwood, where adsorbed NH_3 reacts with adsorbed NO, or an Eley-Rideal mechanism, where adsorbed NH_3 reacts with gas phase NO. Further debate regarding whether the mechanism involves a single or dual site, Brønsted or Lewis acid site, or what is the rate determining step of the reaction have been argued.

Dumesic et al [14,15] proposed insightful conclusions based on kinetic and spectroscopic data where ammonia adsorbs and is activated on a Brønsted acid site, the reaction of the activated ammonia with gaseous or weakly adsorbed NO,

and the reoxidation of the active vanadia site by molecular oxygen. This work was followed up with DFT calculations by Anstrom et al [29] to conclude that the rate limiting process was the reaction of an adsorbed NH_3NHO adduct to form NH_2NO species.

Based on the arguments presented, the mechanism appears to evolve through surface sites being covered first by ammonia, which reacts to provide ammonium species, being those active for the SCR of NO with NH_3 . A similar conclusion was reached by Topsøe et al [14] in the studies of unpromoted $\text{V}_2\text{O}_5/\text{TiO}_2$ catalysts. It is then likely that species are continuously regenerated by ammonia coordinated with the surface, which is evident when the ammonium IR signal reaches a maximum steady state value. When ammonia is reintroduced by isotopic substitution, a short induction time is observed before ammonium is created and converted again. This suggests the following type of mechanism:



Wachs et al [16] has shown that there is a direct relationship between Brønsted acidity and SCR activity and that the reaction proceeds through a dual site mechanism involving a surface redox site and an adjacent surface nonreducible metal oxide site.

4.4 SCR NO-NH₃ Reaction Kinetics

The reaction kinetics may be derived from these mechanistic equations based on the knowledge that (1) gaseous ammonia adsorbs on both Lewis and Brønsted acid sites (2) NO is not formed in appreciable amounts on the surface during the SCR reaction and (3) NH₄⁺* is the most reactive species.

As such, it appears that the rate determining step should be the conversion of NH₃* to the active NH₄⁺*, since Brønsted acid sites appear to be key in the SCR reaction. The rate of the overall reaction can be derived from Eq (6) as $r = k_{\text{rds}}[\text{NH}_3^*][\text{H}^*]$. Amiridies et al. [17] did not find a correlation between the reducibility of vanadia in the promoted samples, suggesting the surface reaction between NO and the SCR intermediate may not be kinetically significant. They were able to correlate however, the Brønsted acidity with the SCR activity, which led them to suggest that the activation of an adsorbed ammonia species could be rate determining. Topsøe et al [14], found a correlation between the NO_x conversion and the product of the concentration of the Brønsted acid sites and the exit partial pressure of NO with 8% O₂, with an unpromoted V₂O₅/TiO₂ catalyst. Therefore, it was proposed that under high O₂ concentrations (most industrial SCR conditions) the rate is equal to the rate of reaction of NO with activated ammonia. Specifically, $r = k[\text{B.A}][\text{V=O}]P_{\text{NO}}$ or $r \propto k[\text{B.A}]P_{\text{NO}}$ since [V=O] is approximately constant. Based on the in situ spectroscopic data presented in this study, we are certainly of similar conclusions to Amiridies [17] and Topsøe [14]. Further,

operando-IR under SCR conditions reveals that the surface is saturated with NH_3 , suggesting step (5) is kinetically insignificant.

4. CONCLUSIONS

The *operando* TP-IR-MS spectroscopy experiments revealed that in the lower SCR reaction temperature regime of $\sim 200\text{-}250^\circ\text{C}$, the surface NH_4^+ species on Brønsted acid sites are preferentially consumed and some surface NH_3^* species on Lewis acid sites are converted to surface NH_4^+ species in the presence of moisture. In the intermediate temperature regime of $\sim 250\text{-}320^\circ\text{C}$, both surface NH_x species are consumed in the production of N_2 . At the highest temperature regime of $\sim 350\text{-}400^\circ\text{C}$, the surface NH_3 species are predominantly responsible for N_2 formation. Additionally, steady state *operando*-IR-MS SCR experiments showed that at the low temperature regime (250°C), both surface NH_3^* and NH_4^+ react to form the SCR products. With an increase in temperature, the NH_4^+ species markedly decreased due to its higher reactivity, and at the highest temperature (350°C), coordinated NH_3^* were largely responsible for the SCR activity.

The combined *operando* IR-MS spectroscopy experiment were able to distinguish between the different reactivities of the surface NH_4^+ species on Brønsted acid sites and the surface NH_3^* species on Lewis acid sites during the SCR reaction, and revealed that both species are active during the SCR of NO, however, the Brønsted acid surface sites were found to have a higher reactivity compared to Lewis acid sites.

ACKNOWLEDGMENTS

The authors gratefully acknowledge the financial support by the NSF NIRT Grant 0609018.

REFERENCES

1. P. Forzatti, *Catalysis Today* **62** (2000) 51
2. I. Chorkendorff, J.W. Niemantsverdriet, *Concepts of Modern Catalysis and Kinetics*; Wiley-VCH Verlag GmbH & Co. KGa, 2003
3. M. Takagi, T. Kawai, M. Soma, T. Onishi, K. Tamaru, *J. Catal.* **50** (1977) 441
4. A. Miyamoto, M. Inomata, Y. Yamazaki, Y. Murakami, *J. Catal.* **57** (1979) 526
5. M. Inomata, A. Miyamoto, Y. Murakami, *J. Catal.* **62** (1980) 140
6. A. Miyamoto, K. Kobayashi, M. Inomata, Y. Murakami, *J. Phys. Chem.* **86** (1982) 2945
7. N.Y. Topsøe, T. Slabæk, B.S. Clausen, T.Z. Srnak, J.A. Dumesic, *J. Catal.*, **134** (1992) 742
8. T.Z. Srnak, J.A. Dumesic, B.S. Clausen, E. Törnqvist, N.Y. Tøpsoe, *J. Catal.*, **135** (1992) 246
9. J.P. Chen, R.T. Yang, *J. Catal.*, **139** (1993) 277
10. N.Y. Topsøe, *Science* **265** (1994) 1217
11. M. Kantcheva, V. Bushev, D. Klissurski, *J. Catal.* **145** (1994) 96
12. H. Schneider, S. Tschudin, M. Schneider, A. Wokaun, A. Baiker, *J. Catal.* **147** (1994) 5
13. N.Y. Topsøe, H. Topsøe, J.A. Dumesic, *J. Catal.* **151** (1995) 226

14. N.Y. Topsøe , J.A. Dumesic, H. Topsøe , *J. Catal.* **151** (1995) 241
15. J.A. Dumesic, N.Y. Topsøe , H. Topsøe , Y. Chen, T. Slabiak, *J. Catal.* **163**
(1996) 409
16. I.E. Wachs, G. Deo, B.M. Weckhuysen, A. Andreini, M.A. Vuurman, M. de
Boer, M.D. Amiridis, *J. Catal.* **161** (1996) 211
17. (a) M.D. Amiridis, I.E. Wachs, G. Deo, J.M. Jehng, D.S. Kim, *J. Catal.* **161**
(1996) 247 (b) M.D. Amiridis, R.V. Duevel, I.E. Wachs, *App. Catal.*
B: Environ. **20** (1999) 111
18. G. Ramis, G. Busca, F. Bregani, P. Forzatti, *Appl. Catal.* **64** (1990) 259
19. L. Lietti, J. Svachula, P. Forzatti, G. Busca, G. Ramis, P. Bregani, *Catal.*
Today **17** (1993) 131
20. L. Lietti, J.L. Alemany, P. Forzatti, G. Busca, G. Ramis, E. Giamello, F.
Bregani, *Catal. Today* **29** (1996) 143
21. G. Ramis, L. Yi, G. Busca, *Catal. Today* **28** (1996) 373
22. G. Busca, L. Lietti, G. Ramis, F. Berti, *Appl. Catal. B: Environmental* **18**
(1998) 1
23. L. Lietti, G. Ramis, F. Berti, G. Toledo, D. Robba, G. Busca, P. Forzatti,
Catal. Today **42** (1998) 101
24. V.I. Parvulescu, S. Boghosian, V. Parvulescu, S.M. Jung, P. Grange, *J.*
Catal. **217** (2003) 172
25. G. Busca, M.A. Larrubia, L. Arrighi, G. Ramis, *Catal. Today* **107-108**

(2005) 139

26. F. Gilardoni, J. Weber, A. Baiker, *J. Phys. Chem. A* **101** (1997) 6069
27. F. Gilardoni, J. Weber, A. Baiker, *Intern. J. Quantum Chem.* **61** (1997) 683
28. X. Yin, H. Han, I. Gunji, A. Endou, S.S.C. Ammal, M. Kubo, A. Miyamoto, *J. Phys. Chem. B* **103** (1999) 4701
29. M. Anstrom, N.Y, Topsøe , J.A. Dumesic, *J. Cata.* **213** (2003) 115
30. K. Jug, T. Homann, T. Bredow, *J. Phys. Chem. A* **108** (2004) 2966
31. A. Vittadini, M. Casarin, A. Selloni, *J. Phys. Chem. B* **109** (2005) 1652
32. S. Soyer, A. Uzun, S. Senkan, I. Onal, *Catal. Today* **118** (2006) 268
33. R.M. Yuan, G. Fu, X. Xu, H.L. Wan, *Phys. Chem. Chem. Phys.* **13** (2011) 453
34. E.I. Ross-Medgaarden, I.E. Wachs, W.V. Knowles, A. Burows, C.J. Kiely, M.S. Wong, *J. Am. Chem. Soc.* **131** (2009) 680
35. F. Sarria, O. Marie, P. Bazin, J. Saussey, J. Lesage, A. Guesdon, M. Daturi, *Phys. Chem. Chem. Phys.*, **5** (2003) 4435
36. I.E. Wachs, *Catal. Today* **27** (1996) 437.
37. I.E. Wachs, *Catal. Today* **100** (2005) 79.
38. X. Gao, S.R. Bare, J.L. Fierro, M.A. Banaras, I.E. Wachs, *J. Phys. Chem. B* **102** (1998) 5653.
39. G.Deo, A. M. Turek and I.E. Wachs, *Appl. Catal. A: Gen*, **91** (1992) 27.
40. E. Lee, I.E. Wachs, *J. Phys. Chem. C.* **111** (2007) 14410-14425.

41. D.S. Kim, M. Ostromecki, I.E. Wachs, *J. Mol. Catal. A Chem.* **106** (1996) 93.
42. M.A. Vuurman, I.E. Wachs, *J. Phys. Chem.* **96** (1992) 5008.
43. J. Jarupatrakorn, M.P. Coles and T.D. Tilley, *Chem. Mater.*, **17** (2005) 818.
44. K. Nakamoto, *Infrared and Raman Spectra of Inorganic Coordination Compounds* (5th ed); Wiley & Sons: New York, 1997.
45. X. Gao, S.R. Bare, B. M. Weckhuysen and I.E. Wachs, *J. Phys. Chem. B* **102** (1998) 10842.
46. H. Eckert, I.E. Wachs, *J. Phys. Chem.* **93** (1989) 6796.
47. N. Das, H. Eckert, H. Hu, I.E. Wachs, J.F. Walzer and F. Feher, *J. Phys. Chem.* **97** (1993) 8240.
48. X. Gao, S.R. Bare, I.E. Wachs, *J. Phys. Chem. B* **103** (1999) 618.
49. G. Deo and I.E. Wachs, *J. Catal.* **146** (1994) 335.
50. M.A. Centeno, I. Carrizosa, J.A. Odriozola, *Appl. Catal. B: Environmental* **29** (2001) 307
51. T. Kim, A. Burrows, C.J. Kiely, I.E. Wachs, *J. Catal.* **246** (2007) 370
52. T. Kim, I.E. Wachs, *J. Catal.* **255** (2008) 197
53. M.A. Banaras, *Catal. Today* **100** (2005) 71
54. G.T. Went, L-J. Leu, R.R. Rosin, A.T. Bell, *J. Catal.* **134** (1992) 492

FIGURES

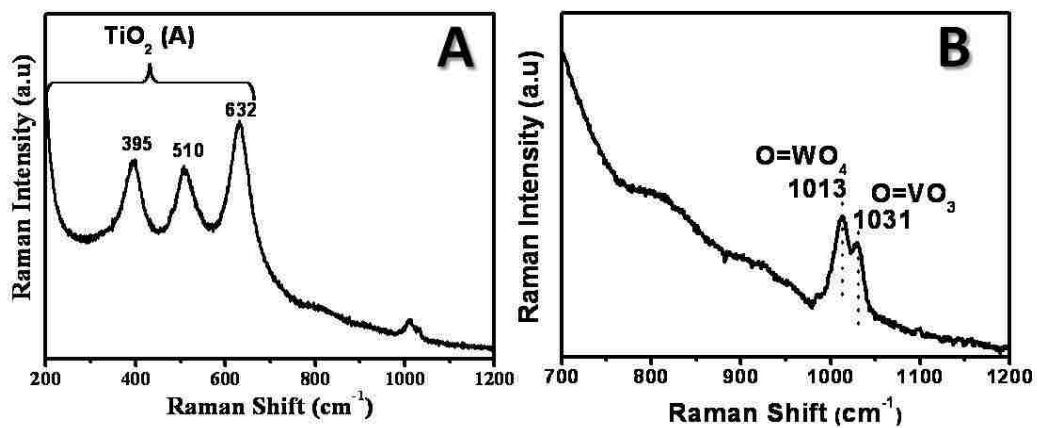


Figure 2.1. *In situ* Raman spectrum (532 nm) of the dehydrated supported 1% V₂O₅–5% WO₃/ 30% TiO₂/SiO₂ catalyst in the [A] 200-1200 cm⁻¹ region that is dominated by TiO₂(A) bands and [B] 700-1200 cm⁻¹ region that is dominated by the surface WO_x and VO_x vibrations.

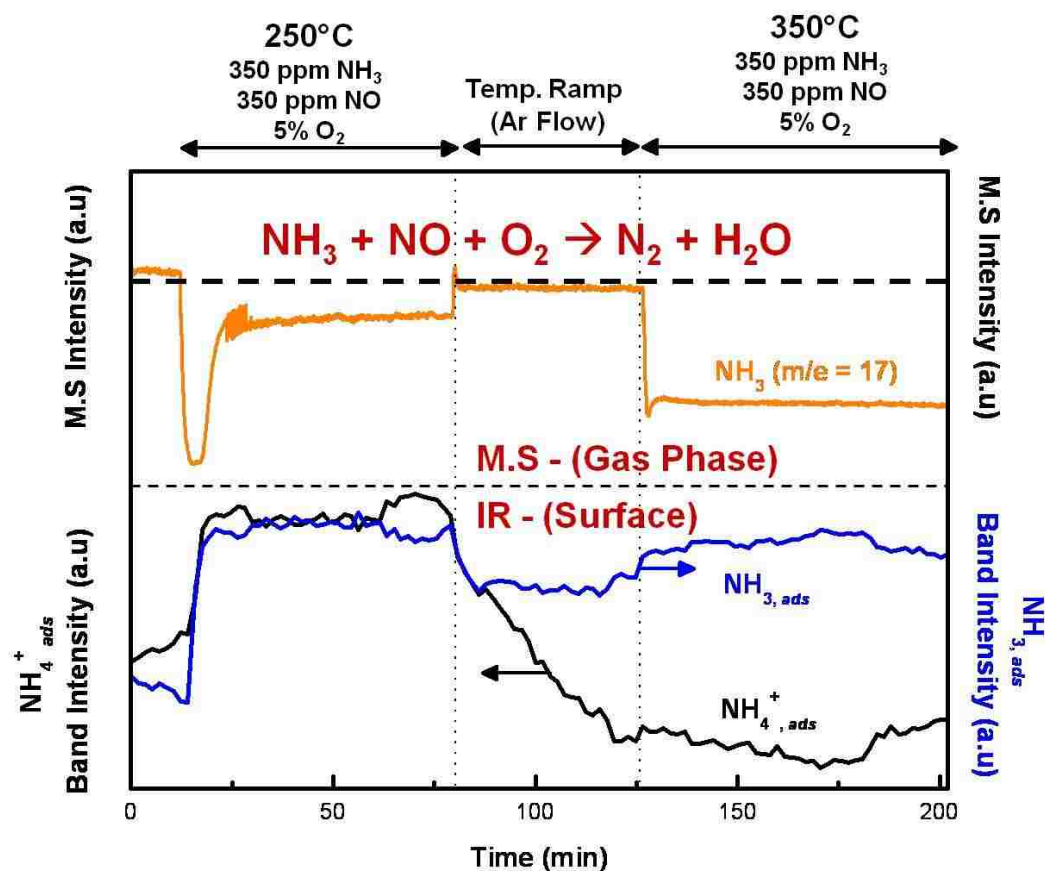


Figure 2.2. TOP: Time-resolved MS spectrum of gas phase NH_3 and BOTTOM: Time-resolved IR intensity of the surface NH_3 (1610 cm^{-1}) and NH_4^+ (1450 cm^{-1}) reaction intermediates during steady-state SCR of NO-NH_3 reaction.

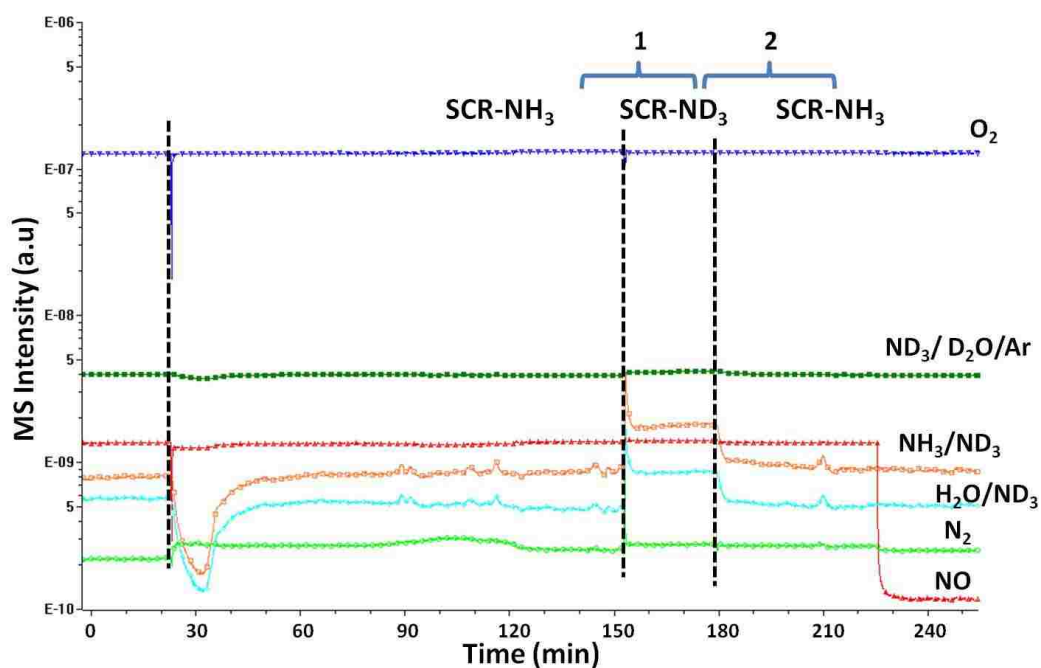


Figure. 2.3: MS signal profiles for reaction products during ammonia isotopic switch over the model supported 1%V₂O₅-5%WO₃/30%TiO₂/SiO₂ catalyst at the reaction temperature of 250°C. The MS signals for various gases are monitored as follows: NH₃ (17), ND₃ (20), NO (30), O₂ (32), N₂ (28), H₂O, (18) and D₂O (20). The specific isotope employed during each part of the study is indicated above the figure.

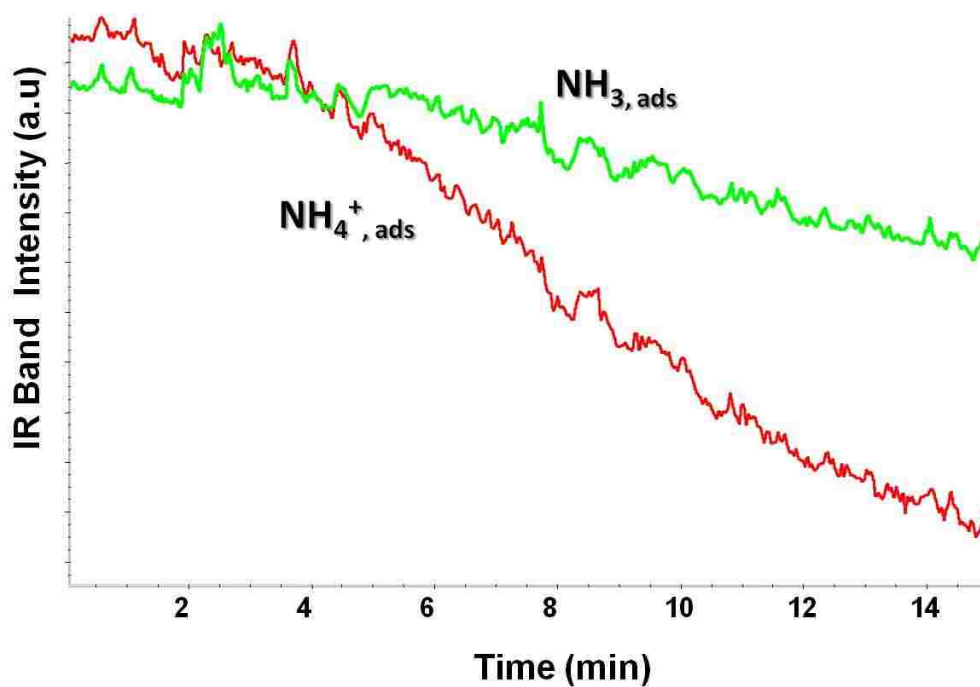


Fig. 2.4: Evolution of the integrated bands for surface NH_3^{+*} (green) and NH_4^{+*} (red) species during the isotopic switch $\text{NH}_3 + \text{NO} + \text{O}_2 \rightarrow \text{ND}_3 + \text{NO} + \text{O}_2$ at 250°C . The chosen integration limits are $1622\text{-}1594\text{ cm}^{-1}$ for the adsorbed ammonia and $1481\text{-}1382\text{ cm}^{-1}$ for the ammonium ion.

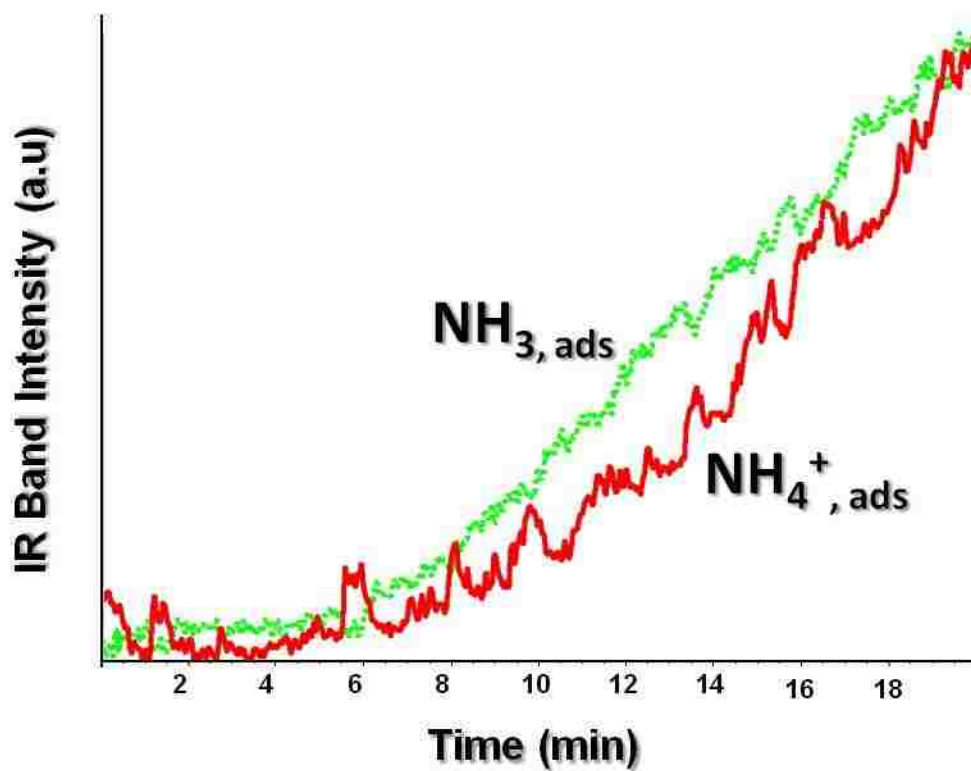


Fig. 2.5: Evolution of the integrated bands for NH_3^* (green) and NH_4^{+*} (red) species during the isotopic switch $\text{ND}_3 + \text{NO} + \text{O}_2 \rightarrow \text{NH}_3 + \text{NO} + \text{O}_2$ at 250°C . The chosen integration limits are $1622\text{-}1594\text{ cm}^{-1}$ for the adsorbed ammonia and $1481\text{-}1382\text{ cm}^{-1}$ for the ammonium ion.

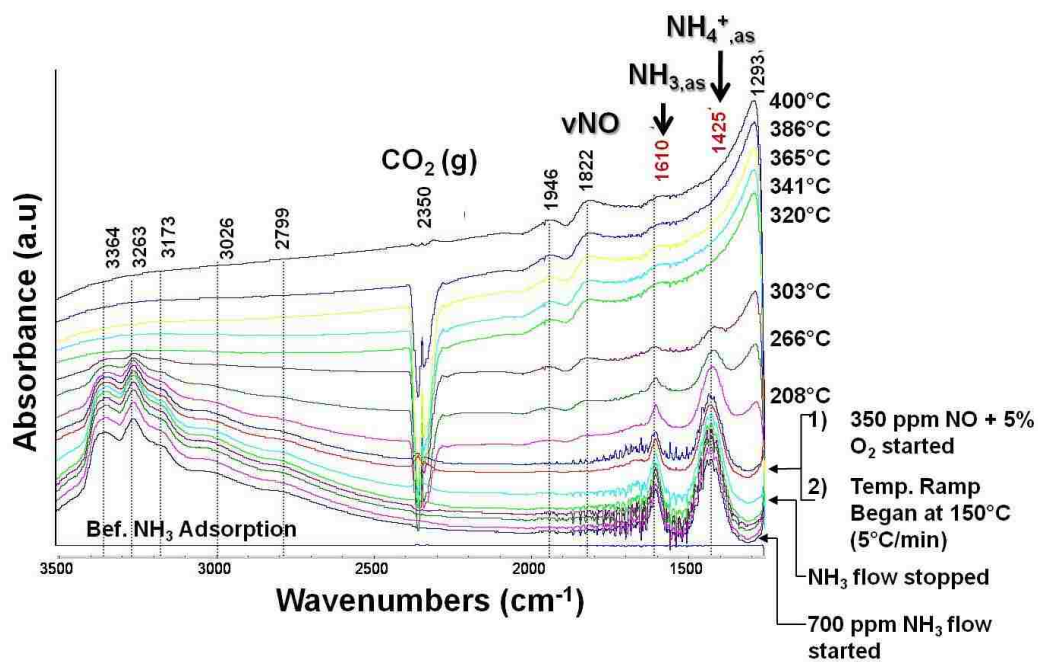


Figure 2.6. *In situ* FT-IR spectra of NH_3 adsorption at 150°C and temperature programmed surface reaction from 150°C to 400°C at 5°C/min under flowing $\text{NO}/\text{O}_2/\text{Ar}$.

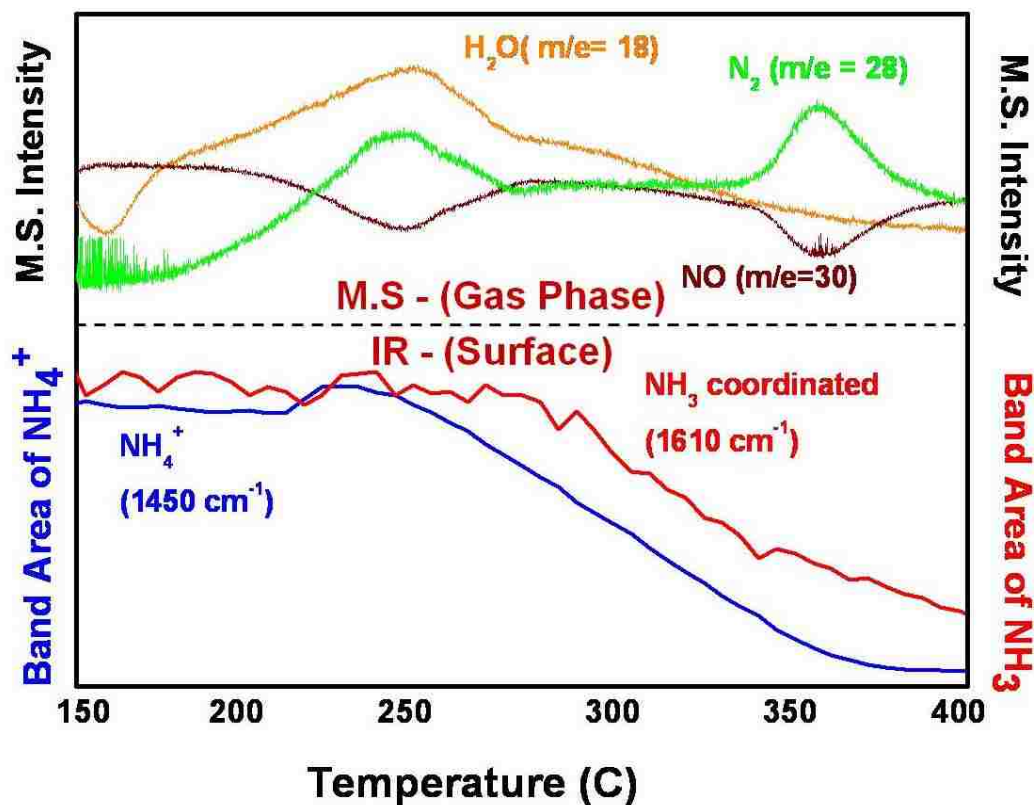


Figure 2.7. TOP: MS spectrum of gas phase SCR products (N₂, H₂O, NO) and BOTTOM: IR intensity of surface NH₃* (1610 cm⁻¹) and NH₄⁺* (1450 cm⁻¹) reaction intermediates during temperature programmed surface reaction in flowing NO/O₂/Ar.

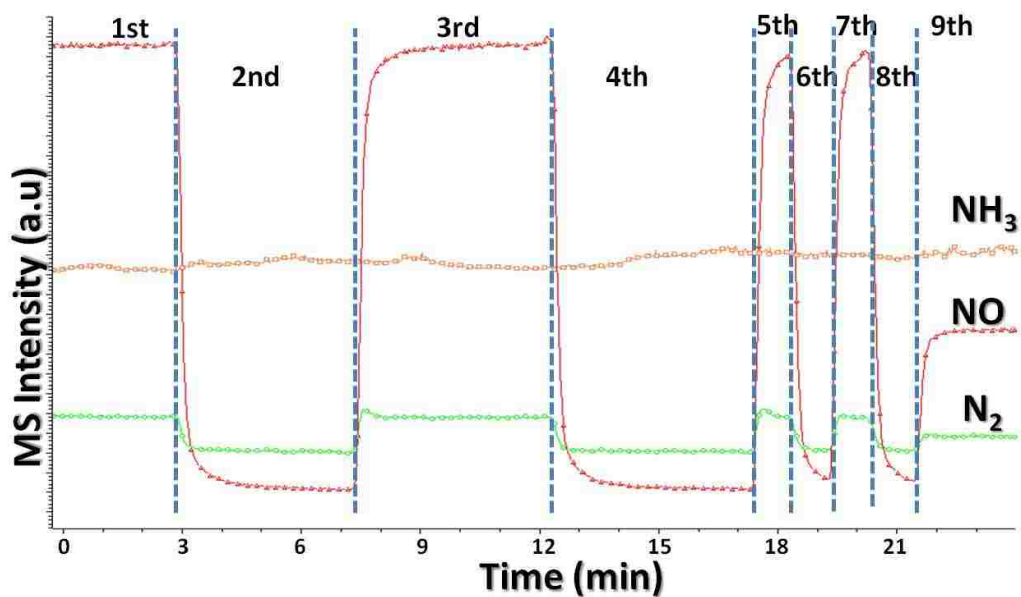


Fig. 2.8: MS signal profiles for the pulsed NO SCR experiments on the model supported 1% V_2O_5 -5% WO_3 /30% TiO_2 / SiO_2 catalyst at a reaction temperature of 250°C. MS analysis of gaseous NH_3 , N_2 , NO molecules during removal and re-introduction of the NO reducing agent: 1st: 350 ppm NH_3 + 5% O_2 + 350 ppm NO (steady-state, 30s scan); 2nd: 350 ppm NH_3 + 5% O_2 ; 3rd: 350 ppm NH_3 + 5% O_2 + 350 ppm NO; 4th: 350 ppm NH_3 +5% O_2 ; 5th: 350 ppm NH_3 +5% O_2 + 350 ppm NO; 6th: 350 ppm NH_3 + 5% O_2 ; 7th: 350 ppm NH_3 + 5% O_2 + 350 ppm NO; 8th: 350 ppm NH_3 + 5% O_2 ; 9th: 350 ppm NH_3 +5% O_2 + 125 ppm NO.

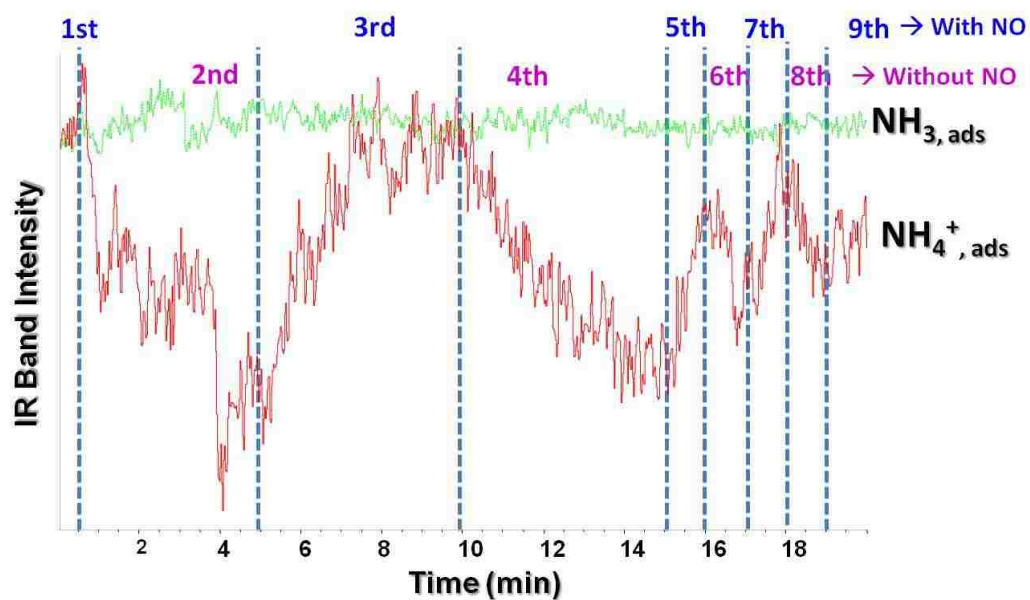


Fig. 2.9: Evolution of the integrated bands for surface NH_3^* (green-dotted) and NH_4^{+*} (red) species under the $\text{NH}_3 + \text{NO} + \text{O}_2$ flow during intermittent NO supply at 250°C . The chosen integration limits are $1621\text{-}1590\text{ cm}^{-1}$ for adsorbed ammonia and $1470\text{-}1386\text{ cm}^{-1}$ for ammonium ion. Zoomed in common scale.

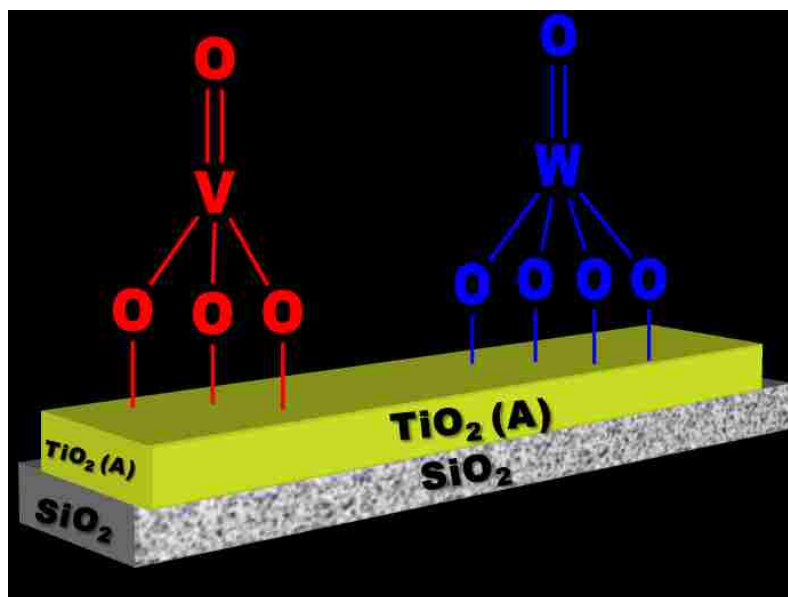
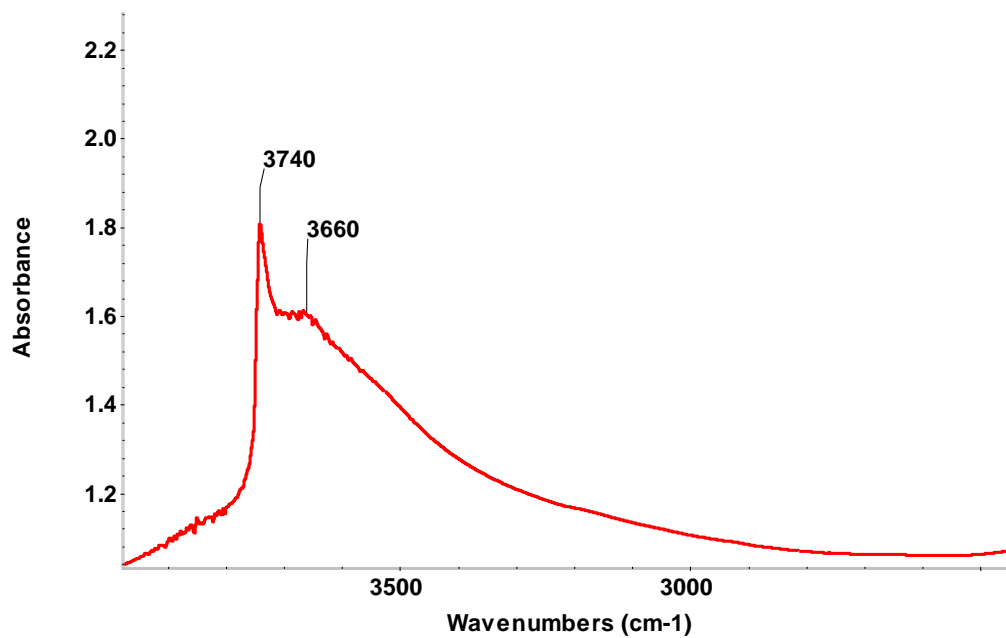
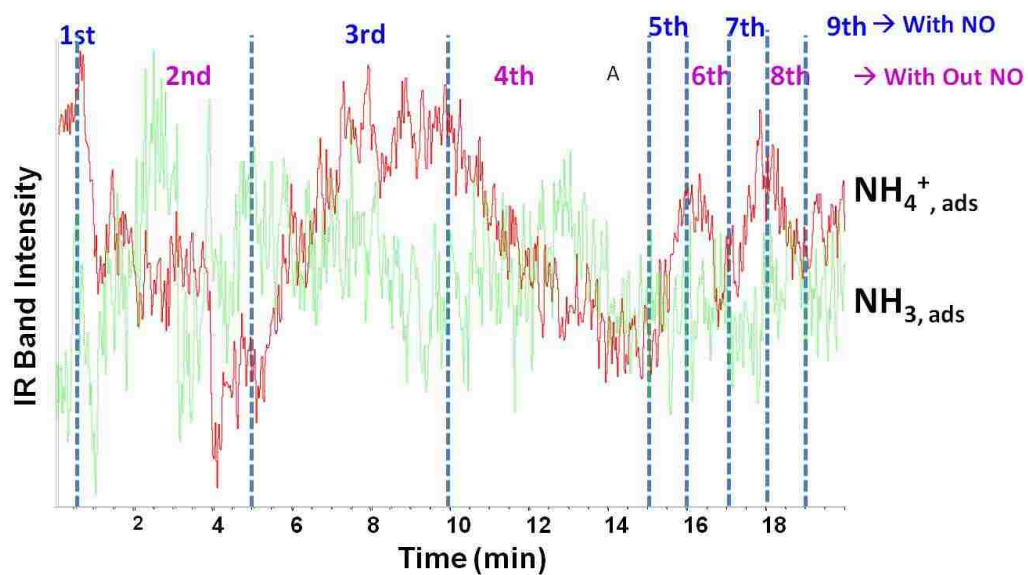


Figure 2.10. Schematic of the dehydrated supported 1% V_2O_5 -5% WO_3 /30% TiO_2 catalyst that corresponds to the *in situ* Raman spectra in Figure 1.

Supplemental Information

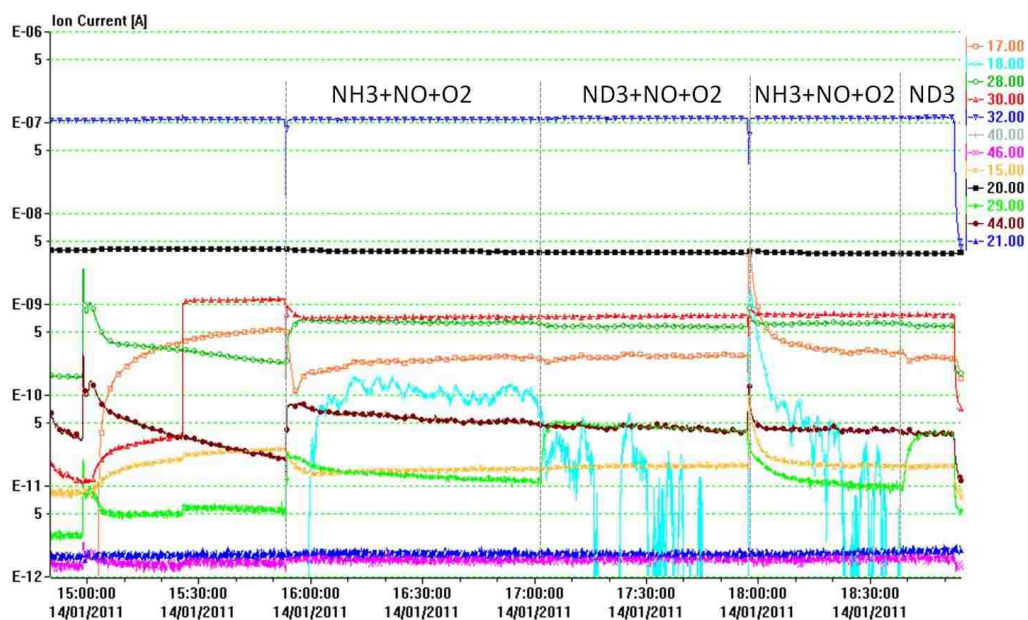


2.S1. Dehydrated FT-IR spectrum of the supported 1% V₂O₅-5% WO₃/30% TiO₂/SiO₂ catalyst in the OH stretching region in flowing O₂/Ar.

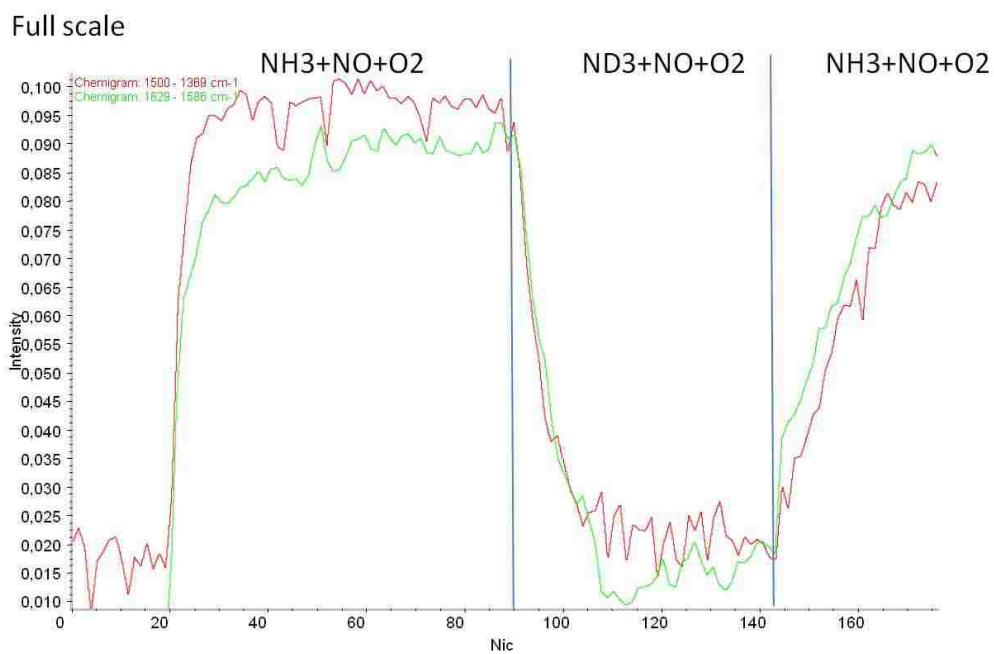


2.S2: Evolution of the integrated bands for surface NH_3^* (green-dotted) and NH_4^{+*} (red) species under the $\text{NH}_3 + \text{NO} + \text{O}_2$ flow during intermittent NO supply at 250°C . The chosen integration limits are $1621\text{-}1590\text{ cm}^{-1}$ for adsorbed ammonia and $1470\text{-}1386\text{ cm}^{-1}$ for ammonium ion. Full scale shown.

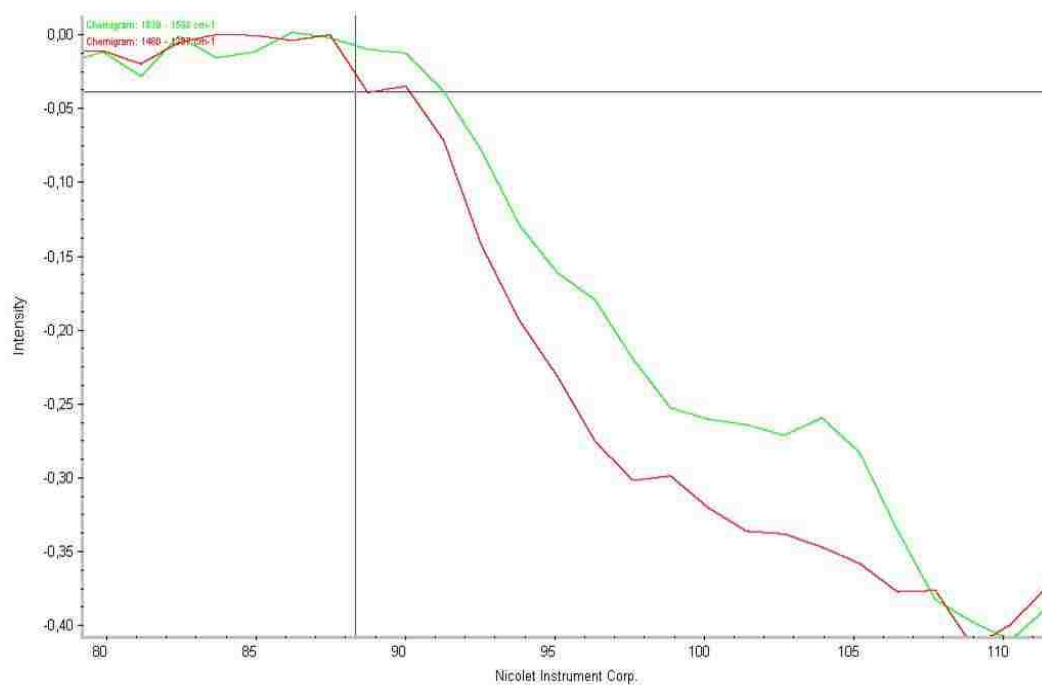
1%V₂O₅-5%WO₃/30%TiO₂/SiO₂ 350°C
 MS Analysis of NH₃, ND₃, NO, O₂, N₂, H₂O, D₂O, NO₂



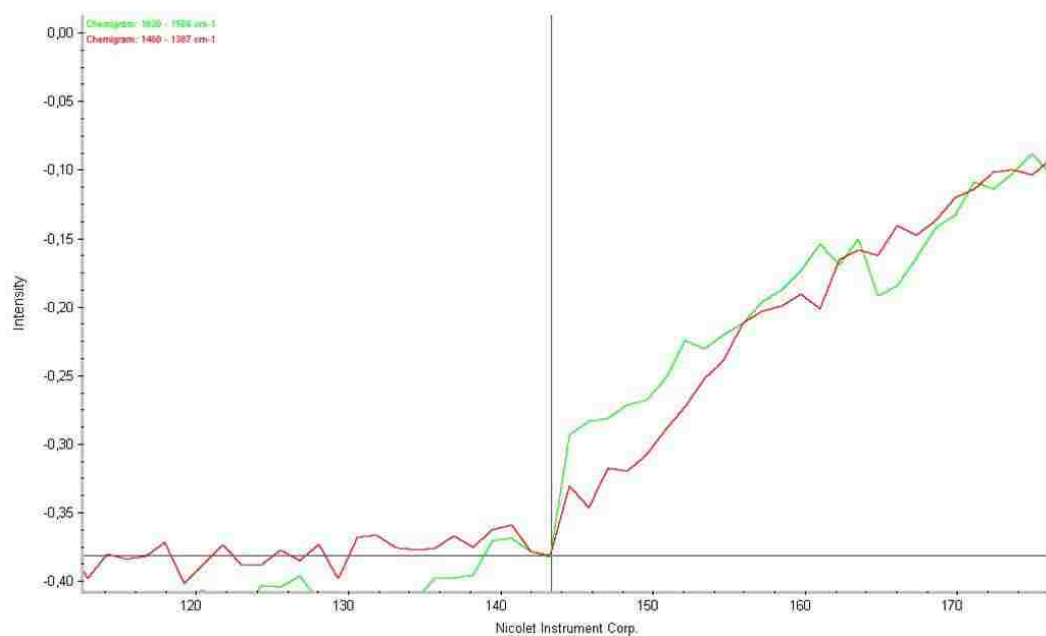
2.S3: MS signal profiles at 350°C for the ammonia isotopic substitution on 1%V₂O₅-5%WO₃/30%TiO₂/SiO₂ sample. Reaction temperature 350°C. MS Analysis of NH₃ (17), ND₃ (20), NO (30), O₂ (32), N₂ (28), H₂O, (18), D₂O (20) species. In the region indicated above, the reaction has been followed by IR spectra of the surface recorded in the rapid scan mode.



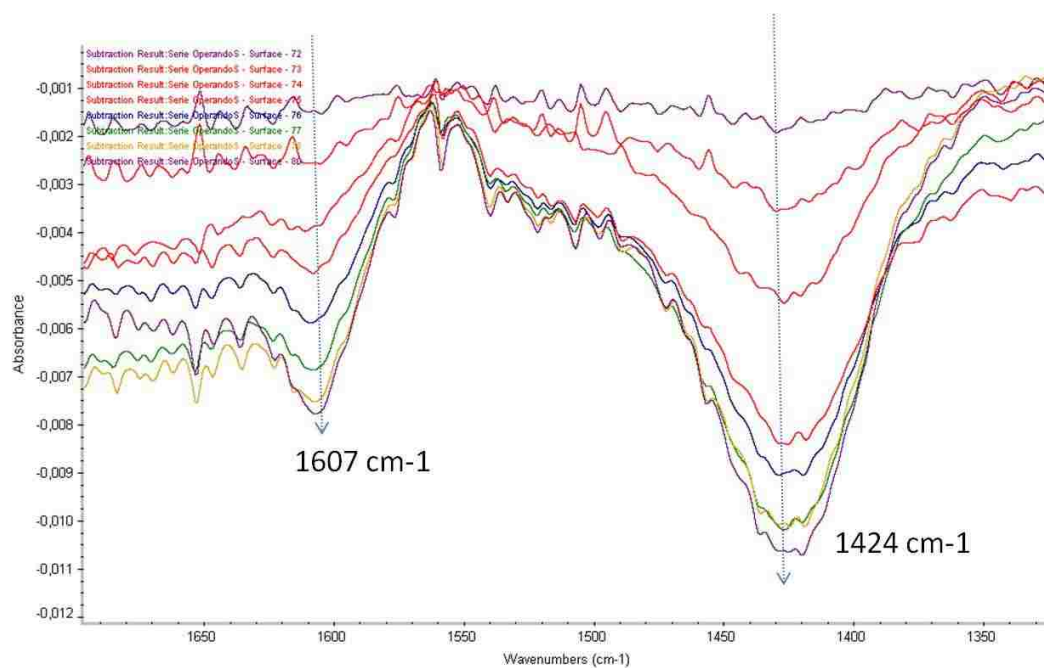
2.S4: Evolution of the integrated bands for ammonia (green) and ammonium (red) species during isotopic substitution at 350°C. The chosen integration limits are 1622-1594 cm^{-1} for adsorbed ammonia and 1481-1382 cm^{-1} for ammonium ion.



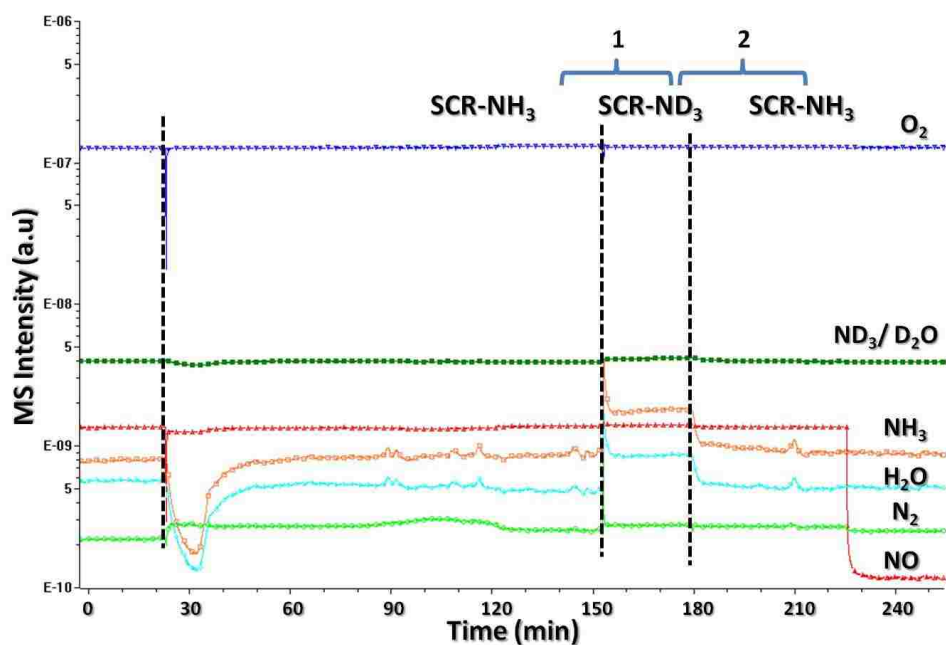
2.S5: Evolution of the integrated bands for ammonia (green) and ammonium (red) species during the $\text{NH}_3 + \text{NO} + \text{O}_2 \rightarrow \text{ND}_3 + \text{NO} + \text{O}_2$ substitution at 350°C . The chosen integration limits are $1622\text{-}1594\text{ cm}^{-1}$ for adsorbed ammonia and $1481\text{-}1382\text{ cm}^{-1}$ for ammonium ion.



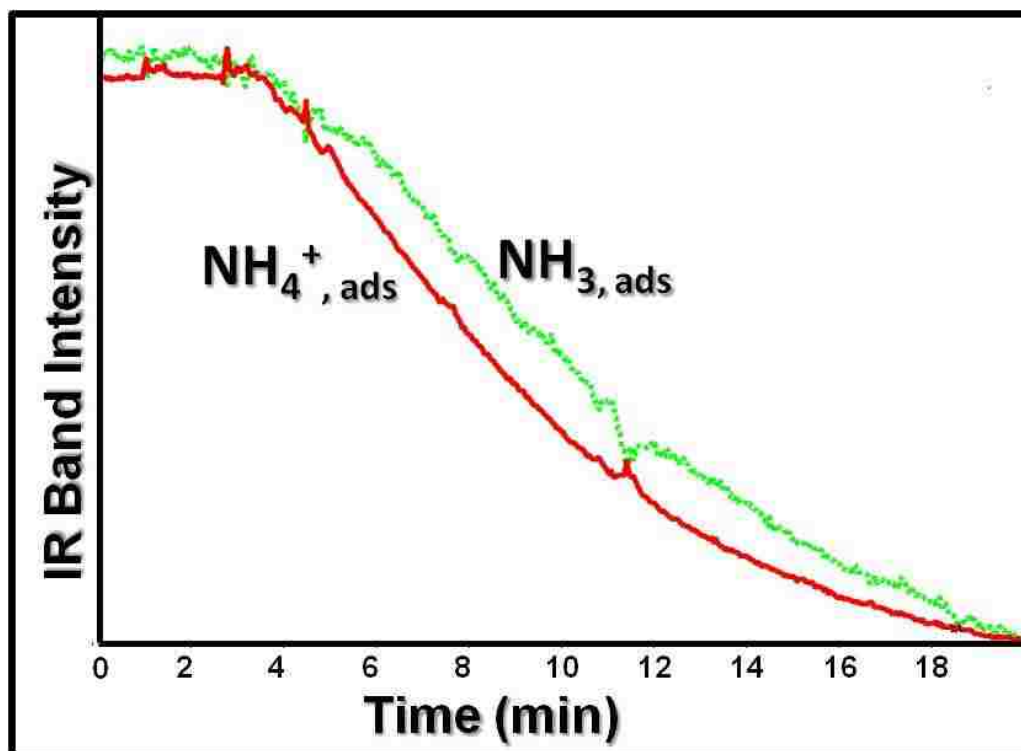
2.S6: Evolution of the integrated bands for ammonia (green) and ammonium (red) species during the $\text{ND}_3 + \text{NO} + \text{O}_2 \rightarrow \text{NH}_3 + \text{NO} + \text{O}_2$ substitution at 350°C . The chosen integration limits are $1622\text{-}1594\text{ cm}^{-1}$ for adsorbed ammonia and $1481\text{-}1382\text{ cm}^{-1}$ for ammonium ion.



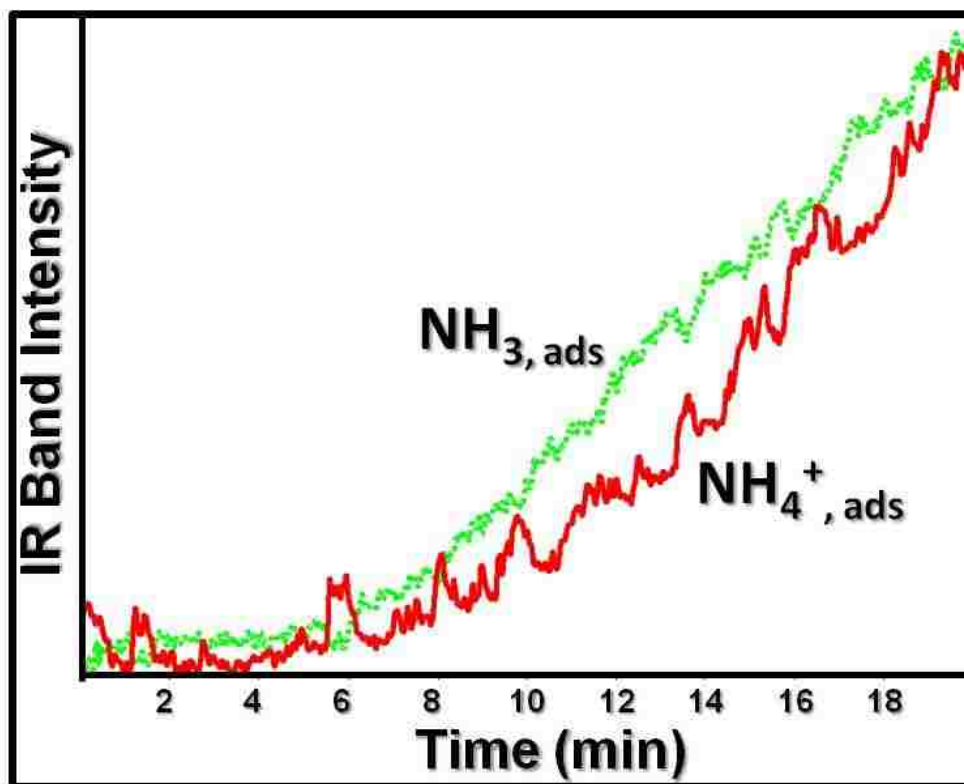
2.S7: IR bands associated to NH_4^{+*} (1424 cm^{-1}) and NH_3^* (1607 cm^{-1}) disappearing during $\text{NH}_3 + \text{NO} + \text{O}_2 \rightarrow \text{ND}_3 + \text{NO} + \text{O}_2$ substitution at 350°C .



2.S8: MS signal profiles for the ammonia isotopic substitution on 1%V₂O₅-5%WO₃/30%TiO₂/SiO₂ sample. Reaction temperature 150°C. MS Analysis of NH₃ (17), ND₃ (20), NO (30), O₂ (32), N₂ (28), H₂O, (18), D₂O (20) species. In the region indicated above, the reaction has been followed by IR spectra of the surface recorded in the rapid scan mode.



2.S9: Evolution of the integrated bands for ammonia (green) and ammonium (red) species during the $\text{NH}_3 + \text{NO} + \text{O}_2 \rightarrow \text{ND}_3 + \text{NO} + \text{O}_2$ substitution at 150°C. The chosen integration limits are 1622-1594 cm^{-1} for adsorbed ammonia and 1481-1382 cm^{-1} for ammonium ion.



2.S10: Evolution of the integrated bands for ammonia (green) and ammonium (red) species during the $\text{ND}_3 + \text{NO} + \text{O}_2 \rightarrow \text{NH}_3 + \text{NO} + \text{O}_2$ substitution at 150°C . The chosen integration limits are $1622\text{-}1594\text{ cm}^{-1}$ for adsorbed ammonia and $1481\text{-}1382\text{ cm}^{-1}$ for ammonium ion.

CHAPTER 3

Fundamental Mechanistic Insights into the Selective Oxidation of CH₃OH to H₂C(OCH₃)₂ over Bifunctional Supported V₂O₅-WO₃/TiO₂/SiO₂ Catalysts

ABSTRACT

The selective oxidation of methanol to dimethoxymethane (DMM) was investigated over a bifunctional V₂O₅-WO₃/TiO₂/SiO₂ catalyst, where VO_x and WO_x were molecularly dispersed and self-assembled onto 5-9 nm TiO₂ (A) nanoparticles that were consequently anchored to an inert silica surface. *In Situ* Raman spectroscopy revealed the catalytic active sites are present as VO₄ and WO₅ mono-oxo species under reaction conditions. *In Situ* FT-IR spectroscopy revealed that surface CH₃O* species are the most abundant reactive intermediate during DMM formation. Temperature programmed surface reaction experiments coupled with mass spectrometry, whereby a monolayer of CH₃O* and CH₃OH* reacted with flowing isotopically labeled molecules (CD₃OD or CH₃¹⁸OH) revealed that C-H bond breaking of surface CH₃O* species is the rate determining step in DMM formation, which was found to occur at surface VO_x sites. The molecularly designed catalyst provided a “green” one step synthetic route to the formation of DMM, whereby toxic HCHO is generated *in situ* from the catalytic active VO₄ sites and synergistically couples with CH₃O* on surface WO₅ sites to produce DMM. Finally, steady state kinetics revealed that DMM formation proceeds via a Mars-

van Krevelen mechanism and that the reaction is zero order in molecular O₂ and methanol partial pressure.

1. INTRODUCTION

Dimethoxymethane (DMM) is currently being used as an industrial organic solvent throughout the pharmaceutical and perfume industries [1]. DMM's potential as an oxygenated diesel fuel additive that reduces soot formation [2-5] has recently sparked intense interest [5-9] as an alternative to methanol and dimethyl ether (DME). All three oxygenates reduce diesel engine smoke and exhaust emissions, but methanol and DME have significant limitations due to their high vapor pressures, low solubility in diesel fuel and poor ignition quality [3].

The surface chemistry and mechanism of methanol oxidation has been thoroughly investigated over catalytic surface VO_x redox [10-12] sites that produce formaldehyde (HCHO) and over surface WO_x acidic sites [10,11] that form dimethyl ether (DME), CH₃OCH₃. Conversely, the mechanism for the selective oxidation of methanol to dimethoxymethane (DMM), H₂C(OCH₃)₂, has received little attention in the literature. The synthesis of DMM has been proposed to require both redox and acidic functionalities [11], and its mechanism has been probed separately by transient kinetic [13] and *in situ* IR spectroscopy [14]. However, the spectroscopic investigations have all been done in vacuum examining the adsorption and desorption of probe molecules with FT-IR. As such there has been much extrapolation of data to provide a speculative reaction mechanism. It

has also been proposed [13] through transient reaction kinetic experiments over unsupported V_2O_5 , that methanol reacts with the V_2O_5 surface to form methoxy groups or strongly adsorbed methanol species. The methanol can also react with the V_2O_5 oxidation sites to form a radical species ($\bullet CH_2OH$) that can quickly react with methoxy groups or adsorbed methanol to form a CH_3OCH_2OH intermediate. This intermediate (CH_3OCH_2OH) can then go on to react with methoxy groups or with adsorbed methanol to form DMM.

The recent advances in characterization techniques however, has allowed an unprecedented look at catalytic reactions under actual reaction conditions, where changes in catalytic active sites and surface reaction intermediates can be directly monitored and compared with the catalytic activity/selectivity performance. The objective of the present study is to obtain fundamental insights into the nature of the catalytic active sites (VO_x and WO_x), surface reaction intermediates, and the reaction mechanism during the selective oxidation of methanol to dimethoxymethane.

2. EXPERIMENTAL

2.1. Catalyst Synthesis

2.1.1. Preparation of Supported TiO_x/SiO_2 Catalysts

The synthesis procedure previously described by Ross-Medgaarden *et al.* [15] was used to prepare the x% TiO_2/SiO_2 (x =12 and 40) supports. The silica support material, amorphous SiO_2 (Cabot, Cab-O-Sil fumed silica EH-5, S.A. ~332

m²/g), was employed and found to be more easily handled by an initial water pretreatment and calcination at 500°C for 4 h without changing the material properties. The supported TiO₂/SiO₂ catalysts were prepared by the incipient-wetness impregnation of isopropanol solutions of titanium isopropoxide (Ti(O-Prⁱ)₄, Alfa Aesar, 99.999%). The silica support was initially dried for 2 h at 120°C to remove the physisorbed water prior to catalyst preparation inside a glovebox (Vacuum Atmospheres, Omni-Lab VAC 101965) under a continuously flowing N₂ (Airgas, Ultra High Purity) environment. After impregnation at room temperature, the sample was kept inside the glovebox to dry overnight under flowing N₂. The calcination of the supported TiO₂/SiO₂ samples entailed ramping at 1°C/min to 120°C in flowing N₂ for 2 h, and then subsequently followed by another 1°C/min ramp under flowing air (Airgas, Zero Grade) to 500°C for 4 h. A multi-step preparation procedure was employed to prepare the TiO₂/SiO₂ supports, where incremental loadings of 8 wt% TiO₂ were impregnated onto SiO₂ followed by drying overnight and calcining as described above for each step.

2.1.2. Preparation of Supported WO₃/TiO₂/SiO₂ Catalysts

The supported x% WO₃/TiO₂/SiO₂ (x= 1, 3 and 5) catalysts were prepared by the incipient-wetness impregnation of aqueous solutions of ammonium metatungstate, (NH₄)₁₀W₁₂O₄₁·5H₂O (Pfaltz & Bauer, 99.5% purity) on the TiO₂/SiO₂ supports. The supported (1,3,5)% WO₃/12% TiO₂/SiO₂ and 5% WO₃/40% TiO₂/SiO₂ catalysts were dried overnight under ambient conditions

and subsequently dried in flowing air (Airgas, Zero Grade) at 120°C for 1 h and further calcined in flowing air at 450°C for 4 h.

2.1.3. Preparation of Supported $\text{VO}_x\text{-WO}_3/\text{TiO}_2/\text{SiO}_2$ Catalysts

The supported x% $\text{V}_2\text{O}_5\text{-WO}_3/\text{TiO}_2/\text{SiO}_2$ (x= 0.5, 1 and 2) catalysts were prepared by the incipient-wetness impregnation of isopropanol solutions of vanadium tri-isopropoxide ($\text{VO}[\text{CHO}(\text{CH}_3)_2]_3$, Alfa Aesar, 97%) onto the supported $\text{WO}_3/\text{TiO}_2/\text{SiO}_2$ catalysts. The preparation was performed inside a glovebox with continuously flowing N_2 (Airgas, Ultra High Purity) whereby the $\text{WO}_3/\text{TiO}_2/\text{SiO}_2$ catalysts were initially dried at 120°C to remove the physisorbed water before impregnation. After impregnation at room temperature, the samples were kept inside the glovebox under flowing N_2 overnight. The calcination of the supported (0.5, 1, 2)% $\text{V}_2\text{O}_5\text{-WO}_3/12\%\text{TiO}_2/\text{SiO}_2$ samples and 1% $\text{V}_2\text{O}_5\text{-5}\%\text{WO}_3/40\%\text{TiO}_2/\text{SiO}_2$ sample entailed ramping at 1°C/min to 120°C in flowing N_2 for 2 h, and then by another 1°C/min ramp under flowing air (Airgas, Zero Grade) up to 500°C for 4 h.

2.2. Catalyst Characterization

2.2.1. In Situ Raman Spectroscopy

The molecular structures of the V_2O_5 , WO_3 , TiO_2 and SiO_2 components of the supported $\text{V}_2\text{O}_5\text{-WO}_3/\text{TiO}_2/\text{SiO}_2$ catalysts were determined with *in situ* Raman spectroscopy employing visible (532 nm) laser excitation. The single stage Raman spectrometer (Horiba-Jobin Yvon, Lab Ram-HR) was equipped with a confocal

microscope (Olympus BX-30), a notch filter (Kaiser Super Notch), a Nd-YAG doubled diode pumped laser (Coherent Compass 315M-150; output power of 150 mW with sample power 10 mW), and the scattered photons were detected by a UV-sensitive liquid-N₂ cooled CCD detector (Horiba-Jobin Yvon, CCD-3000V). Laser excitation was at 532 nm and a spectral resolution of $\sim 2 \text{ cm}^{-1}$ was obtained for the given parameters, with 900 grooves/mm grating. The Raman spectrometer was also equipped with an environmentally-controlled high-temperature cell (Harrick) that examined the catalyst samples in loose powder form ($\sim 20 \text{ mg}$) that allowed for control of both the catalyst temperature and gaseous composition. *In situ* Raman spectra were collected for the supported catalysts under dehydrated conditions (400°C, 10% O₂/He). The spectral acquisition time employed was 20 scans for 20 seconds/scan for a total of $\sim 7 \text{ min/spectrum}$. System alignment was verified daily using a silica reference standard provided by Horiba-Jobin Yvon.

2.2.2. In Situ FT-IR Spectroscopy

The *in situ* IR spectroscopy measurements were performed with a Thermo Nicolet 8700 FT-IR spectrometer equipped with a DTGS detector. The reflectance FT-IR spectra were collected in the total reflection mode every 90 s with a resolution of 4 cm^{-1} and an accumulation of 72 scans. The reactor system employs a modified environmental reactor cell (Harrick, HVC-DR2) with CaF₂ windows and N₂-purged Praying Mantis chamber (DRA-2). The collection of the initial IR gas phase background was performed by placing a reflective mirror in the laser

path, while using the Harrick Praying Mantis attachment, at approximately the same height as a full sample cup of the Harrick Cell. Typically ~20 mg of the sample was placed into the reaction cell as loose powder. The composition of the reactant gas feed was controlled with mass flow controllers (Brooks 5850E) and the total gas flow rate was maintained as 30 mL/min. The procedures for sample pretreatment and exposure to different gaseous environments are described in detail in the CH₃OH-TPSR spectroscopy section below.

2.3 Reactivity Studies

2.3.1 CH₃OH-Temperature Programmed Surface Reaction (TPSR) Spectroscopy

The CH₃OH-TPSR spectroscopy experiments were performed on an AMI-200 temperature programmed system (Altamira Instruments) linked by a capillary tube to an online quadrupole mass spectrometer (Dycor DyMaxion DME200MS, Ametek Process Instruments). Typically, ~100 mg of catalyst was loaded in a U-type quartz tube and initially pretreated in flowing air at 450°C (Airgas, Ultra Zero Grade Air, 30 mL/min) for 45 min to remove any possible adsorbed organic impurities and to dehydrate the sample. To ensure that the surface VO_x and WO_x species remained in a fully oxidized state, the pretreated samples were cooled in air to 100°C. Different experimental CH₃OH-TPSR protocols were employed, with an adsorption step at 100°C, which was followed by a 30 min purge with helium (Airgas, Ultra High Purity, 30 mL/min) to remove any physically adsorbed species. After a He flush, a temperature ramp (10°C /min) from 100°C to 450°C was

employed. In the temperature programmed experiment, the corresponding gases (O_2 and/or He) were bubbled through liquid CH_3OH (Sigma-Aldrich, anhydrous, 99.8%), CD_3OD (Sigma-Aldrich, 100%, 99.96 atom %D) or $CH_3^{18}OH$ (Sigma-Aldrich, 95 atom % ^{18}O) through a saturator connected to the AMI-200 system to ensure a high gas phase concentration where noted.

The gases exiting from the quartz tube reactor were analyzed with the online mass spectrometer throughout the temperature programmed experiment. The following m/e ratios were employed for identification of the various desorbing gases Methanol: CH_3OH ($m/e = 31$) and CD_3OD ($m/e = 34$); Formaldehyde: H_2CO ($m/e = 30$) and D_2CO ($m/e = 32$), DME: CH_3OCH_3 ($m/e = 45$), CD_3OCD_3 ($m/e = 50$), CD_3OCH_3 ($m/e = 48$) and $CH_3^{18}OCH_3$ ($m/e = 47$); CO ($m/e = 28$); CO_2 ($m/e = 44$); H_2O ($m/e = 18$); MF: H_3COOCH ($m/e = 60$); DMM: $(CH_3O)_2CH_2$ ($m/e = 75$), $(CH_3O)_2CD_2$ ($m/e = 76$), $(CD_3O)_2CH_2$ ($m/e = 81$), $(CD_3O)_2CD_2$ ($m/e = 82$), $(CH_3O)(CD_3O)CH_2$ ($m/e = 78$), $(CH_3O)(CD_3O)CD_2$ ($m/e = 79$), $(CH_3^{18}O)_2CH_2$ ($m/e = 79$), and $(CH_3^{16}O)(CD_3^{18}O)CH_2$ ($m/e = 77$). For those desorbing molecules that gave rise to several fragments in the mass spectrometer, additional m/e values were also collected to further confirm their identity.

3. RESULTS

3.1. Characteristics of Supported VO_x - WO_x /TiO₂/SiO₂ Catalysts

3.1.1. In Situ Raman Spectra

The Raman spectrum of the dehydrated supported 1% V_2O_5 -

5%WO₃/40%TiO₂/SiO₂ catalyst is presented in the 200-1200 cm⁻¹ region in Figure 1A and a blowup of the 700-1200 cm⁻¹ region is shown in Figure 1B. The Raman spectrum in the 200-700 cm⁻¹ region is dominated by the vibrations of crystalline TiO₂(anatase) at 394, 508 and 630 cm⁻¹ [16]. The Raman bands associated with crystalline TiO₂(rutile) (142, 445, and 610 cm⁻¹) and crystalline TiO₂(brookite) (242, 320, 363, and 407 cm⁻¹) are not present in Figure 1A [15,16]. The Raman spectrum of the dehydrated supported 1%V₂O₅-5%WO₃/40%TiO₂/SiO₂ catalysts in the 700-1200 cm⁻¹ region, Figure 1B, reveals that neither crystalline WO₃ (strong bands at 804, 710 and 270 cm⁻¹) [17] or crystalline V₂O₅ (strong band at 995, 690 and 525 cm⁻¹) [18] nanoparticles (NPs) are present in the synthesized bifunctional catalyst. The Raman bands at 1013 and 1030 cm⁻¹ are related to the vibrations of the surface WO_x and VO_x species, respectively [15].

The Raman spectrum of the dehydrated supported 2%V₂O₅-5%WO₃/12%TiO₂/SiO₂ catalyst in the 200-1200 cm⁻¹ region is presented in Figure 2A. The 200-700 cm⁻¹ region of the Raman spectrum, however, shows no bands for crystalline TiO₂(anatase) at 394, 508 and 630 cm⁻¹, indicating that all of the titania is 100% molecularly dispersed on the silica support. The 700-1200 cm⁻¹ region of the Raman spectrum in Figure 2A is dominated by the vibrations of surface WO_x and VO_x species. The strong band at 1030 cm⁻¹ is characteristic for surface VO_x species and the shoulder at 1011 cm⁻¹ indicates the presence of surface WO_x species [15].

The Raman spectrum for the dehydrated supported 0.5% V₂O₅-5% WO₃/12% TiO₂/SiO₂ catalyst is shown in Figure 2B. Crystalline TiO₂ phases are not present in this catalyst, as indicated by the absence of Raman bands in the 200-700 cm⁻¹ region, which indicates the presence of highly dispersed surface TiO_x domains on the SiO₂ support. The bands at 1011 and 1030 cm⁻¹ are related to the surface WO_x and VO_x species, respectively.

The Raman spectrum for the dehydrated supported 1% V₂O₅-3% WO₃/12% TiO₂/SiO₂ catalyst is shown in Figure 2C. Similar to the Raman spectrum for the supported 2% V₂O₅-5% WO₃/12% TiO₂/SiO₂ catalyst in Figure 2A, no crystalline TiO₂ Raman bands are observed in the 200-1200 cm⁻¹ region in Figure 2C for the supported 1% V₂O₅-3% WO₃/12% TiO₂/SiO₂ catalyst, again indicating that titania is molecularly dispersed on the SiO₂ surface. The 800-1200 cm⁻¹ region of the Raman spectrum in Figure 2C possesses two distinct Raman bands at 1011 and 1030 cm⁻¹, indicative of surface WO_x and VO_x species, respectively.

The Raman spectrum of the supported 1% V₂O₅-1% WO₃/12% TiO₂/SiO₂ catalyst is presented in Figures 2D. The titania phase must be molecularly dispersed on the SiO₂ support since Raman bands from crystalline TiO₂ phases are absent. Weak Raman bands from the surface VO_x and WO_x species are present in Figure 2D at 1030 and 1011 cm⁻¹, respectively, with the surface WO_x band being a shoulder on the stronger VO_x band. [15]

3.2 Reactivity Studies

3.2.1. *In Situ Raman spectroscopy during methanol chemisorption*

The *in situ* Raman spectra of the supported 1%V₂O₅-5%WO₃/40%TiO₂/SiO₂ catalyst during methanol adsorption at 100°C provide insights about the catalyst structural changes occurring during methanol adsorption and are shown in Figure 3. The Raman bands from the surface WO_x (initially at 1011 cm⁻¹) and the surface VO_x species (initially at 1031 cm⁻¹) decrease in intensity, broaden and red shift upon adsorption of methanol. These changes are related to methanol coordination at the surface WO_x and VO_x sites [19]. The larger perturbation of the Raman bands of the surface VO_x species may reflect greater interaction between chemisorbed methanol and the surface VO_x sites than at the surface WO_x sites.

3.2.2. *In Situ IR spectroscopy during methanol chemisorption*

The corresponding *in situ* IR spectrum of the supported 1%V₂O₅-5%WO₃/40%TiO₂/SiO₂ catalyst during methanol adsorption at 100°C contain information about the nature of the surface methanol species and are presented in Figure 4. The IR spectrum prior to methanol adsorption on the dehydrated catalyst sample in the O₂/He environment has been subtracted from that of the methanol exposed surface to isolate the surface vibrations resulting from adsorbed methanol. The IR bands at ~2956 ν_s(CH₃) and ~2852 cm⁻¹ [2δ_s(CH₃)] arise from Si-OCH₃ intermediates and is also reflected in the parallel decrease in the sharp Si-OH IR

band at $\sim 3700\text{ cm}^{-1}$ (not shown for brevity)[19,22,23]. The IR bands at 2930 [$\nu_s(\text{CH}_3)$], 2896 [$2\delta_{\text{as}}(\text{CH}_3)$] and 2833 cm^{-1} [$2\delta_s(\text{CH}_3)$] are related to surface M-OCH₃ species [19-23]. Surface Ti-OCH₃ species vibrate at ~ 2920 and 2820 cm^{-1} and are probably not the coordination site for the surface methoxy species, which also reflects coverage of exposed titania sites by the surface WO_x and VO_x species. [15]. It is not, however, possible to discriminate between the surface V-OCH₃ and W-OCH₃ species since they both vibrate at the same frequencies of ~ 2930 and $\sim 2830\text{ cm}^{-1}$ [15, 19,22,23]. Thus, surface Si-OCH₃ and V-OCH₃/W-OCH₃ intermediates are present on the supported 1% V₂O₅-5% WO₃/40% TiO₂/SiO₂ catalyst upon methanol adsorption at 100°C.

3.2.3. CH₃OH-TPSR Spectroscopy DMM/CH₃OH. The CH₃OH-TPSR experiments were performed after the chemisorption of methanol at 100°C as indicated in the above IR and Raman spectroscopy studies and the catalysts were subsequently flushed in flowing He for 30 minutes to desorb physically adsorbed methanol. The CH₃OH-TPSR studies were then initiated in different environments. In flowing O₂/He, the major reaction product from the supported 1% V₂O₅-5% WO₃/40% TiO₂/SiO₂ catalyst is HCHO (T_p=190°C) from the redox surface VO_x sites and DME (T_p=320°C) from the acidic surface WO_x sites as shown in Figure 5. When the reaction is performed with isotopically labeled CD₃OD-TPSR, the T_p value for DCDO formation shifts from 190 to 230°C (see Supporting Information Figure S1). Such a T_p shift reflects the well-known isotopic effect when the rate-

determining-step (rds) involves breaking the C-H bond of the chemisorbed surface methoxy species [41,42]. Surprisingly, DMM is not produced as a reaction product under these reaction conditions.

The absence of DMM production suggests that gas phase methanol must be present during the CH₃OH-TPSR reaction in order for the formation of DMM, which requires coupling of three methanol molecules. Consequently, the CH₃OH-TPSR experiment was repeated with the supported 1% V₂O₅-5% WO₃/40% TiO₂/SiO₂ catalyst in flowing CH₃OH/O₂/He during the temperature ramp and indeed DMM now formed with a T_p value of ~180°C as shown in Figure 6.

Repeating the methanol-TPSR experiment with deuterium labeled CD₃OD, CD₃OD-TPSR, in flowing CD₃OD/O₂/He over the supported 1% V₂O₅-5% WO₃/40% TiO₂/SiO₂ catalyst shifts the DMM T_p value from 180 to 200°C as presented in Figure 7.

The T_p shift from 180 to 200°C in formation of DMM indicates that breaking the surface methoxy C-H/C-D bond is involved in the rds of DMM formation.

DMM/CH₃¹⁸OH. When the methanol-TPSR experiment is repeated with oxygen-18 labeled CH₃¹⁸OH in flowing CH₃¹⁸OH/O₂/He over the supported 1% V₂O₅-5% WO₃/40% TiO₂/SiO₂ catalyst, the DMM T_p value occurs at 175°C in comparison to 180°C with unlabeled CH₃OH as shown in Figure 8.

The similar T_p values for DMM formation during the CH_3OH -TPSR and $\text{CH}_3^{18}\text{OH}$ -TPSR experiments reveals that breaking of the C-O bond is not involved in the rds of DMM formation. If C-O bond breaking were involved in the rds of DMM formation, then the T_p value from $\text{CH}_3^{18}\text{OH}$ -TPSR would have moved to slightly higher values than found from CH_3OH -TPSR.

Source of Oxygen. To examine the roles of surface lattice oxygen and gas phase molecular O_2 in DMM production, the CH_3OH -TPSR studies were performed over the supported 1% V_2O_5 -5% WO_3 /40% TiO_2 /SiO₂ catalyst in the presence and absence of gas phase molecular O_2 . As shown in Figure 9, the T_p value for DMM formation is 180°C and independent of the presence of molecular O_2 during the CH_3OH -TPSR experiment. The ability of the supported 1% V_2O_5 -5% WO_3 /40% TiO_2 /SiO₂ catalyst to be able to conduct the experiment in the absence of molecular O_2 indicates that the redox step during DMM formation is occurring with surface lattice oxygen (Mars-van Krevelen reaction mechanism) and that gas phase molecular O_2 is not involved in the rds for DMM formation. The constant DMM T_p 's during the CH_3OH -TPSR experiments with or without gas phase O_2 suggests that the surface VO_x and WO_x sites remain fully oxidized by the supply of bulk lattice oxygen since the T_p value is known to increase as the surface species become reduced [37].

Influence of TiO_2 Domain Size. The influence of TiO_2 domain size upon DMM formation was examined by varying the TiO_2 loading from 12 to 40% of the

supported 1% V₂O₅-5% WO₃/TiO₂/SiO₂ catalysts. Increasing the TiO₂ domain size from surface TiO₅ polymers (12% TiO₂) to 5-9 nm TiO₂ NPs (30 and 40% TiO₂) [15] systematically decreases the T_p value for DMM formation as shown in Figure 10. The same trend was previously found for methanol oxidation to formaldehyde by the surface VO_x sites [15] suggesting that the redox surface VO_x sites are intimately involved in the rds of DMM formation.

Influence of Redox Surface VO_x Loading. To further investigate the participation of the surface VO_x in the formation of DMM, CH₃OH-TPSR experiments where the surface VO_x loading is varied from 0.5 to 2% V₂O₅ were investigated and the findings are presented in Figure 11. In the absence of vanadia, the supported 5% WO₃/12% TiO₂/SiO₂ catalyst only yields a trace amount of DMM. Increasing the surface VO_x concentration increases the amount of DMM formed and decreases the DMM T_p value. The dependence of DMM formation amount on surface VO_x concentration indicates that the redox surface VO_x sites are involved in the rds of the DMM formation reaction, which is further reflected by the decreasing T_p value for DMM formation with the surface VO_x concentration.

Influence of Acidic WO_x Loading. The corresponding studies examining the influence of the acidic surface WO_x concentration upon DMM formation varied the WO_x loading from 1 to 3% WO₃ and the results are shown in Figure 12. In the absence of tungsten, the supported 1% V₂O₅/12% TiO₂/SiO₂ catalyst only yields a trace amount of DMM. Although the DMM T_p temperatures do not change with

surface WO_x concentration, the amount of DMM produced increases with acidic surface WO_x concentration indicating that the acidic surface WO_x sites are involved in the formation of DMM. [The constant T_p value for DMM formation suggests, however, that the acidic surface WO_x sites may not be involved in the rds of DMM formation.]

DMM/ CH_3OH // CD_3OD . To obtain additional insights about the interactions between gas phase methanol and chemisorbed methanol species during the methanol-TPSR experiment, CH_3OH was initially chemisorbed and the flowing gas during the methanol-TPSR experiment consisted of isotopically labeled $\text{CD}_3\text{OD}/\text{O}_2/\text{He}$. Under such reaction conditions, $\text{H}_2\text{C}(\text{OCH}_3)_2$ was not formed and D-containing DMM isotopes represented the major reaction products. As shown in Figure 13, the relative concentration of the DMM isotopes was $\text{D}_2\text{C}(\text{OCD}_3)_2$ ($T_p=190^\circ\text{C}$) > $\text{H}_2\text{C}(\text{OCH}_3)(\text{OCD}_3)$ ($T_p=178^\circ\text{C}$) > $\text{H}_2\text{C}(\text{OCD}_3)_2$ ($T_p=184^\circ\text{C}$).

3.2.4. DMM/ CH_3OH // CD_3OD Methanol-Temperature Programmed-IR (TP-IR) Spectroscopy

To learn more about the surface intermediates present on the supported 1% V_2O_5 -5% WO_3 /40% $\text{TiO}_2/\text{SiO}_2$ catalyst during the methanol-TPSR experiment, the previous reaction with initial adsorption of CH_3OH and flowing $\text{CD}_3\text{OD}/\text{O}_2/\text{He}$ was monitored with methanol-TP-IR and the resulting IR spectra are presented in Figure 14.

As described in the previous section, surface V-OCH₃, W-OCH₃ and Si-OCH₂ species are present on the catalyst surface after CH₃OH chemisorption at 100°C. The dynamic equilibrium between gas phase CD₃OD and surface CH₃O* and intact CH₃OH* is reflected in the immediate decrease in the intensity of the C-H vibrations of the surface CH₃O* intermediates at ~2800-3000 cm⁻¹ and increase in the C-D vibrations of surface CD₃O* intermediates at ~2050-2250 cm⁻¹, which are presented in Figure 18A. The rapid exchange between gas phase CD₃OD and weakly adsorbed intact surface CH₃OH in the presence of the methanol-containing atmosphere is also indicated by the shift of the broad methanol ν(OH) vibrations at ~3350 cm⁻¹ to the broad methanol ν(OD) vibrations ~2514 cm⁻¹. In addition, the sharp Si-OH IR vibration at 3745 cm⁻¹ (not shown in Figure 14A for brevity) is also replaced with the sharp Si-OD IR vibration at 2756 cm⁻¹. With increasing reaction temperature, the surface concentration of all the surface intermediates (CH₃O*, CH₃OH*, CD₃O* and CD₃OD*) progressively decrease signifying their consumption by the catalyzed reactions and desorption from the catalyst.

New surface reaction intermediates are also formed with increasing catalyst temperature as displayed in the TP-IR spectra of Figure 14B. Once the reaction is initiated, the IR bands for the surface CH₃O* species (~1459 and ~1437 cm⁻¹) decrease and new vibrations from surface H₂COO* species (~1485 and ~1453 cm⁻¹) are present until above 200°C. These new IR bands compare well with dioxymethylene-organic compounds such as H₂C(OCD₃)₂, dioxolane-d₄, and

several dioxymethylene aromatics [14]. At higher temperatures of 260-332°C, a new IR peak appears at $\sim 1540\text{ cm}^{-1}$ from the surface HCOO* intermediate [14,20]. At 400°C, the surface reaction intermediates are almost absent due to their very fast reaction rates towards products at such high temperature. Thus, the IR spectrum at 400°C mostly consists of vibrations from Si-OD and gas phase CD₃OD.

4. DISCUSSION

Molecular Structure of Silica-Supported TiO₂, V₂O₅ and WO₃ Phases. The *in situ* Raman spectra of the dehydrated supported V₂O₅-WO₃/TiO₂/SiO₂ catalysts demonstrate that the supported vanadium oxide and tungsten oxide phases are exclusively present as dispersed surface metal oxide phases, but the titania phase is present as either a surface phase or crystalline TiO₂(anatase) depending on the titania loading. Although the surface TiO_x phase doesn't give rise to strong Raman bands, the presence of the surface TiO_x phase is reflected by the absence of the strong TiO₂(anatase) Raman vibrations [16]. For the 12% TiO₂/SiO₂ catalyst, it is estimated from UV-vis spectroscopy measurements that the surface TiO_x phase consists of ~ 1 nm domains of surface polymeric TiO_x species [15]. For higher titania loadings of TiO₂/SiO₂, the supported TiO₂/SiO₂ catalysts possess ~ 2 -9 nm sized crystalline TiO₂(anatase) NPs with increasing crystallite size as a function of titania loading.

The *in situ* Raman spectra of the dehydrated supported V₂O₅-WO₃/TiO₂/SiO₂ catalysts also contain molecular structural information about the

surface WO_x and VO_x species. For dehydrated supported WO_3/SiO_2 , the primary Raman vibration occurs at $\sim 980 \text{ cm}^{-1}$, characteristic of dioxo surface $(\text{O}=\text{O})_2\text{WO}_2$ species [15,25], with a weaker vibration at $\sim 1010 \text{ cm}^{-1}$, associated with mono-oxo surface $\text{O}=\text{WO}_4$ species [25-30]. For dehydrated supported WO_3/TiO_2 , only one Raman vibration occurs at $\sim 1010 \text{ cm}^{-1}$ from mono-oxo surface $\text{O}=\text{WO}_4$ species [15,25-30]. The surface WO_x species present in the supported $\text{V}_2\text{O}_5\text{-WO}_3/\text{TiO}_2/\text{SiO}_2$ catalysts exhibit a Raman band at $\sim 1011 \text{ cm}^{-1}$ and, thus, are present as mono-oxo surface $\text{O}=\text{WO}_4$ species. The surface VO_x species present in the supported $\text{V}_2\text{O}_5\text{-WO}_3/\text{TiO}_2/\text{SiO}_2$ catalysts exhibit a Raman band at $\sim 1031 \text{ cm}^{-1}$ characteristic of mono-oxo surface $\text{O}=\text{VO}_3$ species [15, 31-34].

The Raman spectra of the surface WO_x and VO_x species present in the dehydrated supported $\text{V}_2\text{O}_5\text{-WO}_3/\text{TiO}_2/\text{SiO}_2$ catalysts also contain information about the specific location of these surface species. The mono-oxo surface WO_5 species give rise to a Raman band at $\sim 1011 \text{ cm}^{-1}$ that indicates they are coordinated to TiO_x sites since supported WO_3/SiO_2 exhibits Raman bands at 980 (s) and 1010 (w) cm^{-1} while supported WO_3/TiO_2 possesses only one Raman band at $\sim 1010 \text{ cm}^{-1}$ [25]. This conclusion is directly confirmed with aberration corrected-TEM imaging that shows that the surface WO_5 species are located on the titania domains [43]. For the dehydrated supported $\text{V}_2\text{O}_5/\text{SiO}_2$ and $\text{V}_2\text{O}_5/\text{TiO}_2$ catalysts, the mono-oxo surface VO_4 species vibrate at $\sim 1036\text{-}1040 \text{ cm}^{-1}$ [33] and $\sim 1027\text{-}1031 \text{ cm}^{-1}$ [35], respectively. The appearance of the mono-oxo VO_4 vibration for the

dehydrated supported $V_2O_5WO_3/TiO_2/SiO_2$ catalysts at $\sim 1031\text{ cm}^{-1}$ signifies that the surface VO_4 species also preferentially coordinates to the TiO_x sites rather than the exposed SiO_2 sites. Additionally, the *in situ* IR spectroscopy measurements of the surface CH_3O^* species only reveal vibrations for Si-OCH₃ and V-OCH₃/W-OCH₃ and not for Ti-OCH₃ consistent with the conclusion that the exposed TiO_x sites are covered by the surface VO_x and WO_x species. Thus, both the surface WO_4 and VO_4 self-assemble at the exposed TiO_x sites rather than the exposed SiO_2 support sites.

Surface Reaction Intermediates. The *in situ* IR spectroscopic investigation of the bifunctional supported $V_2O_5-WO_3/TiO_2/SiO_2$ catalysts reveals that surface CH_3O^* is the most abundant reaction intermediates (MARI) after methanol chemisorption at 100°C (see Figure 4). The TP-IR and CH_3OH -TPSR spectroscopy studies in the presence of flowing gas phase $CH_3OH/O_2/He$ demonstrate that the surface CH_3O^* species are being consumed and converted to the reaction products. The isotopically labeled CD_3OD/CH_3OH -TPSR experiment yielded the mixed isotopic products $H_2C(OCH_3)(OCD_3)$ and $H_2C(OCD_3)_2$ reflecting the participation of the initial surface CH_3O^* species and their reaction with the deuterated methanol in the formation of DMM. Under the temperature programmed reaction conditions, a surface dioxymethylene (H_2COO^*) intermediate is also present in the temperature range of ~ 120 - 200°C . The surface H_2COO^* intermediate forms by oxidation of HCHO that is produced from the oxidative dehydrogenation of the surface CH_3O^*

species. The surface dioxymethylene intermediate has been proposed by Busca *et al.* [14], as the key reaction intermediate involved in coupling surface CH_3O^* species to form DMM. The formation of the mixed isotopes $\text{H}_2\text{C}(\text{OCH}_3)(\text{OCD}_3)$ and $\text{H}_2\text{C}(\text{OCD}_3)_2$ from $\text{CD}_3\text{OD}/\text{CH}_3\text{OH}$ -TPSR experiment is consistent with the participation of the initial surface CH_3O^* species, and presumably via its corresponding surface H_2COO^* intermediate, in the coupling of surface methoxy intermediates in the formation of DMM.

The selective oxidation of CH_3OH to DMM involves the participation of three methanol molecules and, thus, requires high surface CH_3O^* coverage that approaches monolayer coverage to allow this trimerization reaction to occur. In the absence of gas phase CH_3OH , monolayer or high surface methoxy coverage cannot be sustained and the surface CH_3O^* reaction intermediates are almost completely converted to HCHO (see Figure 5). In the presence of gas phase CH_3OH , DMM formation can only be sustained between the temperatures of ~ 100 - 250°C since this corresponds to the temperature range where the surface CH_3O^* and H_2COO^* reaction intermediates still maintain appreciable surface coverage on the supported V_2O_5 - $\text{WO}_3/\text{TiO}_2/\text{SiO}_2$ catalysts during the $\text{CH}_3\text{OH}/\text{CH}_3\text{OH}$ -TPSR study (see Figure 14). The surface CH_3O^* and H_2COO^* reaction intermediates are almost nonexistent above 300°C during the $\text{CH}_3\text{OH}/\text{CH}_3\text{OH}$ -TPSR spectroscopy study (see Figure 14). The formation of the mixed isotope product $\text{H}_2\text{C}(\text{OCH}_3)(\text{OCD}_3)$ during the $\text{CD}_3\text{OD}/\text{CH}_3\text{OH}$ -TPSR experiment reveals that DMM can form from

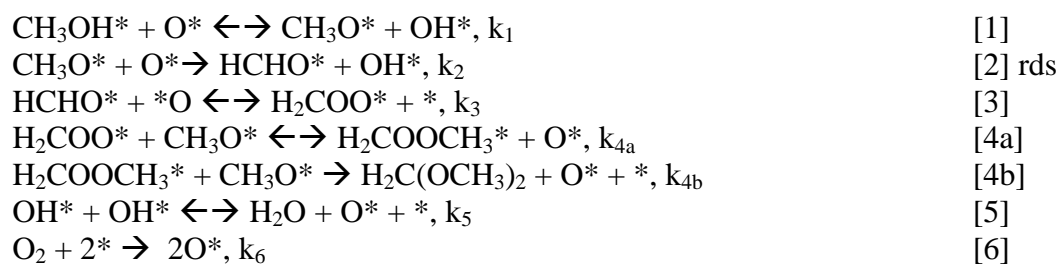
surface CH_3O^* intermediates. This implies that gas phase CD_3OD does not directly participate in formation of DMM via an Eley-Rideal mechanism, but CD_3OD needs to first dissociatively adsorb as surface CD_3O^* species. Thus, the role of gas phase CH_3OH during methanol oxidation to DMM in the $\text{CH}_3\text{OH}/\text{CH}_3\text{OH}$ -TPSR experiment is to maintain a high surface coverage of the surface CH_3O^* reaction intermediate and its oxidation products of HCHO or H_2COO^* that couple two additional surface methoxy species to form DMM trimer.

Catalytic Active Sites. The CH_3OH -TPSR experiments reveal that both surface VO_x and surface WO_x species are involved in DMM formation since DMM barely forms in the absence of either of these sites and the DMM amount increases with surface coverage of surface WO_x and VO_x species. The formation of DMM/ CH_3OH occurs in the same temperatures range as formation of $\text{HCHO}/\text{CH}_3\text{OH}$ suggesting that it is the redox surface VO_x sites that are dominating the rds for DMM formation. This conclusion is further supported by the increase of DMM formation and decrease in DMM T_p temperature with increasing TiO_2 domain size that is known to enhance the activity of redox surface VO_x sites, but decrease the activity of the acidic surface WO_x sites [15]. Another significant difference between the influence of the surface VO_x and WO_x species is that the DMM T_p values decrease with increasing surface VO_x coverage and the DMM T_p values remain constant with increasing surface WO_x coverage. These collective characteristics of the redox surface VO_x sites suggest that they are the catalytic

active sites responsible for coupling of surface H_2COO^* reaction intermediate with two additional surface CH_3O^* species to form DMM. The constant DMM T_p value with varying surface WO_x coverage suggests that the surface WO_x sites just store the surface CH_3O^* species that are needed to couple with the surface H_2COO^* involved in the rds for DMM formation. This conclusion, thus, suggests that the acidic surface WO_x species are not contributing to the kinetics of the surface rds for DMM formation, and the redox surface VO_x sites control the kinetics for DMM formation.

Surface Reaction Mechanism. The rapid exchange between surface CH_3O^* intermediates and gas phase CD_3OD during the $\text{CD}_3\text{OD}/\text{CH}_3\text{OH}$ -TPSR study reveals the facile reversible exchange between the surface methoxy species on the surface VO_x and WO_x sites and gas phase methanol (reaction step 1 below). The selective oxidation of CH_3OH to $\text{H}_2\text{C}(\text{OCH}_3)_2$ over the bifunctional supported $\text{V}_2\text{O}_5\text{-WO}_3/\text{TiO}_2/\text{SiO}_2$ catalysts involves both the redox surface VO_x sites and the acidic surface WO_x sites, but the rds involves the irreversible breaking of the C-H bond of the surface CH_3O^* reaction intermediate to form HCHO by the redox surface VO_x sites (reaction step 2 below). The conversion of surface HCHO^* to H_2COO^* also occurs on the surface redox VO_x sites (reaction step 3) and has been shown to be a facile reversible reaction [44]. The coupling of surface H_2COO^* with two additional surface CH_3O^* species is facilitated by adjacent or nearby acidic surface WO_x sites that store the surface CH_3O^* intermediates and is a rapid kinetic

step (reaction steps 4a and 4b below). Although the first surface methoxy coupling step 4a may be reversible, the second surface methoxy coupling step 4b is irreversible since the DMM reaction products immediately desorb from the catalyst. The recombination of the product surface hydroxyls to form water (step 5) is reversible since H₂O efficiently dissociates on surface O* species to form surface hydroxyls [45]. In the final reaction step (reaction step 6), the reduced surface VO_x sites are reoxidized by dissociative adsorption of gas phase molecular O₂. The reoxidation of the reduced surface VO_x sites by gas phase O₂ is irreversible since surface O* does not recombine to form gas phase molecular O₂ at these low reaction temperatures. From these fundamental molecular level insights, the following surface reaction mechanism is proposed for the selective oxidation of methanol to dimethoxymethane over the bifunctional supported V₂O₅-WO₃/TiO₂/SiO₂ catalysts.



The in situ spectroscopic results have provided molecular level insights into the mechanism of methanol oxidation to dimethoxymethane for the first time. The fundamental studies presented have shown that the selective oxidation of methanol to DMM is influenced by the surface vanadium density in the sub-monolayer

region and sensitive to the nature of acid sites, possibly favoring Brønsted acidity and redox activity.

5. CONCLUSIONS

A bifunctional acidic-redox supported V_2O_5 - WO_3 / TiO_2 / SiO_2 catalyst was molecularly designed whereby catalytic active VO_4 and WO_5 surface sites were 100% dispersed and self assembled onto an underlying TiO_2 surface that was anchored to an inert silica surface. The selective oxidation of methanol to dimethoxymethane reaction proceeds via surface CH_3O^* species as the most abundant reactive intermediate, and the rate determining step is C-H bond breaking of surface CH_3O^* species. The catalytically active VO_x sites are directly involved in the rate determining step, whereas the surface WO_x sites are involved in coupling of CH_3O^* with HCHO to form DMM.

ACKNOWLEDGEMENTS

The authors gratefully acknowledge the financial support by the NSF NIRT Grant 0609018.

REFERENCES

1. Y. Fu, J. Shen, *Chem. Commun.*, (2007) 2172
2. P. Pepiot-Desjardins, H. Pitsch, R. Malhotra, S.R. Kirby, A.L. Boehman, *Combustion and Flame* **154** (2008) 191
3. G.P. Hagen, M.J. Spangler, *U.S. Patent* 6,437,195 (2002)
4. E. Stroofer, H. Hasse, S. Blagov, *U.S. Patent* 7,700,809 (2010)
5. Y. Ren, Z. Huang, H. Miao, Y. Di, D. Jiang, K. Zeng, B. Liu, X. Wang, *Fuel* **87** (2008) 2691
6. J. Liu, Y. Fu, Q. Sun, J. Shen, *Microporous and Mesoporous Materials* **116** (2008) 614
7. Q. Sun, Y. Fu, J. Liu, A. Auroux, J. Shen, *Appl. Catal. A: General* **334** (2008) 26
8. H. Zhao, S. Bennici, J. Cai, J. Shen, A. Auroux, *Catal. Today* **152** (2010) 70
9. X. Lu, Z. Qin, M. Dong, H. Zhu, G. Wang, Y. Zhao, W. Fan, J. Wang, *Fuel* (2011) doi: 10.1016/j.fuel.2011.01.007
10. M. Badlani, I.E. Wachs, *Catal. Lett.* **75** (2001) 137
11. J. M. Tatibouet, *Appl. Catal. A: General* **148** (1997) 213
12. T. Kim, I.E. Wachs, *J. Catal.* **255** (2008) 197
13. J.M. Tatibouet, H. Lauron-Pernot, *J. Mol. Catal. A: Chemical* **171** (2001) 205
14. G. Busca, A.S. Elmi, P. Forzatti, *J. Phys. Chem.* **91** (1987) 5263

15. E.I. Ross-Medgaarden, I.E. Wachs, W.V. Knowles, A. Burows, C.J. Kiely, M.S. Wong, *J. Am. Chem. Soc.* **131** (2009) 680
16. X. Gao, S.R. Bare, J.L. Fierro, M.A. Banaras, I.E. Wachs, *J. Phys. Chem. B* **102** (1998) 5653.
17. T. Kim, A. Burrows, C.J. Kiely, I.E. Wachs, *Journal of Catalysis* **246** (2007) 370
18. T. Kim, I.E. Wachs, *Journal of Catalysis* **255** (2008) 197
19. L.J. Burcham, G. Deo, X. Gao, I.E. Wachs, *Topics in Catalysis* **11/12** (2000) 85
20. L.J. Burcham, I.E. Wachs, *Catalysis Today* **49** (1999) 467
21. L.J. Burcham, L.E. Briand, I.E. Wachs, *Langmuir* **17** (2001) 6164
22. L.J. Burcham, L.E. Briand, I.E. Wachs, *Langmuir* **17** (2001) 6175
23. L.J. Burcham, M. Badlani, I.E. Wachs, *Journal of Catalysis* **203** (2001) 104
24. P. Mars, D.W. van Krevelen, *Chem. Eng. Sci. (Spec. Suppl)* **3** (1954) 41
25. E. Lee, I.E. Wachs, *J. Phys. Chem. C.* **111** (2007) 14410-14425.
26. I.E. Wachs, *Catal. Today* **27** (1996) 437
27. D.S. Kim, M. Ostromecki, I.E. Wachs, *J. Mol. Catal. A Chem.* **106** (1996) 93.
28. M.A. Vuurman, I.E. Wachs, *J. Phys. Chem.* **96** (1992) 5008.
29. J. Jarupatrakorn, M.P. Coles and T.D. Tilley, *Chem. Mater.*, **17** (2005) 1818.

30. K. Nakamoto, *Infrared and Raman Spectra of Inorganic Coordination Compounds* (5th ed); Wiley & Sons: New York, 1997.
31. H. Eckert, I.E. Wachs, *J. Phys. Chem.* **93** (1989) 6796.
32. N. Das, H. Eckert, H. Hu, I.E. Wachs, J.F. Walzer and F. Feher, *J. Phys. Chem*
33. X. Gao, S.R. Bare, B. M. Weckhuysen and I.E. Wachs, *J. Phys. Chem. B* **102** (1998) 10842.
34. X. Gao, S.R. Bare, I.E. Wachs, *J. Phys. Chem. B* **103** (1999) 618.
35. G. Deo and I.E. Wachs, *J. Catal.* **146** (1994) 335.
36. M.A. Vuurman, I.E. Wachs, A.M. Hirt, *J. Phys. Chem.* **95** (1991) 9928
37. I.E. Wachs, J-M. Jehng, W. Ueda, *J. Phys. Chem. B* **109** (2005) 2275
38. A.M. Turek, I.E. Wachs, E. DeCanio, *J. Phys. Chem.* **96** (1992) 5000
39. M.V. Martinez-Huerta, X. Gao, H. Tian, I.E. Wachs, J.L.G. Fierro, M.A. Banares, *Catalysis Today* **118** (2006) 279
40. T. Kim, *Fundamental Structure-Activity Relationships for Supported Metal Oxide Catalysts*, (2007) Lehigh University Dissertation
41. I.E. Wachs, R.J. Madix, *J. Catal.* **30** (1978) 208
42. W.E. Farneth, F. Ohuchi, R.H. Staley, U. Chowdhry, A. Sleight, *J. Phys. Chem.* **89** (1985) 2493

43. W. Zhou, K.F. Doura, M. Watanabe, A.A. Herzing, E. Okunishi, E.I. Ross-Medgaarden, I.E. Wachs, C.J. Kiely, *ChemCatChem* (2011); DOI: 10.1002/cctc.201000273
44. I.E. Wachs, R.J. Madix, *App. of Surf. Sci.* **5** (1980) 426
45. E.L. Lee, I.E. Wachs, *J. Phys. Chem. C* **112** (2008) 6487

FIGURES

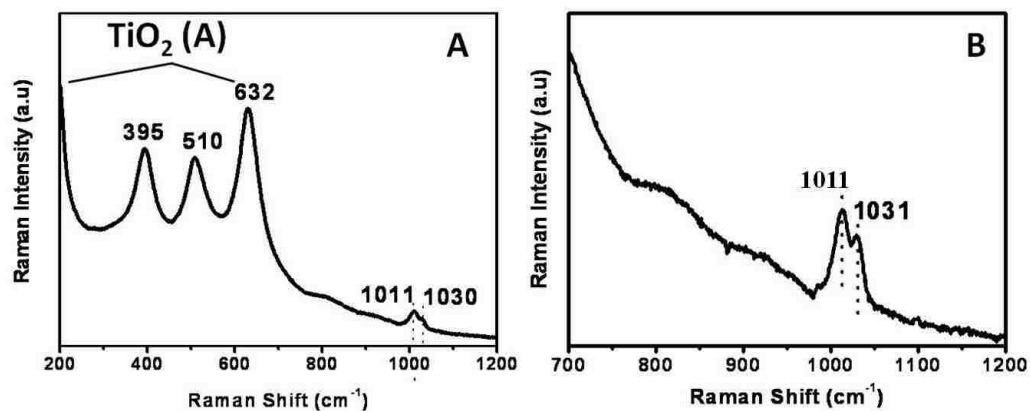


Figure 3.1. *In situ* Raman spectrum (532 nm) of the dehydrated supported 1%V₂O₅-5% WO₃/ 40%TiO₂/SiO₂ catalyst in [A] 200-1200 cm⁻¹ region that is dominated by TiO₂(A) bands and [B] 700-1200 cm⁻¹ region that is dominated by the WO_x and VO_x vibrations.

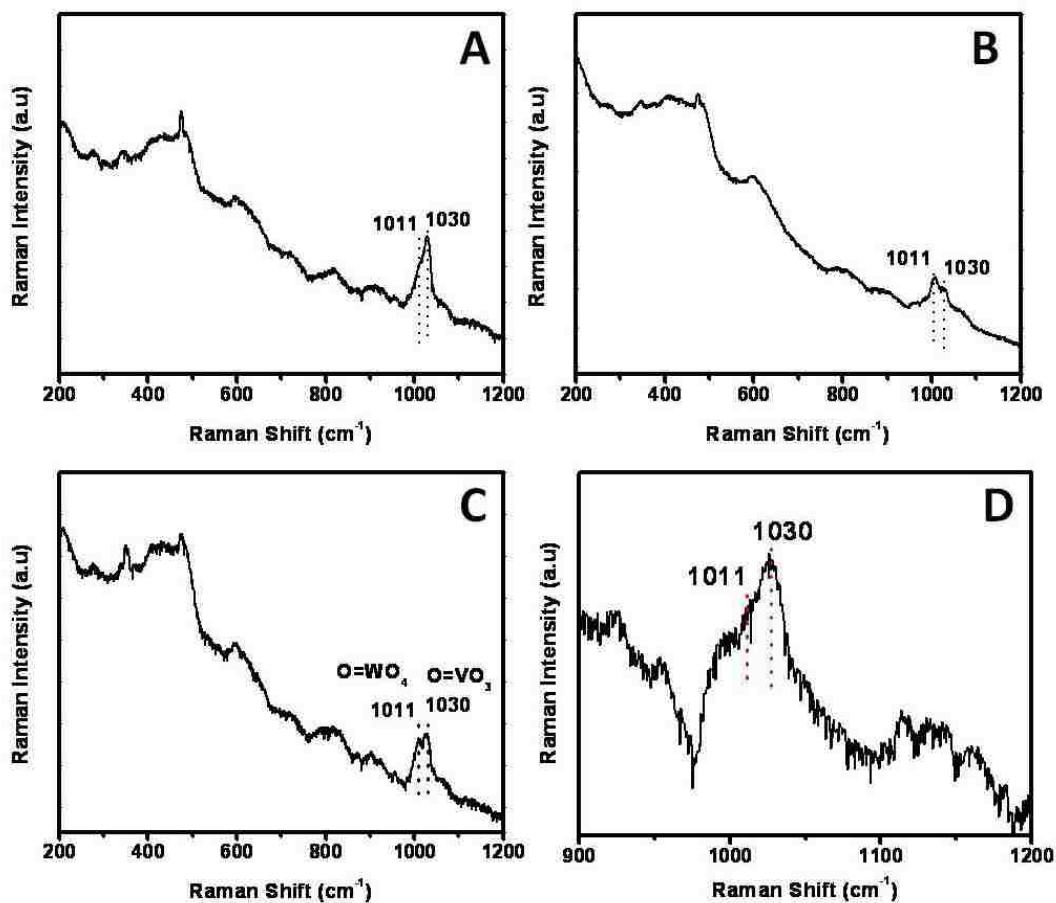


Figure 3.2. *In situ* Raman spectrum (532 nm) of the dehydrated 12% TiO₂/SiO₂ supported catalysts [A] 2% V₂O₅–5% WO₃/12% TiO₂/SiO₂ catalyst [B] 0.5% V₂O₅–5% WO₃/12% TiO₂/SiO₂ catalyst [C] 1% V₂O₅–3% WO₃/12% TiO₂/SiO₂ catalyst [D] 1% V₂O₅–1% WO₃/ 12% TiO₂/SiO₂ catalyst in the 900-1200 cm⁻¹ region that is dominated by the WO_x and VO_x vibrations.

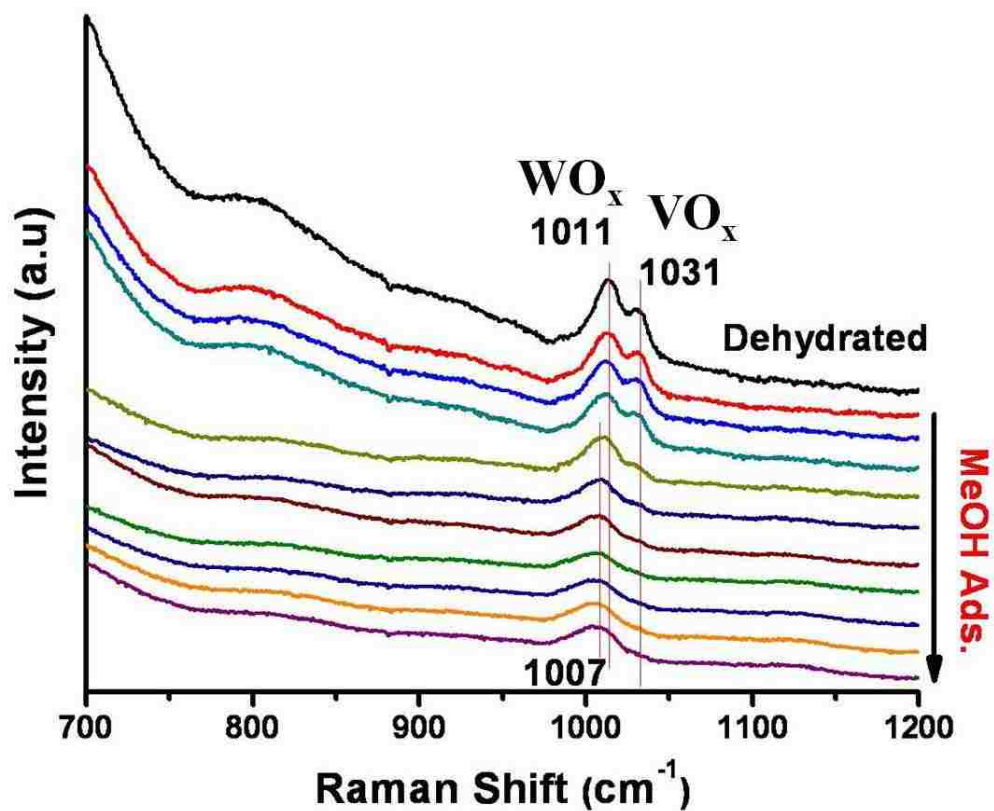


Figure 3.3. *In Situ* Raman spectra during methanol chemisorption at 100°C on the supported 1% V_2O_5 –5% WO_3 /40% TiO_2 / SiO_2 catalyst in the 700–1200 cm^{-1} region .

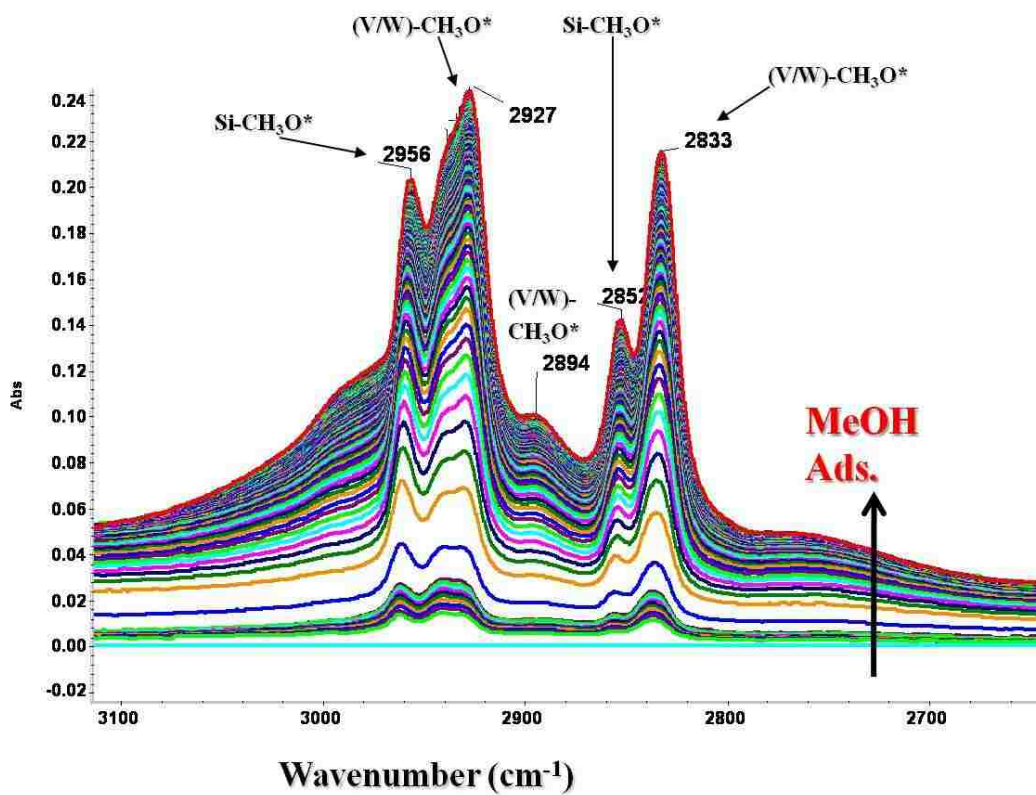


Figure 3.4. *In Situ* IR spectra during methanol chemisorption at 100°C on the supported 1% V_2O_5 –5% WO_3 /40% TiO_2 / SiO_2 catalyst

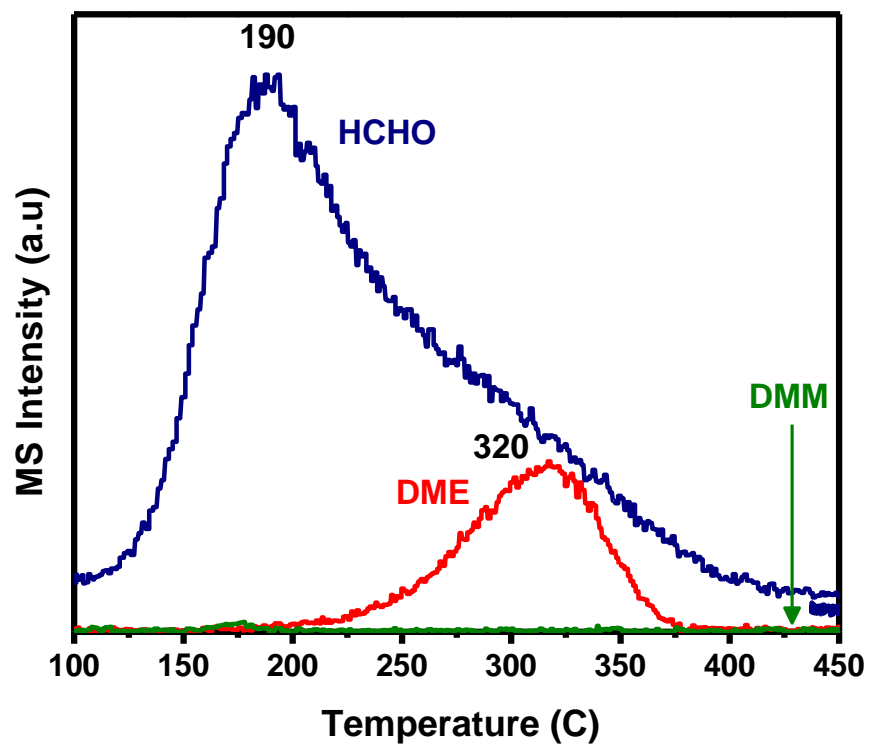


Figure 3.5. Methanol-TPSR spectra where CH_3OH is initially chemisorbed and the TPSR experiment is conducted in flowing O_2/He with the supported $1\% \text{V}_2\text{O}_5-5\% \text{WO}_3/40\% \text{TiO}_2/\text{SiO}_2$ catalyst

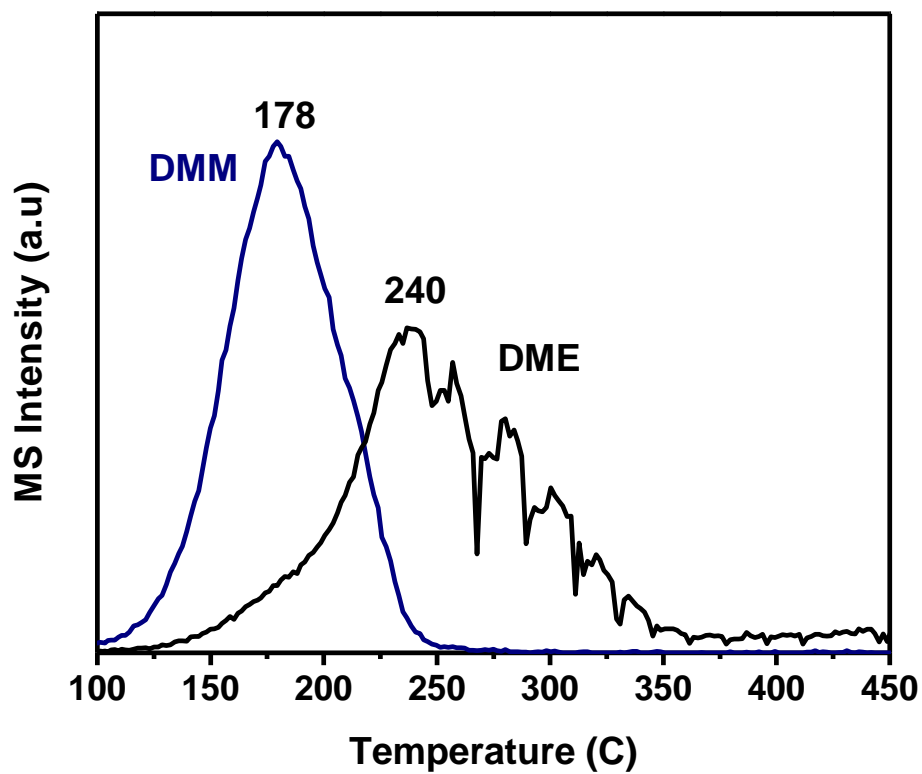


Figure 3.6. Methanol-TPSR spectra where CH₃OH is initially chemisorbed and the TPSR experiment is conducted in flowing CH₃OH/O₂/He with the supported 1% V₂O₅-5% WO₃/40% TiO₂/SiO₂ catalyst

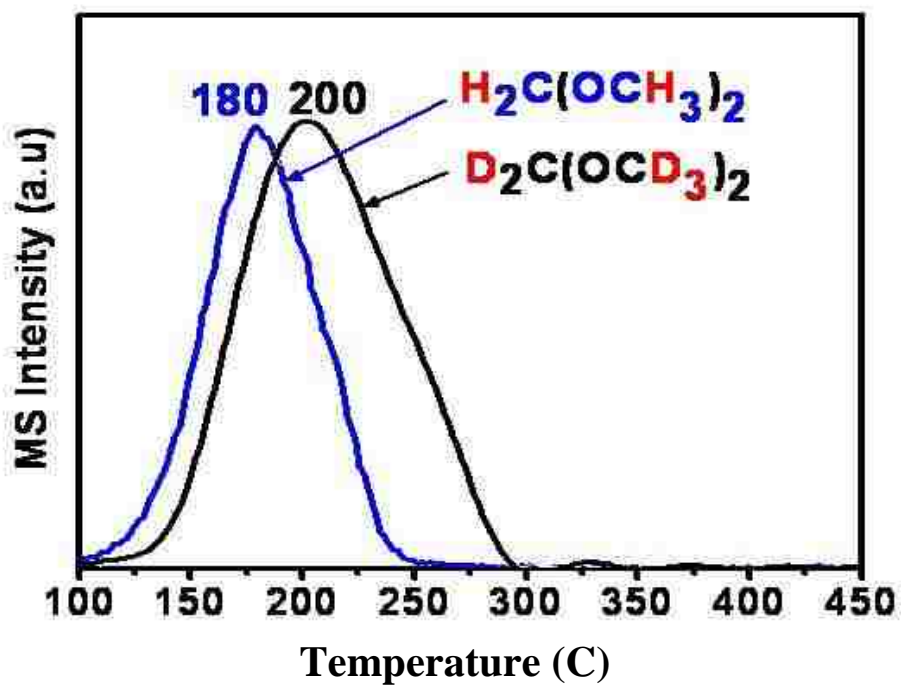


Figure 3.7. Methanol -TPSR spectra during $\text{CH}_3\text{OH}/\text{CH}_3\text{OH}$ -TPSR and $\text{CD}_3\text{OD}/\text{CD}_3\text{OD}$ -TPSR over the supported 1% V_2O_5 -5% WO_3 /40% $\text{TiO}_2/\text{SiO}_2$ catalyst

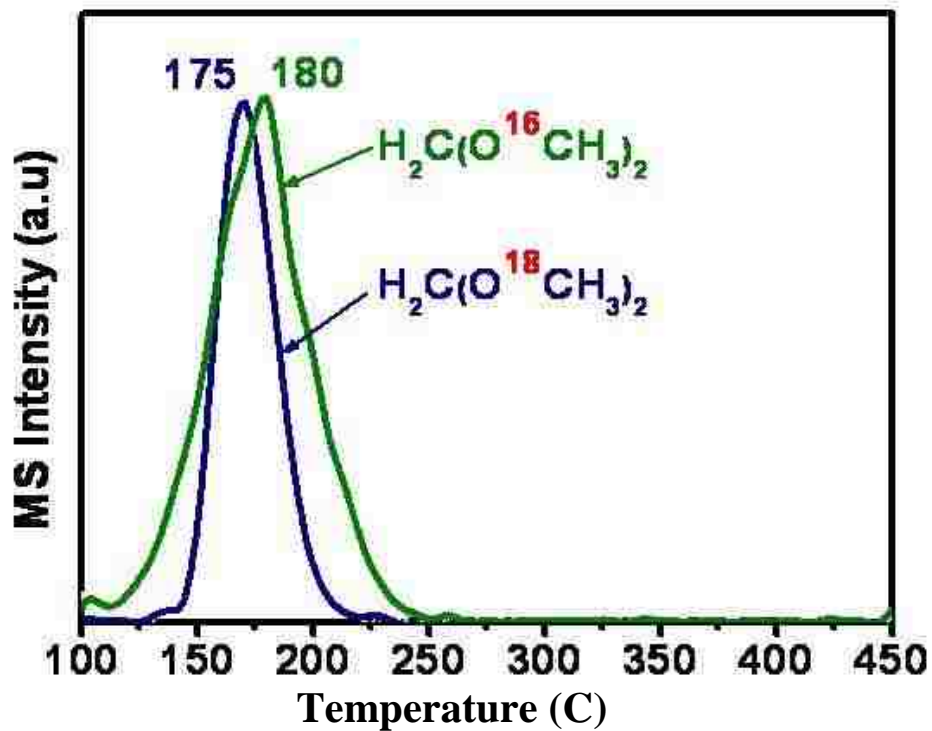


Figure 3.8. Methanol -TPSR spectra during $\text{CH}_3^{16}\text{OH}/\text{CH}_3^{16}\text{OH}$ -TPSR and $\text{CH}_3^{18}\text{OH}/\text{CH}_3^{18}\text{OH}$ -TPSR over supported 1% V_2O_5 -5% WO_3 /40% TiO_2 / SiO_2 catalyst

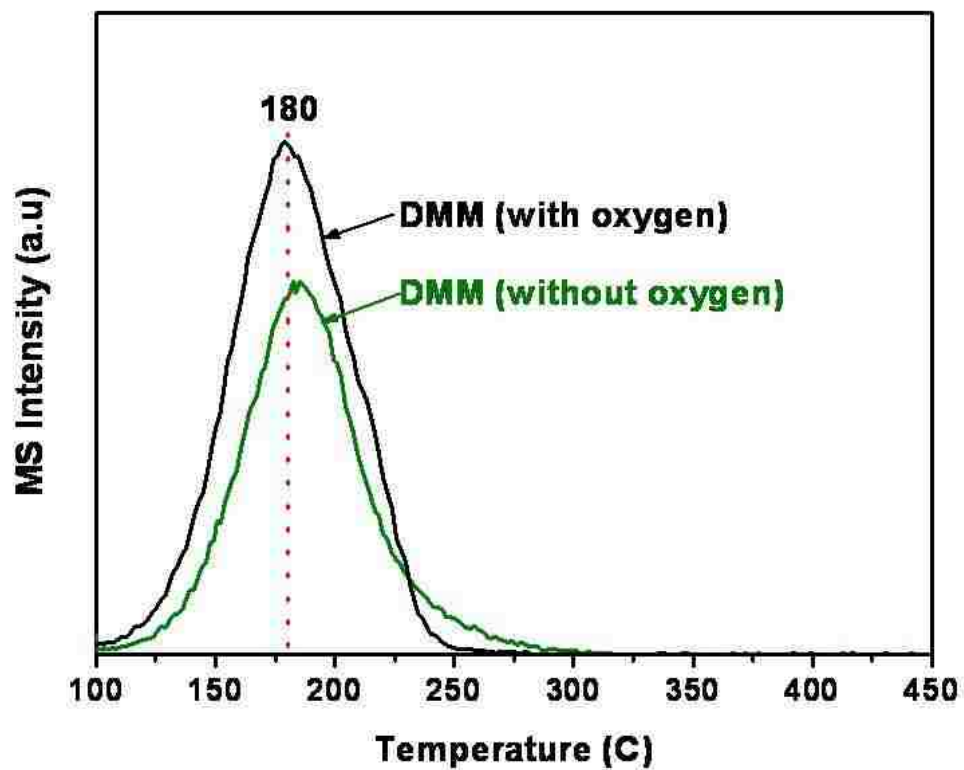


Figure 3.9. Methanol -TPSR spectra in the presence and absence of gas phase oxygen over the supported 1%V₂O₅-5%WO₃/40%TiO₂/SiO₂ catalyst

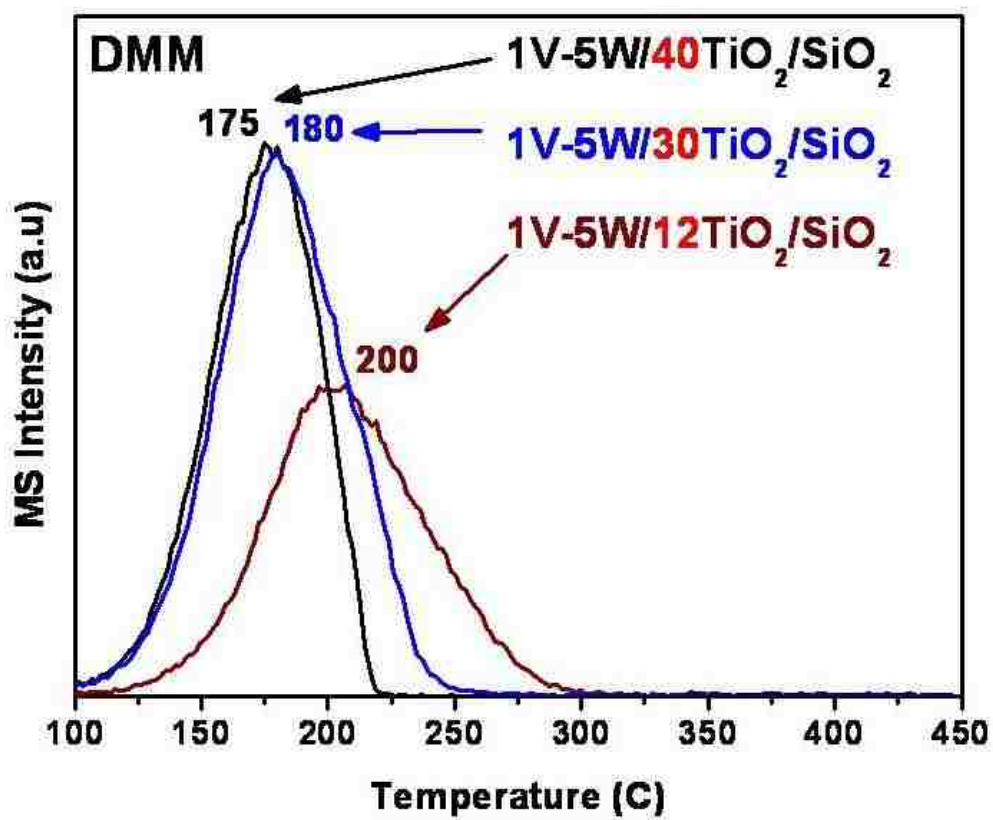


Figure 3.10. Methanol-TPSR spectra over the supported 1% V₂O₅-5% WO₃/12% TiO₂/SiO₂, 1% V₂O₅-5% WO₃/30% TiO₂/SiO₂, and 1% V₂O₅-5% WO₃/40% TiO₂/SiO₂ catalysts

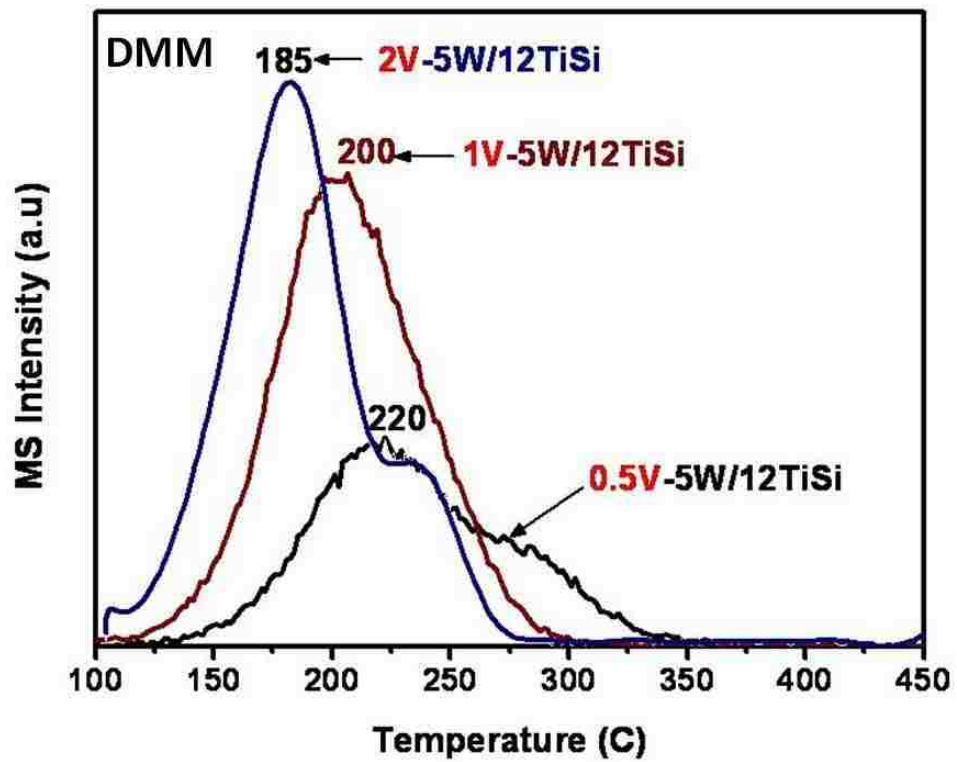


Figure 3.11. Methanol-TPSR spectra over the supported 2%V₂O₅-5%WO₃/12%TiO₂/SiO₂, 1%V₂O₅-5%WO₃/12%TiO₂/SiO₂, and 0.5%V₂O₅-5%WO₃/12%TiO₂/SiO₂ catalysts

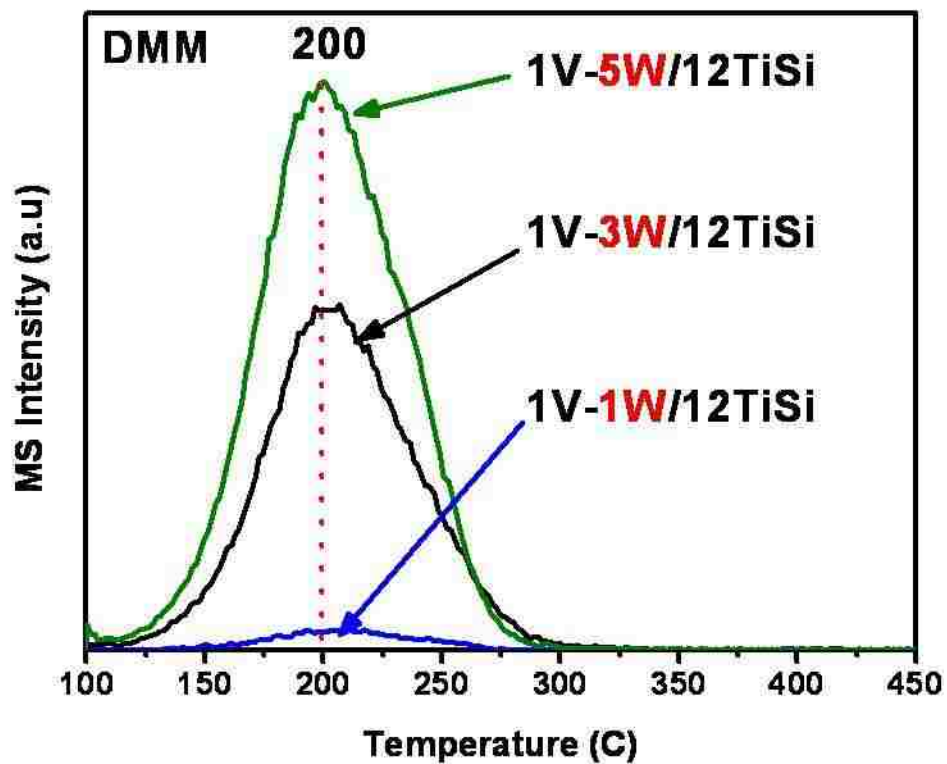


Figure 3.12. Methanol-TPSR spectra over the supported 1% V_2O_5 -5% WO_3 /12% TiO_2 /SiO₂, 1% V_2O_5 -3% WO_3 /12% TiO_2 /SiO₂, and 1% V_2O_5 -1% WO_3 /12% TiO_2 /SiO₂ catalysts

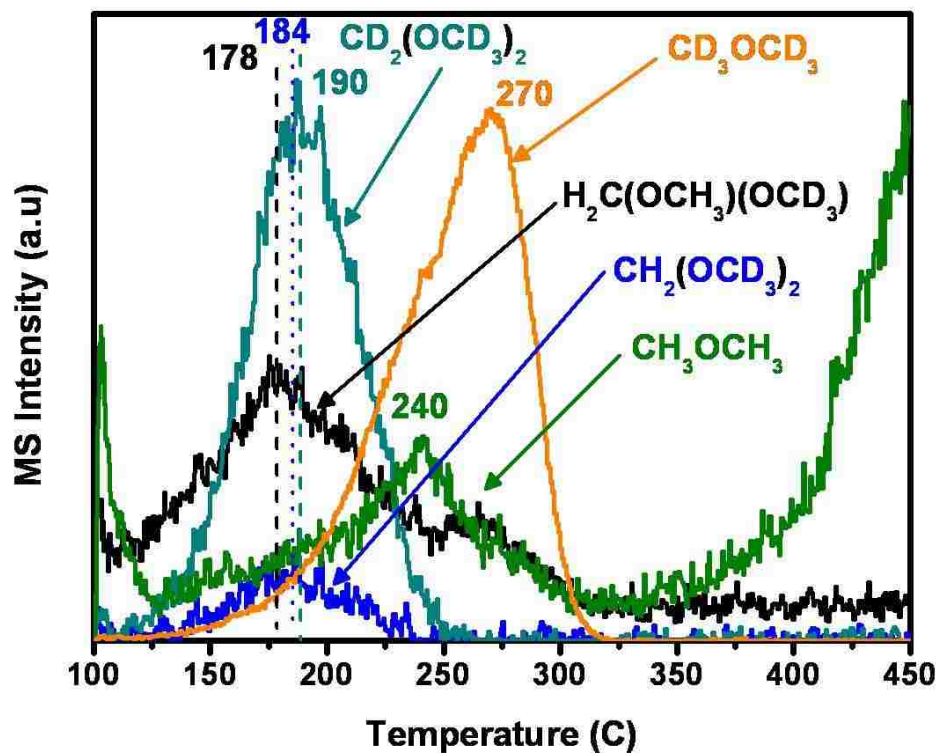


Figure 3.13. Methanol-TPSR spectra where CH_3OH is initially chemisorbed and the TPSR experiment is conducted in flowing $CD_3OD/O_2/He$ with the supported 1% V_2O_5 -5% WO_3 /40% TiO_2/SiO_2 catalyst

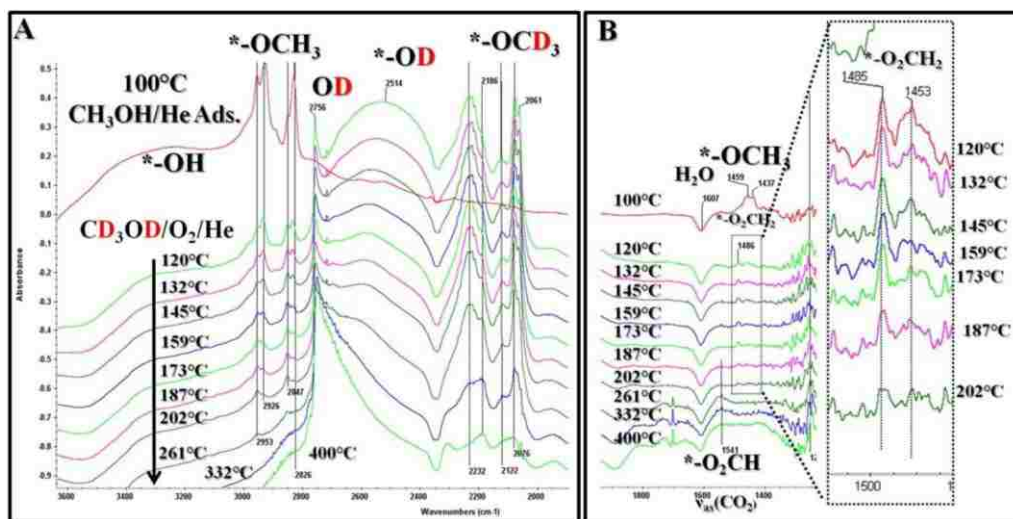


Figure 3.14. *In Situ* TP-IR spectra during methanol-TPSR where CH₃OH was initially chemisorbed at 100°C and the temperature programmed reaction was conducted with flowing CD₃OD/O₂/He over the supported 1% V₂O₅-5% WO₃/40% TiO₂/SiO₂ catalyst (A) 1800-3700 cm⁻¹ region and (B) 1100-2100 cm⁻¹ region with zoomed in inset for the 1400-1550 cm⁻¹ region.

Supplemental Information

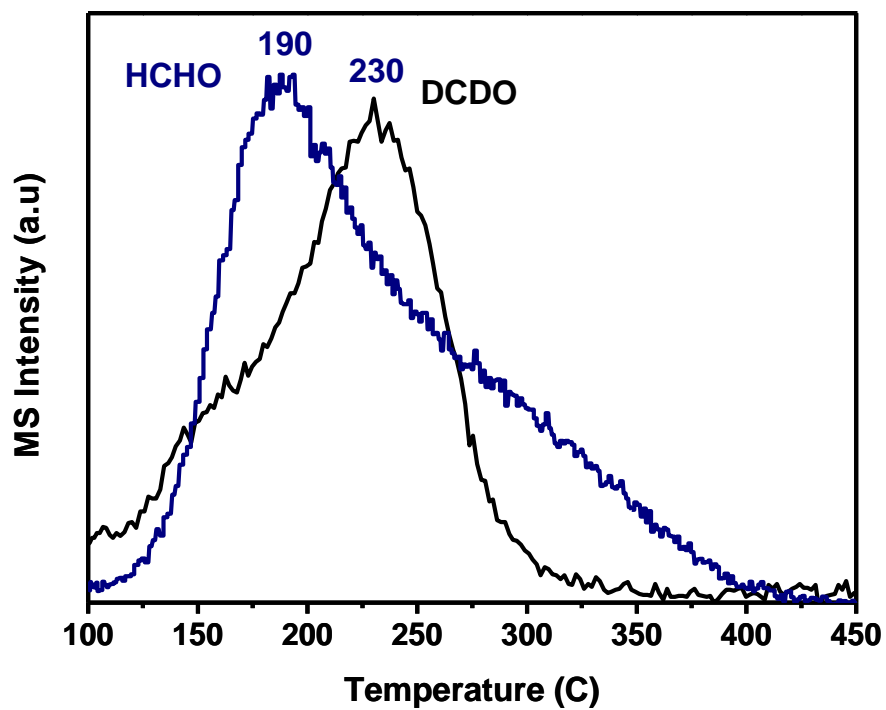


Figure 3.S1. Comparison of HCHO/CH₃OH-TPSR and DCDO/CD₃OD-TPSR spectra over the supported 1%V₂O₅-5%WO₃/40%TiO₂/SiO₂ catalyst

CHAPTER 4

Catalyst by Design: Tuning the Selective Oxidation of CH₃OH to H₂C(OCH₃)₂ over Supported V₂O₅-WO₃/TiO₂/SiO₂ with TiO₂ Nanoligands

ABSTRACT

The selective oxidation of methanol over a catalyst with surface redox sites primarily produces formaldehyde (HCHO) as the reaction product, with low selectivity's to other redox products. The conversion of CH₃OH over acid sites, however, primarily yields CH₃OCH₃ as the reaction product. The selective oxidation of CH₃OH to (CH₃O)₂CH₂ (DMM: dimethoxymethane) requires redox sites to initially form HCHO and acid sites to combine HCHO with two methanol molecules to form DMM. Recently, DMM has been investigated for its potential benefit as an oxygenated additive in diesel fuel. The objective of this study was to molecularly design a supported V₂O₅-WO₃/TiO₂/SiO₂ catalyst whereby methanol could be selectively oxidized to give DMM as the main reaction product by changing the titania domain size. The supported catalysts were physically characterized with *in situ* Raman and chemically probed with steady-state CH₃OH oxidation. The experimental results demonstrate that varying the local electron density of oxide nanoligand supports allows tuning of the specific activity characteristics of surface metal oxide catalytic active sites. In the low temperature regime (150°C - 190°C), the selectivity to DMM is highest due to a high concentration of methoxy species present on the surface. These methoxy species

are able to react to form HCHO, and still in a high enough concentration on the surface to further react with HCHO to produce DMM. However, in the high temperature regime (200°C - 230°C), the concentration of methoxy species is significantly lower. As a result, it takes longer for two methoxy species to diffuse on the catalyst surface and react with HCHO to produce DMM. Therefore, we find the selectivity decrease as we approach our highest temperature. Ultimately, the ability to engineer the catalyst structure at the nanoscale and the fundamental understanding of the synthesis-structure-property relationships of supported metal oxides enabled the rational design of a supported metal oxide that could selectively oxidize methanol to DMM.

1. INTRODUCTION

The synthesis of dimethoxymethane (DMM) has been receiving much attention recently due to its potential as an oxygenated diesel fuel additive [1, 2] and potential source of H₂ through reforming for fuel cell applications [3]. Particularly, it has been shown to suppress soot formation from diesel emissions and improve diesel fuel lubricity compared to conventional low-sulfur, low aromatic diesel fuels while maintaining the ignition quality of high quality diesel fuel [4, 5]. The current process for DMM production is the oxidation of methanol over a Ag or Fe(MoO₃)₂ redox catalyst to produce formaldehyde (HCHO) with subsequent condensation of formaldehyde by its reaction with methanol over an acid zeolite catalyst to produce DMM [4, 5]. Several catalyst studies have also appeared where DMM is produced in one step from selective oxidation of methanol, which would represent a more efficient process for the production of DMM [7-11,14].

A number of studies have investigated methanol oxidation reactions over supported vanadia catalysts. Typically, these investigations produced DMM in trace quantities as a byproduct [6] with few studies undertaken to investigate the one step selective oxidation of methanol directly to DMM, where DMM constitutes the major product. The synthesis of DMM has been proposed to require both redox and acid sites [7], with many researchers using a supported V₂O₅/TiO₂ catalyst and incorporated surface sulfates as a way to increase acidity and produce DMM

selectively [8-12]. Wang and Wachs [13] demonstrated that the partial oxidation of methanol over a mixed redox-acidic (20% V_2O_5/Al_2O_3) catalyst could form dimethoxymethane with 40% selectivity at 230°C. The source of the acid sites was attributed to the inherent acidity of the surface VO_x sites that possess both Lewis and Brønsted acidity rather than the underlying Al_2O_3 support since it was covered with the surface VO_x monolayer. Liu *et al.* [14] investigated the synthesis of DMM with unsupported and SiO_2 -supported polyoxometallate Keggin structures [$H_{3+n}PV_nMo_{12-n}O_{40}$ ($n = 0-4$)]. Manipulation of the Keggin clusters, whereby some Mo atoms were replaced by vanadium was found to increase selectivity of DMM production. The ratio of redox and Brønsted acids was further varied by controlled thermal dehydroxylation of the surface Brønsted acidic protons of the Keggin clusters. It was concluded that the concentration of Brønsted acid protons is being affected by the introduced vanadium, temperature treatments and reaction conditions. These studies demonstrated that the production of DMM can be tuned by varying the relative redox and acid catalyst properties.

Although previous studies have extensively focused on single component acidic (WO_x) or redox (VO_x) catalytic active sites supported on nano- TiO_2 domains [16] for methanol oxidation to formaldehyde (redox sites) or dimethyl ether (acidic sites), respectively, no investigation has systematically examined the influence of the oxide substrate dimension in the critical ~0.5-10 nm region upon the resultant catalytic properties of bifunctional redox-acid catalysts. Thus, a unique

nanotechnology opportunity currently exists to investigate the fundamental science of tuning the electronic and molecular structures of bifunctional supported redox-acid catalytic active sites for enhanced catalytic performance. The focus of this paper is the synthesis, rational design, and tunability of bifunctional redox-acidic supported metal oxide catalysts with nanostructured oxide substrate domains for the one step selective oxidation of methanol to dimethoxymethane.

2. EXPERIMENTAL

2.1. Catalyst Synthesis

2.1.1. Preparation of Supported $\text{TiO}_2/\text{SiO}_2$ Catalysts

The synthesis procedure previously described by Ross-Medgaarden *et al.* [16] was used to prepare a series of x% $\text{TiO}_2/\text{SiO}_2$ supports, where x = 1, 12, 20, 30, and 40%. The silica support material, amorphous SiO_2 (Cabot, Cab-O-Sil fumed silica EH-5, S.A. $\sim 332 \text{ m}^2/\text{g}$), was employed and found to be more easily handled by an initial water pretreatment and calcination at 500°C for 4 h without changing the material properties. The supported $\text{TiO}_2/\text{SiO}_2$ catalysts were prepared by the incipient-wetness impregnation of isopropanol solutions of titanium isopropoxide ($\text{Ti}(\text{O-Pr})_4$, Alfa Aesar, 99.999%). The silica support was initially dried for 2 h at 120°C to remove the physisorbed water prior to catalyst preparation inside a glovebox (Vacuum Atmospheres, Omni-Lab VAC 101965) under a continuously flowing N_2 (Airgas, Ultra High Purity) environment. After impregnation at room temperature, the sample was kept inside the glovebox to dry overnight under

flowing N₂. The calcination of the supported x%TiO₂/SiO₂ samples entailed ramping at 1°C/min to 120°C in flowing N₂ for 2 h, and then subsequently followed by another 1°C/min ramp under flowing air (Airgas, Zero Grade) to 500°C for 4 h. A multi-step preparation procedure was employed to prepare the 12, 20, 30, and 40%TiO₂/SiO₂ supports, where incremental loadings of 8 wt% TiO₂ were made followed by drying overnight and calcining as described above, for each step.

2.1.2. Preparation of Supported WO_x/TiO₂/SiO₂ Catalysts

The supported tungsten oxide (1 and 5%) catalysts were prepared by the incipient-wetness impregnation of aqueous solutions of ammonium metatungstate, (NH₄)₁₀W₁₂O₄₁·5H₂O (Pfaltz & Bauer, 99.5% purity) on the x% TiO₂/SiO₂ supports. The supported 1%WO₃/1%TiO₂/SiO₂ and 5%WO₃/x%TiO₂/SiO₂ (x = 12, 20, 30, and 40%) samples were dried overnight under ambient conditions and subsequently dried in flowing air (Airgas, Zero Grade) at 120°C for 1 h and further calcined in the flowing air at 450°C for 4 h.

2.1.3. Preparation of Supported VO_x-WO_x/TiO₂/SiO₂ Catalysts

The supported vanadium oxide (1%) catalysts were prepared by the incipient-wetness impregnation of isopropanol solutions of vanadium triisopropoxide (VO[CHO(CH₃)₂]₃, Alfa Aesar, 97%) onto the supported (1,5)%WO₃/x%TiO₂/SiO₂ catalysts. The preparation was performed inside a glovebox with continuously flowing N₂ (Airgas, Ultra High Purity) whereby the

(1,5)%WO₃/x%TiO₂/SiO₂ catalysts were initially dried at 120°C to remove the physisorbed water before impregnation. After impregnation at room temperature, the samples were kept inside the glovebox under flowing N₂ overnight. The calcination of the supported 1%V₂O₅-(1,5)%WO₃/x%TiO₂/SiO₂ samples entailed ramping at 1°C/min to 120°C in flowing N₂ for 2 h, and then by another 1°C/min ramp under flowing air (Airgas, Zero Grade) up to 500°C for 4 h.

2.2. Catalyst Characterization

2.2.1. In Situ Raman Spectroscopy

The molecular structures of the V₂O₅, WO₃, TiO₂ and SiO₂ components of the supported 1%V₂O₅-(1,5)%WO₃/x%TiO₂/SiO₂ catalysts were determined with *in situ* Raman spectroscopy, with a visible (532 nm) laser excitation. The single stage Raman spectrometer (Horiba-Jobin Yvon, Lab Ram-HR) was equipped with a confocal microscope (Olympus BX-30), a notch filter (Kaiser Super Notch), a Nd-YAG doubled diode pumped laser (Coherent Compass 315M-150; output power of 150 mW with sample power 10 mW), and the scattered photons were detected by a UV-sensitive liquid-N₂ cooled CCD detector (Horiba-Jobin Yvon, CCD-3000V). Laser excitation was at 532 nm and a spectral resolution of ~ 2 cm⁻¹ was obtained for the given parameters, with 900 grooves/mm grating. The Raman spectrometer was also equipped with an environmentally-controlled high-temperature cell (Harrick) that examined the catalyst samples in loose powder form (~5-10 mg) that allowed for control of both the catalyst temperature and gaseous

composition. *In situ* Raman spectra were collected for the supported 1% V₂O₅- (1,5)% WO₃/x% TiO₂/SiO₂ catalyst under dehydrated conditions (400°C, 10% O₂/He). The spectral acquisition time employed was 20 scans for 20 seconds/scan for a total of ~7 min/spectrum. System alignment was verified daily using a silica reference standard provided by Horiba-Jobin Yvon.

2.2.2. Electron Microscopy Procedures

A 5% V₂O₅/30% TiO₂/SiO₂ and 5% WO₃/30% TiO₂/SiO₂ were characterized by aberration corrected HAADF, BF-STEM, STEM-EELS and STEM-XEDS. Details of the experimental procedure can be found elsewhere [17].

2.3. Steady-State Methanol Oxidation

Steady-state methanol dehydrogenation experiments were conducted in an ambient pressure reactor consisting of a single-pass down flow fixed bed quartz reactor (0.16" ID) packed with finely ground catalyst powder and quartz end caps. To mimic thermal resistance and estimate catalyst bed temperature, a thermocouple mounted at the same elevation as the catalyst bed was installed inside an identical quartz tube that was fixed to the reactor tube. Both tubes were mounted side-by-side snugly within a 0.5" ID metal tube wrapped in heat tape and insulation. Pretreatment consisted of calcining each catalyst at 350°C for 30 min in 93 mL/min a dry flowing gas mixture of Oxygen (Ultra High Purity, Airgas) and Helium (Ultra High Purity, Airgas) controlled at a molar O₂-He ratio of 14:79 by two independent Coriolis mass flow controllers. The reactor was then cooled to the desired reaction

temperature and the feed gases were bubbled through a liquid methanol saturator (Alfa Aesar, ACS grade). The gas phase methanol concentration was controlled by the temperature of an overhead condenser, operated at 8°C for these experiments. The final composition of the reactor feed stream was 7%:14%:79% CH₃OH/O₂/He at 100 mL/min total flow. Steady-state performance was determined by averaging 3-4 gas chromatograph (GC) cycles at the reaction temperature and comparing to initial 100°C temperature runs where each catalyst was consistently demonstrated inactive in converting methanol. Blank runs without the catalysts demonstrated negligible methanol conversion in the reactor system. The 0.25" OD stainless steel tubing from the reactor outlet to the GC was maintained between 120-150°C by heat tape and insulation to minimize condensation of the reactor effluents. The reactor effluent gases were analyzed by an HP5890 Series II online GC (Hewlett Packard), operated in split mode (35°C for 6 min, ramp 20°C/min to 225°C hold for 5 min), with a 10-port Valco valve diverting two samples in parallel through a CP-sil 5CB capillary column (30 m x 0.32 mm x 5.0 m, J& W Scientific) to the FID and a 40/60 Carboxene-1000 packed column (5 ft x 1/8", Supelco) to the TCD for determination of the methanol conversion, selectivity and activity.

3. Results

3.1. Characteristics of Supported VO_x-WO_x/TiO₂/SiO₂ Catalysts

3.1.1. In Situ Raman Spectroscopy

The *in situ* Raman spectra of the dehydrated supported 1%V₂O₅-(1 and

5% WO₃/x% TiO₂/SiO₂ catalysts are presented in Figure 1 as a function of titania loading. The Raman spectra in the 200-700 cm⁻¹ region are dominated by the bands of crystalline TiO₂(anatase) at 394, 508 and 630 cm⁻¹ for the supported 1% V₂O₅-5% WO₃/30% TiO₂/SiO₂, 1% V₂O₅-5% WO₃/40% TiO₂/SiO₂ and 1% V₂O₅-5% WO₃/20% TiO₂/SiO₂ catalysts [18]. The Raman bands associated with crystalline TiO₂(rutile) (142, 445, and 610 cm⁻¹) and crystalline TiO₂(brookite) (242, 320, 363, and 407 cm⁻¹) are not present in the Raman spectra [16,18]. The supported 1% V₂O₅-5% WO₃/12% TiO₂/SiO₂ and 1% V₂O₅-1% WO₃/1% TiO₂/SiO₂ catalysts lack the distinct TiO₂(anatase) Raman features, indicating that the supported TiO₂ phase is molecularly dispersed on the SiO₂ surface. Gao *et al.* [18] have shown that the supported 1% TiO₂/SiO₂ catalyst consists of isolated surface TiO₄ species and the supported 12% TiO₂/SiO₂ catalysts consist of polymeric surface TiO₅ species ~ 0.4 and 1 nm in size, respectively.

Structural information about the deposited tungsten and vanadium oxide components in the dehydrated supported 1% V₂O₅-(1,5)% WO₃/x% TiO₂/SiO₂ catalysts is also contained in the 700-1200 cm⁻¹ region of Figure 1. The *in situ* Raman spectra in Figures 1 reveal that neither crystalline WO₃ (strong bands at 804, 710 and 270 cm⁻¹) [19] or crystalline V₂O₅ (strong bands at 995, 690 and 525 cm⁻¹) [20] nanoparticles (NPs) are present in any of the synthesized bifunctional catalysts. The supported tungsten oxide and vanadium oxide phases are exclusively present as surface WO_x and VO_x species that are reflected by the

vibrations at ~ 1011 and 1030 cm^{-1} , respectively. Comparison of the intensity of the Raman bands for the surface WO_x and VO_x bands reveals that the Raman cross-section of the dehydrated surface vanadium oxide species is ~ 4 times larger than the Raman cross-section of the dehydrated tungsten oxide species [21].

3.1.2. Electron Microscopy

Complementary HAADF and BF-STEM imaging, together with STEM-EELS and XEDS chemical analyses were employed to map out the structure and relative distribution of the supported metal oxide components of the double-supported catalysts. The results indicate that for the supported $\text{WO}_3/\text{TiO}_2/\text{SiO}_2$ catalysts, the WO_x surface species tend to be atomically dispersed on the larger TiO_2 rafts, as shown in Figure 2, whereas approximately 1 nm WO_x clusters form on the smaller TiO_2 domains. The aberration corrected-EELS suggests that the surface VO_x species self-assemble at the edges of TiO_2 nanoparticles on SiO_2 for the supported $\text{V}_2\text{O}_5/\text{TiO}_2/\text{SiO}_2$ catalysts, as shown in Figure 3. The combined atomic level structural characterization and chemical analysis effectively maps out the relative spatial distribution of all the metal oxide components. Though the characterization techniques were applied individually to the $\text{WO}_3/\text{TiO}_2/\text{SiO}_2$ and $\text{V}_2\text{O}_5/\text{TiO}_2/\text{SiO}_2$ systems, it is believed that the results are transferable to the bifunctional supported 1% V_2O_5 -(1 and 5)% $\text{WO}_3/x\%$ $\text{TiO}_2/\text{SiO}_2$ catalysts since it has been proposed that the different types of surface metal oxides (V_2O_5 and WO_3) exist independently from each other on the support [21].

3.2 Reactivity Studies

3.2.1 Steady-State Methanol Oxidation

The DMM selectivity of the bifunctional supported catalysts during steady-state methanol oxidation is a function of the surface VO_4/WO_5 ratio, titania domain size and reaction temperature as shown in Figure 4-7 and Tables **S1-S5**. Increasing both the TiO_2 domain size and the number of acid sites initially increases the DMM selectivity in going from 1% to 12% TiO_2 and 1% to 5% WO_3 . Further increasing the TiO_2 domain size, however, decreases DMM selectivity and enhances HCHO formation. All the bifunctional redox-acid catalysts exclusively yield DMM at the reaction temperature of 150°C indicating good coupling of the redox-acid reaction steps. At reaction temperatures above 150°C, however, the DMM selectivity decreases and additional HCHO byproduct is formed indicating poor coupling of the redox-acid reaction steps.

The specific DMM rate per surface VO_x site per second, TOF_{DMM} , is graphically displayed in Figures 5-7 at 150, 190, and 230°C, respectively, as a function of TiO_2 domain size. The TOF_{DMM} values were determined from the formula

$$\text{TOF}_{\text{DMM}} = \text{TOF (Overall)} \times \text{DMM selectivity}, \quad (1)$$

in which the DMM formation has been normalized for the 1% V_2O_5 content in all the catalysts. In the low temperature reaction regime (150-200°C), the TOF_{DMM} is greatest for the larger TiO_2 domain size (supported 1% V_2O_5 -

5%WO₃/40%TiO₂/SiO₂). At the higher reaction temperature regime (>200°C), the TOF_{DMM} is maximum at intermediate TiO₂ domain size for the supported 1% V₂O₅-5%WO₃/12%TiO₂/SiO₂ catalyst because of the significant formation of HCHO and CO for the other catalysts.

3.2.2. Reaction orders for CH₃OH and O₂

The steady state kinetics for the methanol oxidation reaction to dimethoxymethane over a supported 1% V₂O₅-5% WO₃/40% TiO₂/SiO₂ catalyst was investigated to determine the dependence on both CH₃OH and O₂ partial pressures. The kinetic dependence on CH₃OH partial pressures is displayed in Figure 8. The overall CH₃OH dependence during DMM formation reveals a reaction order less than 1. This low reaction order suggests that the catalytic surface is saturated with CH₃O* and CH₃OH* during the formation of DMM. Likewise, the reaction order with respect to molecular oxygen was found to be approximately zero order, as shown in Figure 9. This result is in agreement with TPSR results previously described in chapter 3 showing the formation of DMM in the absence of gas phase oxygen. Overall, the steady state kinetic study corroborates the conclusion of a Mars-van Krevelen mechanism.

4. Discussion

4.1 Structures of the SiO₂-supported VO_x, WO_x and TiO_x phases

The synthesized surface TiO_x structures are schematically shown in Figure 10 that relate to the in situ Raman spectra presented in Figure 1 (200-700 cm⁻¹ region).

The 1%TiO₂/SiO₂ support, consist of isolated TiO₄ species where as the 12%TiO₂/SiO₂ support consist of polymeric TiO₅ species that are grafted onto silica. The domain size from a 1%TiO₂/SiO₂ support to a 12%TiO₂/SiO₂ support varies from ~0.4 nm to ~1 nm, respectively, which decreases the edge energy [15]. Higher loadings (20-40%) of titania impregnated onto silica, result in the formation of crystalline TiO₂ (A). The resulting crystalline phase effectively varies the TiO₂ domain size from 2-4 nm (20%TiO₂/SiO₂) to 3-5 nm (30%TiO₂/SiO₂) to 5-9 nm (40%TiO₂/SiO₂). As such, the synthesized TiO₂/SiO₂ catalysts have varying surface structures (isolated to crystalline) and domain sizes (~0.4 to 9 nm), which ultimately results in electron tunable supports. The Raman spectra of isolated TiO₄ (1%TiO₂/SiO₂) and polymeric TiO₅ species (12%TiO₂/SiO₂) do not give strong Raman vibrations, but their presence is inferred from higher loading TiO₂/SiO₂ samples (20-40%) that do give strong Raman vibrations in the 200-700 cm⁻¹ region (see Figure 1) due to crystalline TiO₂ (A). As such, the chosen synthesis method was able to vary the titania domain size on the inert silica surface with the 1%TiO₂/SiO₂ and 12%TiO₂/SiO₂ catalysts consisting of molecularly dispersed TiO_x species.

For dehydrated supported WO₃/SiO₂, the primary Raman W=O vibration occurs at ~980 cm⁻¹, which is characteristic of dioxo (O=W=O) dehydrated surface WO₄ species [16,24], with a weaker vibration at ~1010 cm⁻¹, associated with mono-oxo (W=O) dehydrated surface WO₅ species [22, 24-28]. The Raman spectra

(Figures 1) for the dehydrated supported 1% V₂O₅-(1 and 5)% WO₃/x% TiO₂/SiO₂ catalysts are dominated by the vibration of the dehydrated mono-oxo surface WO₅ species at ~1011 cm⁻¹. The position of the Raman band at ~1011 cm⁻¹ also reveals that the surface WO_x species preferentially coordinate to the TiO₂ sites rather than exposed SiO₂ sites since dehydrated supported WO₃/TiO₂ exhibits the W=O Raman vibrations at ~1007-1016 cm⁻¹ [19]. The W Aberration Corrected-HAADF images in Figure 2 further corroborate the Raman spectroscopy conclusion and reveals that surface WO_x species are atomically dispersed on the TiO₂(anatase) rafts. The mono-oxo surface O=WO₄ species on the TiO₂ sites are schematically shown in Figure 11.

Supported VO_x species exclusively form mono-oxo V=O structures upon dehydration [30,31]. Previous XANES and solid-state ⁵¹V NMR characterization revealed that the dehydrated surface VO_x species always possess VO₄ coordination [16, 29-32]. For the dehydrated supported V₂O₅/SiO₂ and V₂O₅/TiO₂ catalysts, the Raman bands of the mono-oxo surface VO₄ species vibrate at ~1036-1040 cm⁻¹ [29] and ~1027-1031 cm⁻¹ [33], respectively. The appearance of the V=O vibration for the dehydrated supported 1% V₂O₅-(1 and 5)% WO₃/30% TiO₂/SiO₂ catalyst at ~1031 cm⁻¹ suggests that the surface VO₄ species also preferentially coordinates to the TiO₂ sites rather than the exposed SiO₂ sites. Thus, Abberation Corrected STEM-EELS (Figure 3), *in situ* Raman spectroscopy (Figure 1) and previous *in situ* X-ray absorption near edge spectroscopy (XANES) [16,18] are all in agreement

that the surface VO_4 species preferentially self-assemble on the titania nanoligand domains rather than the exposed silica sites. The mono-oxo surface $\text{O}=\text{VO}_3$ sites on the TiO_2 sites are schematically shown in Figure 11.

4.2 Catalyst Performance for Methanol Oxidation to DMM

The reaction products formed from methanol oxidation over the bifunctional supported $\text{V}_2\text{O}_5\text{-WO}_3/\text{TiO}_2/\text{SiO}_2$ catalysts are quite informative about the role of the redox and acid sites. Formation of DMM requires that the redox and acid sites work in tandem to produce HCHO over the redox site and couple HCHO with two CH_3OH molecules on the acid site. If the number of redox sites is greater than the acid sites or the redox reaction step is faster than the coupling reaction over the acid sites, then excess HCHO will be formed. If the number of acid sites is greater than the redox sites or the acidic active site is more active than the redox sites, then excess DME will be formed.

The almost complete absence of DME formation with all the investigated catalysts indicates that the catalysts did not possess excess acidic sites or activity. For all the catalysts, increasing the reaction temperature produces HCHO and CO as the major byproducts, with CO only observed for the supported 1% $\text{V}_2\text{O}_5\text{-1% WO}_3/1\% \text{TiO}_2/\text{SiO}_2$ catalyst, indicating that the redox sites are more active than the acid sites. The DMM selectivity is lowest for the supported 1% $\text{V}_2\text{O}_5\text{-1% WO}_3/1\% \text{TiO}_2/\text{SiO}_2$ catalyst indicating that there are insufficient acid sites in this catalyst system. Increasing both the WO_3 loading from 1% to 5% WO_3 , which

necessitates having more titania anchoring sites by increasing the TiO_2 domain size from 1% to 12% TiO_2 , provides the needed extra acid sites. It was previously demonstrated that both the surface VO_4 redox and surface WO_5 acid specific reaction rates are affected by the TiO_2 domain size in an inverse fashion [16]. Thus, the surface VO_4 redox activity will monotonically increase with TiO_2 domain size and reaction temperature. The results are that large TiO_2 domains and increasing reaction temperature are responsible for formation of significant HCHO byproduct that decreases DMM selectivity. As a result, the TOF_{DMM} decreases with increasing TiO_2 domain size and reaction temperature with the optimization of DMM formation for the supported 1% V_2O_5 -5% WO_3 /12% TiO_2 /SiO₂ catalyst. Thus, the performance of the bifunctional supported V_2O_5 - WO_3 /TiO₂/SiO₂ catalysts can be tuned by changing the domain size of the TiO_2 nanoligands.

The steady state reaction kinetics over a 1% V_2O_5 -5% WO_3 /40% TiO_2 /SiO₂ catalyst for methanol oxidation to dimethoxymethane exhibit approximately half-order dependence on the partial pressure of methanol. This low reaction order of less than 1 can be understood by considering two methanol partial pressure regimes, where in the low $P_{\text{CH}_3\text{OH}}$ range, the reaction order approaches 1 (~0.6) and at the high $P_{\text{CH}_3\text{OH}}$ range the reaction order approaches zero (~0.1). From in situ IR studies (Chapter 3), CH_3O^* were found to be the MARI and saturate the surface during DMM formation. As such, the near zero order dependence on methanol at high $P_{\text{CH}_3\text{OH}}$ is consistent. At low $P_{\text{CH}_3\text{OH}}$, the decrease in surface CH_3O^*

concentration inhibits the ability for surface HCHO and CH₃O* to react and form DMM, as such approaching the first order case of CH₃OH directly to HCHO. This is consistent with previously described CH₃OH-TPSR results where a monolayer of CH₃O* and CH₃OH* in the absence of gas phase methanol during the temperature programmed ramp only produced HCHO and DME. The steady state reaction kinetics also revealed an approximately zero order dependence on the partial pressure of molecular O₂, which is also consistent with CH₃OH-TPSR experiments showing the production of DMM at identical T_p's with or without gas phase molecular O₂. This reflects the ability of surface VO_x and WO_x sites to utilize lattice oxygen for the oxidation of the surface reaction intermediates to DMM, which is known as the Mars-van Krevelen mechanism.

The reaction kinetics may be derived from the knowledge that the surface decomposition of the adsorbed CH₃O* intermediate is the rate determining step. Thus, the rate of the overall reaction is as follows:

$$\text{Rate} = k_{\text{rds}} * K_{\text{ads}} * P_{\text{CH}_3\text{OH}} / [1 + K_{\text{ads}} * P_{\text{CH}_3\text{OH}}] \quad [2]$$

in which k_{rds} represents the kinetic rate constant for C-H bond breaking of the surface CH₃O* intermediate. In situ IR spectroscopy (Chapter 3) revealed that the catalytic surface is saturated with CH₃O* during DMM formation. As such, K_{ads}*P_{CH₃OH} >> 1 which simplifies the rate expression to:

$$\text{Rate} = k_{\text{rds}} \quad [3]$$

The derived rate equation for methanol oxidation to dimethoxymethane is analogous to the rate expression proposed by Kilos et al [34] for ethanol oxidation to acetaldehyde over $\text{VO}_x/\text{Al}_2\text{O}_3$.

5. CONCLUSIONS

A series of well-defined titania nanoligand-supported bifunctional 1% V_2O_5 -(1,5)% $\text{WO}_3/x\% \text{TiO}_2/\text{SiO}_2$ catalysts consisting of surface VO_4 species and surface WO_5 species were successfully synthesized as determined by Raman spectroscopy and aberration corrected HAADF imaging. The DMM selectivity and TOF_{DMM} as a function of temperature and titania domain size were investigated by steady state methanol oxidation studies.

The catalytic results demonstrated that by varying the local electron density of the titania nanoligand, the relative activity of the surface VO_4 and WO_5 species could be effectively tuned. The ability to tune the catalytically active surface species resulted in molecular control during the selective oxidation of methanol to dimethoxymethane. In the highest temperature regime, 230°C, the S_{DMM} and TOF_{DMM} were found to be at an optimum when the surface VO_4 and WO_5 species were anchored to a 1 nm polymeric TiO_5 support, which was subsequently grafted onto an underlying inert silica support.

Ultimately, the rational design of acidic-redox bifunctional metal oxide nanocatalysts for optimum catalytic performance was successfully achieved.

ACKNOWLEDGEMENTS

The authors gratefully acknowledge the financial support by the NSF NIRT Grant 0609018.

REFERENCES

46. Y. Ren, Z. Huang, H. Miao, Y. Di, D. Jiang, K. Zeng, B. Liu, X. Wang, *Fuel* **87** (2008) 2691
47. P. Pepiot-Desjardins, H. Pitsch, R. Malhotra, S.R. Kirby, A.L. Boehman, *Combustion and Flame* **154** (2008) 191
48. Y. Fu, J. Shen, *Journal of Catalysis* **248** (2007) 101
49. G.P. Hagen, M.J. Spangler, *U.S. Patent* 6,437,195 (2002)
50. E. Stroofer, H. Hasse, S. Blagov, *U.S. Patent* 7,700,809 (2010)
51. G. Deo, I.E. Wachs, *Journal of Catalysis* **146** (1994) 323
52. J.M. Tatibouet, *Applied Catalysis A: General* **148** (1997) 213
53. Y. Fu, J. Shen, *Chem. Commun.*, (2007) 2172
54. J. Liu, Y. Fu, Q. Sun, J. Shen, *Microporous and Mesoporous Materials* **116** (2008) 614
55. Q. Sun, Y. Fu, J. Liu, A. Auroux, J. Shen, *Applied Catalysis A: General* **334** (2008) 26
56. H. Zhao, S. Bennici, J. Cai, J. Shen, A. Auroux, *Catalysis Today* **152** (2010) 70
57. X. Lu, Z. Qin, M. Dong, H. Zhu, G. Wang, Y. Zhao, W. Fan, J. Wang, *Fuel* (2011) doi: 10.1016/j.fuel.2011.01.007
58. X. Wang, I.E. Wachs, *Catalysis Today*, **96** (2004) 211
59. H. Liu, E. Iglesia, *J. Phys. Chem. B*, **107** (2003) 10840

60. L. L. Nakka, J.E. Molinari, I.E. Wachs, *In Press*
61. E.I. Ross-Medgaarden, I.E. Wachs, W.V. Knowles, A. Burows, C.J. Kiely, M.S. Wong, *J. Am. Chem. Soc.* **131** (2009) 680
62. W. Zhou, K.F. Doura, M. Watanabe, A.A. Herzing, E. Okunishi, E.I. Ross-Medgaarden, I.E. Wachs, C.J. Kiely, *ChemCatChem*, n/a. doi: 10.1002/cctc.201000273
63. X. Gao, S.R. Bare, J.L. Fierro, M.A. Banares, I.E. Wachs, *J. Phys. Chem. B* **102** (1998) 5653.
64. T. Kim, A. Burrows, C.J. Kiely, I.E. Wachs, *Journal of Catalysis* **246** (2007) 370
65. T. Kim, I.E. Wachs, *Journal of Catalysis* **255** (2008) 197
66. M.A. Vuurman, I.E. Wachs, A.M. Hirt, *J. Phys. Chem.* **95** (1991) 9928
67. I.E. Wachs, *Catal. Today* **27** (1996) 437.
68. I.E. Wachs, *Catal. Today* **100** (2005) 79.
69. E. Lee, I.E. Wachs, *J. Phys. Chem. C.* **111** (2007) 14410-14425.
70. D.S. Kim, M. Ostromecki, I.E. Wachs, *J. Mol. Catal. A Chem.* **106** (1996) 93.
71. M.A. Vuurman, I.E. Wachs, *J. Phys. Chem.* **96** (1992) 5008.
72. J. Jarupatrakorn, M.P. Coles and T.D. Tilley, *Chem. Mater.*, **17** (2005) 818.
73. K. Nakamoto, *Infrared and Raman Spectra of Inorganic Coordination Compounds* (5th ed); Wiley & Sons: New York, 1997.

74. X. Gao, S.R. Bare, B. M. Weckhuysen and I.E. Wachs, *J. Phys. Chem. B* **102** (1998) 10842.
75. H. Eckert, I.E. Wachs, *J. Phys. Chem.* **93** (1989) 6796.
76. N. Das, H. Eckert, H. Hu, I.E. Wachs, J.F. Walzer and F. Feher, *J. Phys. Chem.* **97** (1993) 8240.
77. X. Gao, S.R. Bare, I.E. Wachs, *J. Phys. Chem. B* **103** (1999) 618.
78. G. Deo and I.E. Wachs, *J. Catal.* **146** (1994) 335.
79. B. Kilos, A.T. Bell, E. Iglesia, *J. Phys. Chem. C* **113** (2009) 2830

FIGURES

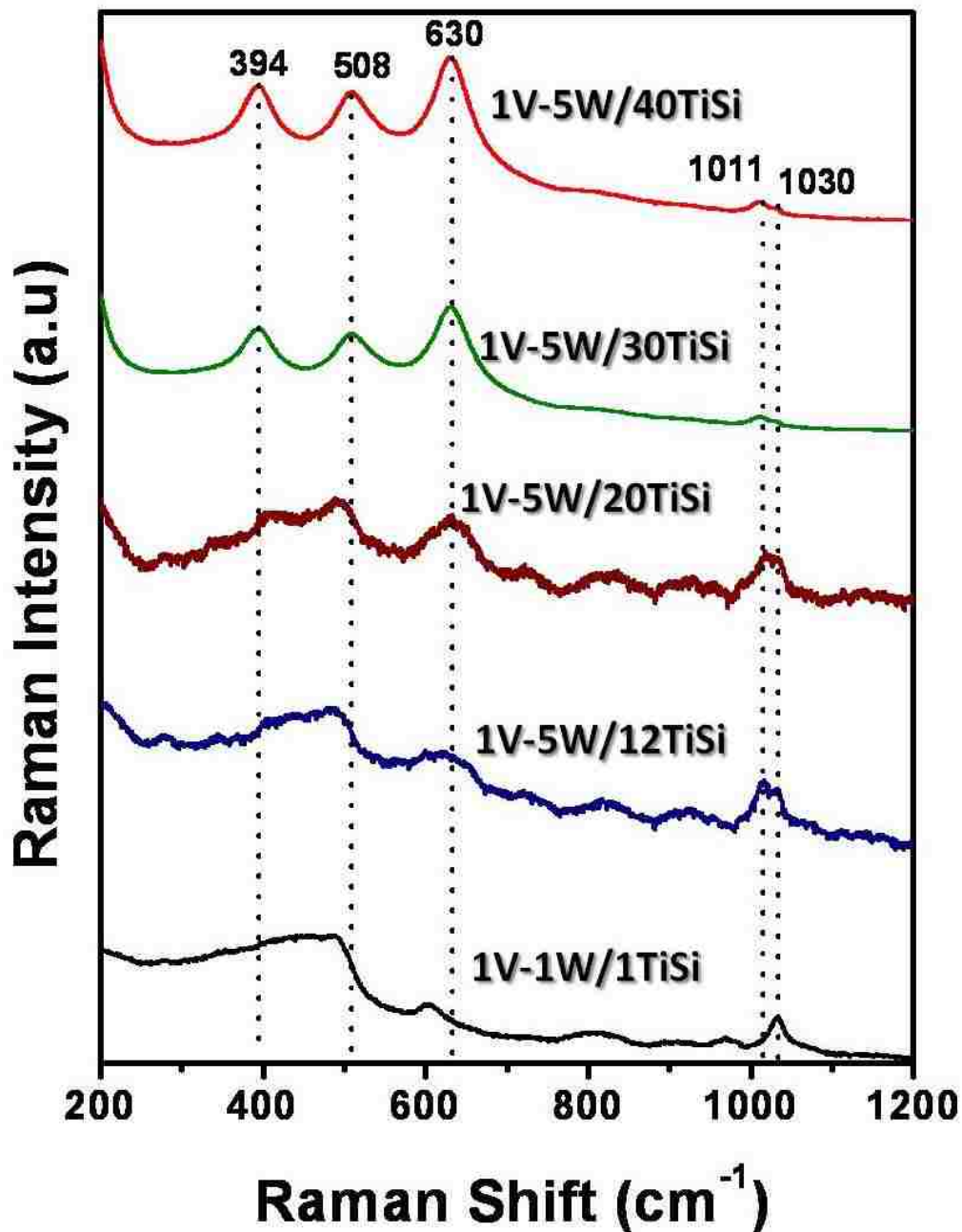
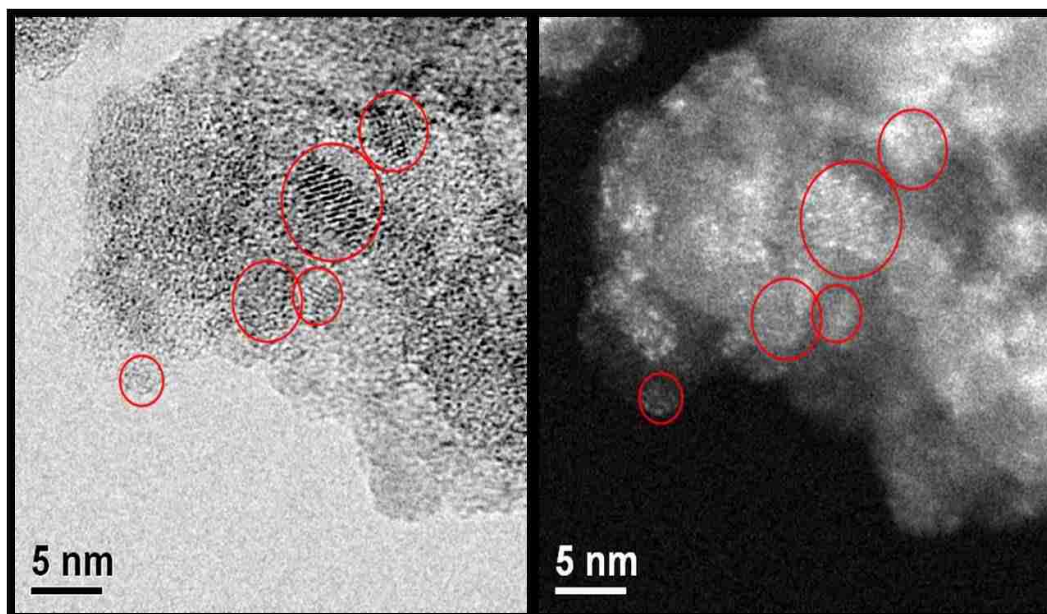


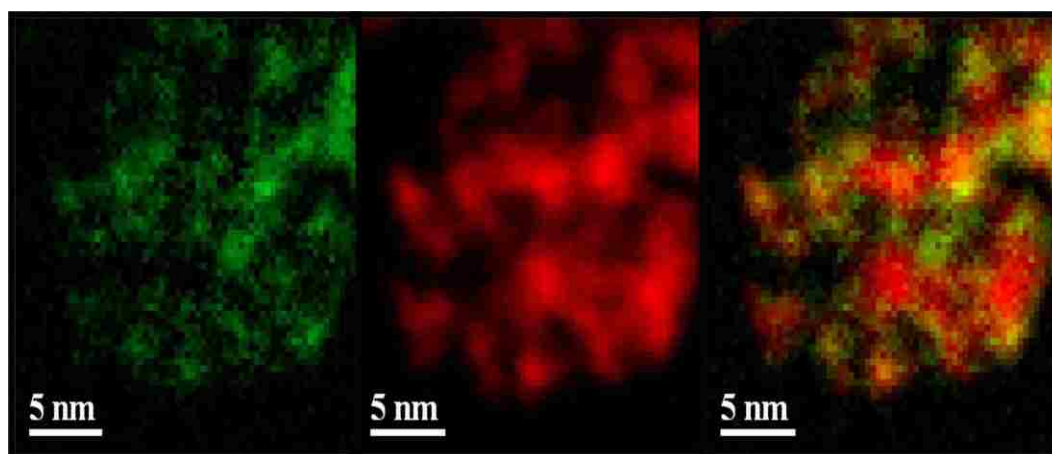
Figure 4.1. Dehydrated Raman (532 nm) spectra of bifunctional redox-acid supported $\text{V}_2\text{O}_5\text{-WO}_3/\text{TiO}_2/\text{SiO}_2$ catalysts



[A]

[B]

Figure 4.2. [A] BF-STEM image of $\text{TiO}_2(\text{anatase})$ rafts and [B] HAADF of atomically dispersed W atoms. Note the superposition of the surface W atoms in B on the $\text{TiO}_2(\text{anatase})$ rafts in A.



[A]

[B]

[C]

Figure 4.3. Aberration Corrected STEM-EELS of supported 5% V_2O_5 /30% TiO_2 /SiO₂ [A] V edge [B] Ti edge [C] superposition of the V edge and Ti edge

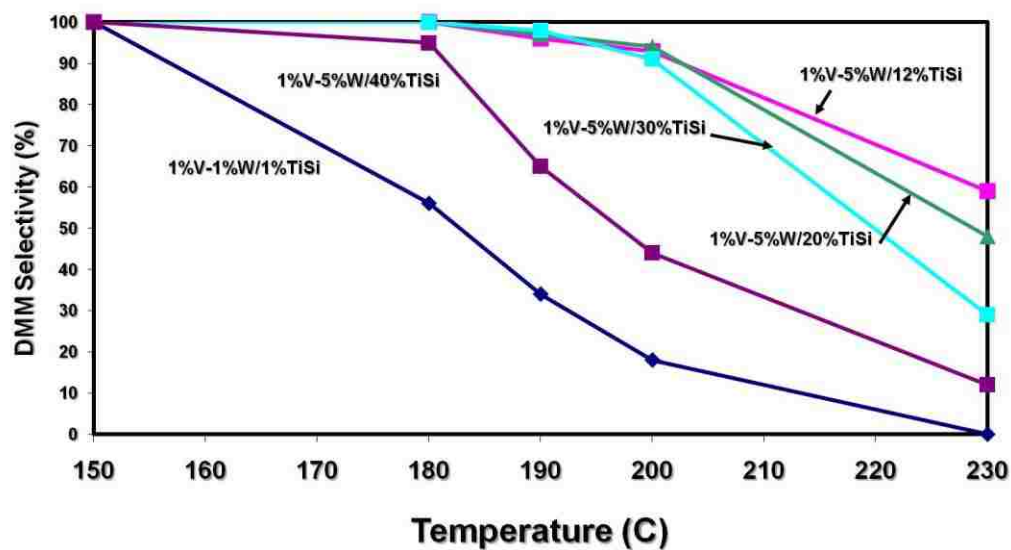


Figure 4.4. DMM selectivity of bifunctional supported V_2O_5 - WO_3 / TiO_2 / SiO_2 catalysts as a function of VO_4/WO_5 ratio, titania domain size and reaction temperature [V= V_2O_5 , W= WO_3 , TiSi = TiO_2/SiO_2].

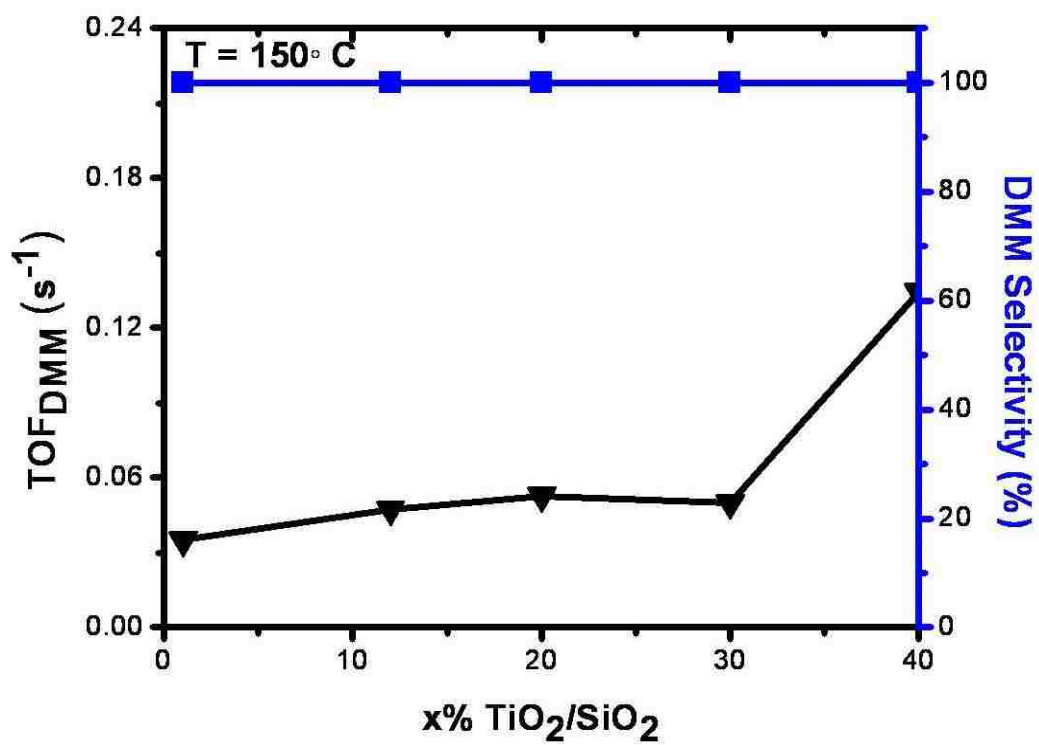


Figure 4.5. DMM selectivity and TOF_{DMM} during methanol oxidation at 150°C as a function of titania domain size

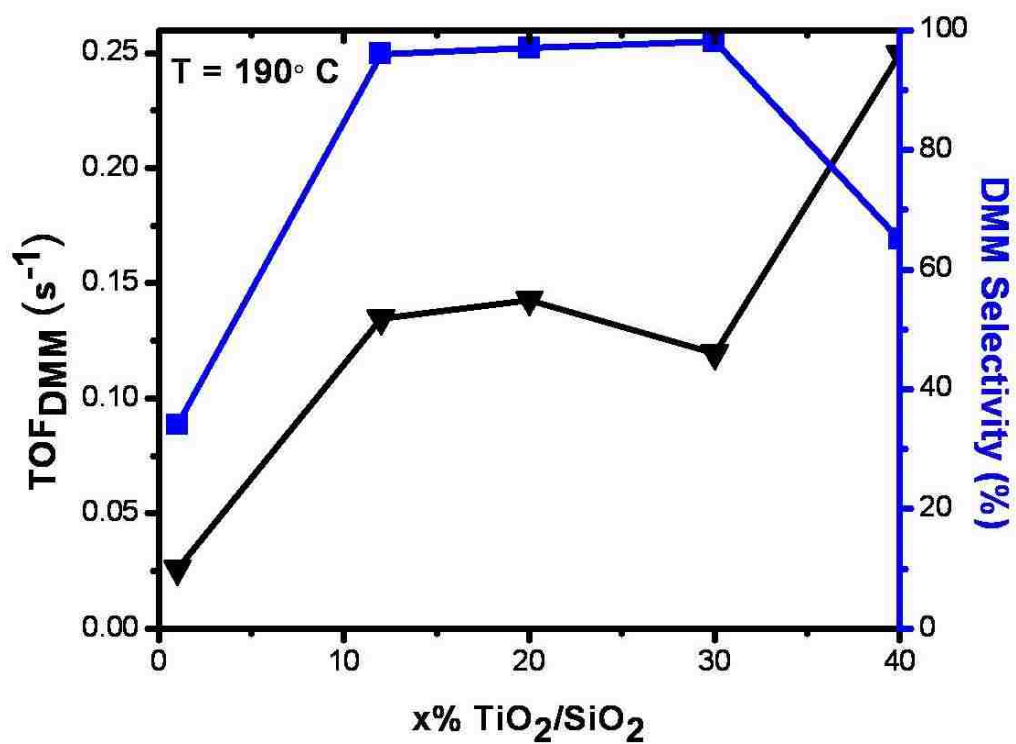


Figure 4.6. DMM selectivity and TOF_{DMM} during methanol oxidation at 190°C as a function of titania domain size

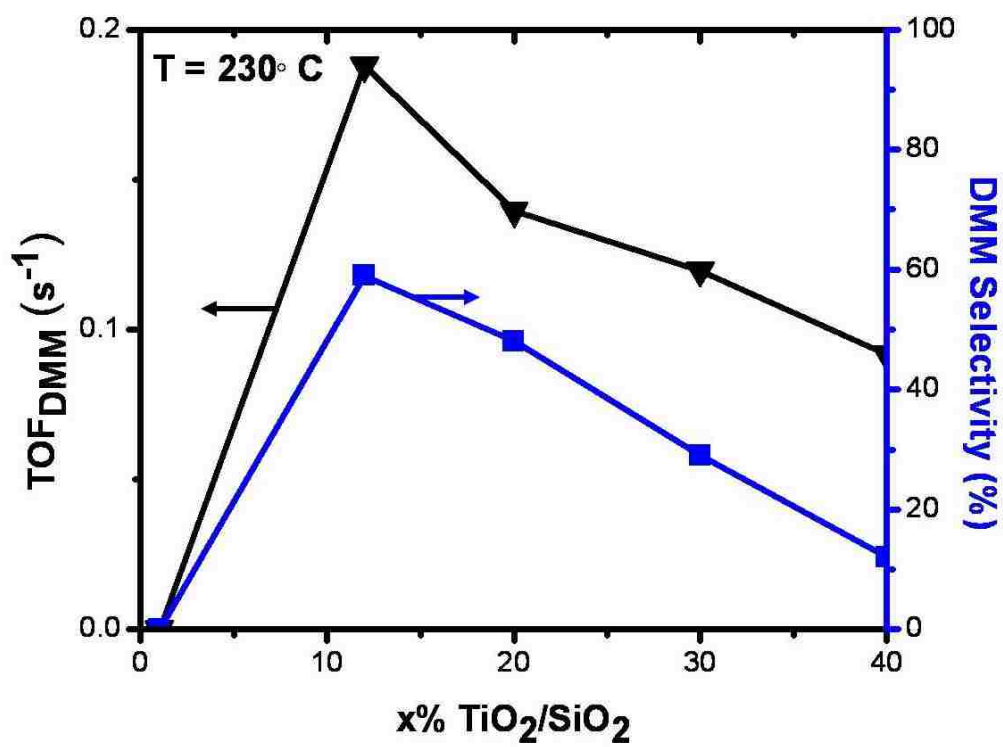


Figure 4.7. DMM selectivity and TOF_{DMM} during methanol oxidation at 230°C as a function of titania domain size

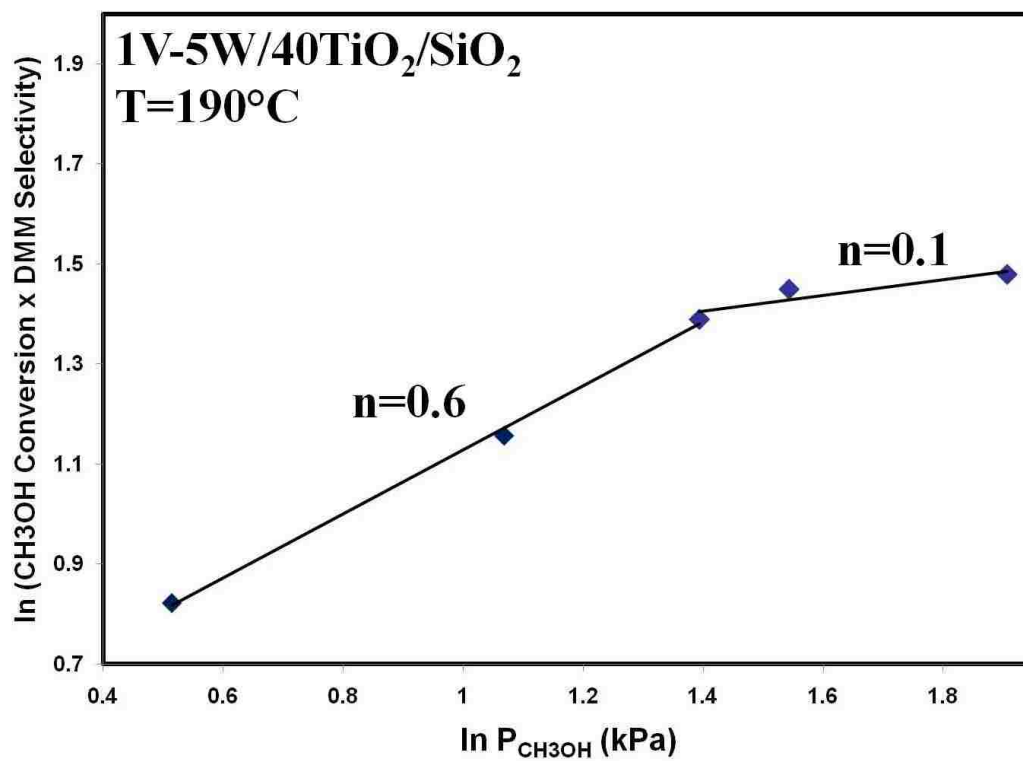


Figure 4.8. Dependence of kinetics for methanol oxidation to DMM on the gas phase CH₃OH partial pressure at 190°C for the supported 1%V₂O₅-5%WO₃/40%TiO₂/SiO₂ catalyst

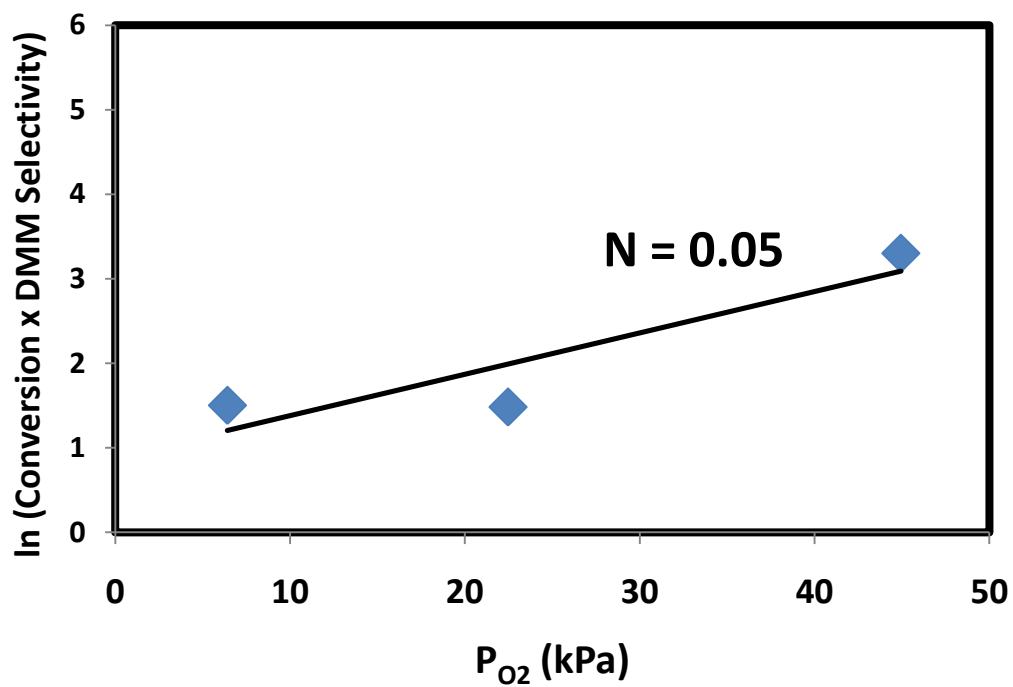


Figure 4.9. Dependence of kinetics for methanol oxidation to DMM on the gas phase molecular O_2 partial pressure at 190°C for the supported $1\%V_2O_5$ – $5\%WO_3/40\%TiO_2/SiO_2$ catalyst

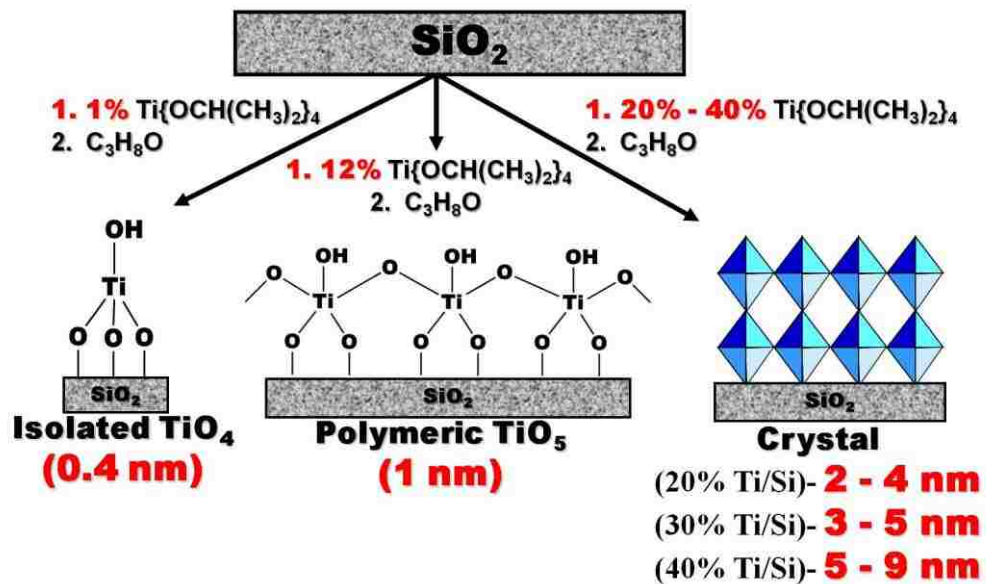


Figure 4.10. Schematic of titania nanoligand structures on the SiO₂ support

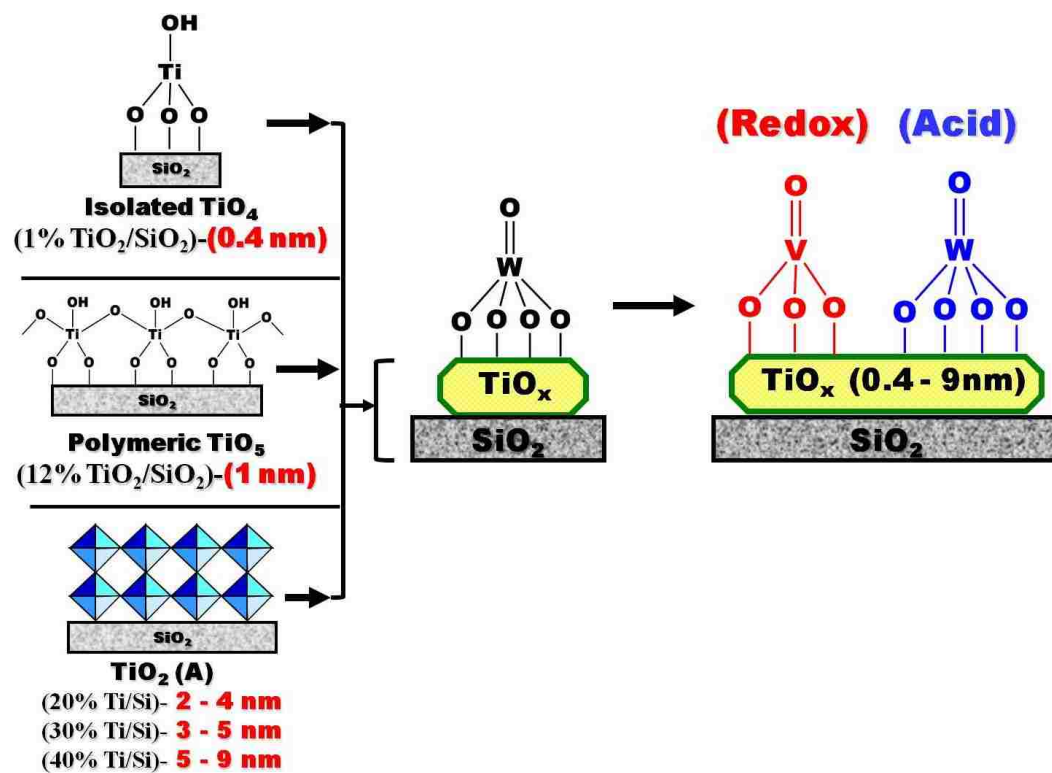


Figure 4.11. Molecular design of bifunctional redox-acid catalysts by self-assembly of surface VO_x and WO_x species on titania nanoligand domains.

SUPPLEMENTAL INFORMATION

Catalysts	Selectivity (%)			
	DMM	MF	HCHO	DME
1V-1W/1TiSi	100	0	0	0
1V-5W/12TiSi	100	0	0	0
1V-5W/20TiSi	100	0	0	0
1V-5W/30TiSi	100	0	0	0
1V-5W/40TiSi	100	0	0	0

Table 4.S1. Selectivity of bifunctional redox-acid catalysts at 150°C [V= V₂O₅, W=WO₃, TiSi = TiO₂/SiO₂].

Catalysts	Selectivity (%)			
	DMM	MF	HCHO	DME
1V-1W/1TiSi	56	8	36	0
1V-5W/12TiSi	100	0	0	0
1V-5W/20TiSi	100	0	0	0
1V-5W/30TiSi	100	0	0	0
1V-5W/40TiSi	95	5	0	0

Table 4.S2. Selectivity of bifunctional redox-acid catalysts at 180°C [V= V₂O₅, W=WO₃, TiSi = TiO₂/SiO₂].

Catalysts	Selectivity (%)			
	DMM	MF	HCHO	DME
1V-1W/1TiSi	34	12	51	3
1V-5W/12TiSi	96	4	0	0
1V-5W/20TiSi	97	3	0	0
1V-5W/30TiSi	98	2	0	0
1V-5W/40TiSi	65	9	24	2

Table 4.S3. Selectivity of bifunctional redox-acid catalysts at 190°C [V= V₂O₅, W=WO₃, TiSi = TiO₂/SiO₂].

Catalysts	Selectivity (%)			
	DMM	MF	HCHO	DME
1V-1W/1TiSi	18	18	61	3
1V-5W/12TiSi	93	7	0	0
1V-5W/20TiSi	94	6	0	0
1V-5W/30TiSi	91	9	0	0
1V-5W/40TiSi	44	13	41	2

Table 4.S4. Selectivity of bifunctional redox-acid catalysts at 200°C [V= V₂O₅, W=WO₃, TiSi = TiO₂/SiO₂].

Catalysts	Selectivity (%)					
	DMM	MF	HCHO	DME	CO	CO ₂
1V-1W/1TiSi	0	8	31	1	55	5
1V-5W/12TiSi	59	13	25	3	0	0
1V-5W/20TiSi	48	10	40	2	0	0
1V-5W/30TiSi	29	11	57	3	0	0
1V-5W/40TiSi	12	32	53	3	0	0

Table 4.S5. Selectivity of bifunctional redox-acid catalysts at 230°C [V= V₂O₅, W=WO₃, TiSi = TiO₂/SiO₂].

CHAPTER 5

CONCLUSIONS and PROPOSED FUTURE STUDIES

The primary objectives of the research presented in this dissertation are to (1) gain new molecular level insights about the catalytic active sites and surface reaction intermediates for complex, multisite and multistep catalytic reaction mechanisms and (2) develop a fundamental understanding that will allow for the rational design of bifunctional supported metal oxide catalytic materials by tuning the characteristics of dual redox-acidic catalytic active sites.

1. Molecular and Electronic Structures of SiO₂-Supported VO_x, WO_x and TiO_x Phases

The chosen synthesis method was able to vary the titania surface structures, and titania domain sizes, on the inert silica surface. A series of rationally designed TiO₂/SiO₂ supports were synthesized, whereby molecularly dispersed isolated TiO₄ and polymeric TiO₅ structures could be carefully controlled on a silica surface. In addition, the synthesis method employed allowed higher loadings of titania on silica to form crystalline TiO₂ (A). The wide array of titania surface structures created resulted in variable domain sizes (0.4 – 9 nm) which impacted the electron density of the TiO_x species, that consequently affects the resulting catalytic active sites. Using novel synthetic techniques, catalytically active acidic (WO_x) and redox (VO_x) surface sites were impregnated onto the various TiO₂/SiO₂ supports, forming a tunable bifunctional redox-acidic catalyst. Raman spectroscopy revealed that

mono-oxo WO_5 and VO_4 surface species exclusively formed and self-assembled onto the TiO_x domains rather than the exposed silica, in order to lower the thermodynamic free energy of the system.

2. Selective Catalytic Reduction (SCR) of NO_x with NH_3

The molecularly designed experiments showed that both surface NH_3^* and NH_4^{+*} species are present on the model supported $\text{V}_2\text{O}_5\text{-WO}_3/\text{TiO}_2/\text{SiO}_2$ catalyst during the SCR of NO with NH_3 under steady-state (250-350°C) as well as temperature programmed reaction conditions (150-350°C). The steady-state *operando* IR-MS spectroscopy measurements demonstrated that the surface NH_4^{+*} species on the Brønsted acid sites are more reactive than the surface NH_3^* species on Lewis acid sites during the NO- NH_3 SCR reaction over supported $\text{V}_2\text{O}_5\text{-WO}_3/\text{TiO}_2/\text{SiO}_2$ catalysts. During the steady-state SCR NO- NH_3 reaction, the $\text{NH}_3 \rightarrow \text{ND}_3$ isotopic switch revealed that the surface NH_4^{+*} concentration decreases more rapidly than that of the surface NH_3^* concentration reflecting the greater consumption rate of the surface NH_4^{+*} species relative to the surface NH_3^* species. During the $\text{ND}_3 \rightarrow \text{NH}_3$ isotopic switch, repopulation of the surface NH_4^{+*} species is slightly more sluggish than the repopulation of the surface NH_3^* species because of the greater consumption rate of the surface NH_4^{+*} species than the surface NH_3^* species by the SCR NO- NH_3 reaction.

The transient NO pulsing experiments into the NH_3/Ar reaction mixture provide additional insights into the relative reactivity of the surface NH_4^{+*} and NH_3^*

intermediates during the SCR NO-NH₃ reaction. In the presence of gas phase NO reactant, the surface NH₄⁺* concentration markedly increases while the surface NH₃* concentration is relatively unaffected. The insensitivity of the surface NH₃* species on the Lewis acid sites and the significant perturbation of the surface NH₄⁺* species on Brønsted acid sites to the presence/absence of the gaseous NO reactant definitively demonstrates the greater reactivity of the surface NH₄⁺* species on Brønsted acid sites during the SCR NO-NH₃ reaction over supported V₂O₅-WO₃/TiO₂/SiO₂ catalysts.

The reactivity of the surface NH₄⁺* and NH₃* species was also chemically probed by temperature programmed *operando* IR-MS spectroscopy where the chemisorbed ammonia species were reacted with gas phase NO while the catalyst temperature was continuously increased. The chemisorbed ammonia species react with the gaseous NO in two temperature regimes: ~295 and 390°C. At the lower temperature region, the surface NH₄⁺* species are preferentially consumed by the SCR NO-NH₃ reaction. At the higher temperature region, only surface NH₃* species on Lewis acid sites remain and are consumed by the SCR NO-NH₃ reaction. The temperature programmed *operando* IR-MS spectroscopy experiment reveals that both surface NH₄⁺* and NH₃* species are able to participate in the NO-NH₃ SCR reaction, but that the surface NH₄⁺* species on Brønsted acid sites are significantly more reactive than the surface NH₃* species on Lewis acid sites during the SCR NO-NH₃ reaction over supported V₂O₅-WO₃/TiO₂/SiO₂ catalysts.

3. Selective Oxidation of Methanol to Dimethoxymethane

From the fundamental molecular level insights developed in the current research study, a fundamental surface reaction mechanism is proposed for the selective oxidation of methanol to dimethoxymethane over bifunctional supported V_2O_5 - $WO_3/TiO_2/SiO_2$ catalysts. The rapid exchange between surface CH_3O^* intermediates and gas phase CD_3OD during the CD_3OD/CH_3OH -TPSR study reveals the facile reversible exchange between the surface methoxy species on the surface VO_x and WO_x sites and gas phase methanol. The selective oxidation of CH_3OH to $H_2C(OCH_3)_2$ over the bifunctional supported V_2O_5 - $WO_3/TiO_2/SiO_2$ catalysts involves both the redox surface VO_x sites and the acidic surface WO_x sites, but the rds involves the irreversible breaking of the C-H bond of the surface CH_3O^* reaction intermediate to form HCHO by the redox surface VO_4 sites. The conversion of surface $HCHO^*$ to H_2COO^* also occurs on the surface redox VO_4 sites, whereas the coupling of surface H_2COO^* with two additional surface CH_3O^* species is facilitated by adjacent or nearby acidic surface WO_5 sites that store the surface CH_3O^* intermediates and is a rapid kinetic step.

The selective oxidation of methanol to DMM was investigated as a function of temperature and titania domain size by steady state methanol oxidation studies. The catalytic results demonstrated that by varying the local electron density of the titania nanoligand, the relative activity of the surface VO_4 and WO_5 species could be effectively tuned. The ability to tune the catalytically active surface species

resulted in molecular control during the selective oxidation of methanol to dimethoxymethane. In the highest temperature regime, 230°C, the S_{DMM} and TOF_{DMM} were found to be at an optimum when the surface VO_4 and WO_5 species were anchored to a 1 nm polymeric TiO_5 support, which was subsequently grafted onto an underlying inert silica support.

4. Future Studies

The selective catalytic reduction (SCR) of NO_x is a well studied and developed technology that has been in place since the late 1970s. Typical industrial SCR $\text{NO}-\text{NH}_3$ reactions take place at high temperatures (300-400°C). The limitation with this technology is that the current high temperature SCR catalysts deactivate due to exposure to particulates and high SO_2 concentrations when the flue gas is at 300-400°C, which is before the scrubbers in a standard power plant. Thus, there is a current industrial need to have a low temperature SCR catalyst after the scrubbers where the particulate and SO_2 concentrations are significantly lower, but the flue gas is much cooler at this point (< 150°C). In addition, due to the tightening of regulations of NO_x , older power plants are required to install SCR units and low temperature SCR is the preferred option. The crux of the problem is that, the standard catalysts used for high temperature SCR applications (supported VO_x/TiO_2 catalysts) are not very reactive below 150°C. As such, a catalyst that can operate at such low reaction temperatures has not been found yet and represents an exciting research opportunity for future studies.

Finally, the molecularly designed bifunctional redox-acidic catalysts developed within this research represent a stepping stone for the “next generation” in catalytic materials that can easily be integrated in today’s SCR catalytic reactors. There are also a number of reactions requiring dual redox-acidic sites, such as the ammoxidation of propane to acrylonitrile and the ability to tune the catalytic active sites would provide molecular level structure-activity/selectivity relationships about this important catalyst system. In addition, other composition (CeO₂, TiO₂, ZrO₂, Al₂O₃) of the nanoligands and the catalytic active sites (such as acidic P₂O₅ and redox MoO₃) could be controlled to tune the catalytic activity/selectivity. With the recent advancement in atomic and molecular level characterization techniques, the electronic and molecular structures of the catalytic active sites and oxide nanoligands can be determined by a wide array of *in situ* and *operando* spectroscopic, microscopic and probe molecules that assure complete characterization of each catalyst component. The surface chemistry, surface reaction intermediates, surface reaction mechanism and kinetics of the supported catalysts can be thoroughly mapped out similar to the designed experiments presented within this dissertation. This rich collection of experimental electronic/molecular structural and catalytic activity/selectivity information can now be obtained and provide a plethora of innovative ideas for the rational design of improved catalysts.

VITAE

EDUCATION

Ph.D., Chemical Engineering, Lehigh University **2006 - Present**

Dissertation Title: *Tuning Bifunctional Surface Redox-Acid Sites for Enhanced Catalytic Performance*

Advisor: *Israel E. Wachs*

B.S., Chemical Engineering, Howard University **1998 - 2002**

AWARDS

- Catalysis and Reaction Engineering Division Student Travel Award (2010)
- 2nd Place Student Poster Award, Catalysis Club of Philadelphia (2010)
- Rossin Doctoral Fellow (2008 – Present)
- 2nd Place Student Poster Award, Catalysis Society of Metropolitan New York Spring Symposium (2009)
- Dean's Doctoral Fellowship, Lehigh University, P.C. Rossin College of Engineering (9/1/06-8/31/07)
- Elected to Tau Beta Pi (National Engineering Honor Society) (9/1/00-5/1/02)
- Trustee Scholar, Howard University (9/1/99-5/1/02)
- Eli Lilly Scholar and Monsanto Scholar (9/1/01-5/1/02)
- Ford Scholar (9/1/00-5/1/01)
- Howard University Science, Engineering, and Mathematics Scholar (9/1/99-5/1/02)
- 2nd Place Award, Student Paper Competition, Chesapeake Water Environment Association Annual Conference, Ocean City Maryland, (2002)
- Best Student Paper, Kansas State University Environmental Conference, (2001)

WORK EXPERIENCE

Lehigh University, Bethlehem, PA **2006 –Present**

Graduate Research Assistant

- Performed doctoral studies in the broad area of environmental and energy related applications focusing on the molecular design, *in situ* characterization, and performance of novel heterogeneous catalytic materials.

differentiate fuel that is proximal to the site of the biological activity from bulk fuel within a tank.

- Implemented a multivariate analysis (ANOVA, covariance analysis, eigenvalue computation, factor analysis) and modeling effort, using SAS, between microbial contamination test data and operational parameters to design a cost-effective condition monitoring process.
- Analyzed and tested the effect of drag reducing additives (DRA) in pipelines across the country, resulting in an estimated savings in pump electricity for ExxonMobil of \$5MM/yr.

PROFESSIONAL SOCIETY MEMBERSHIPS

- American Institute of Chemical Engineers (AIChE)
- National Society of Black Engineers (NSBE)
- Society of Hispanic Professional Engineers (HSPE)

PUBLICATIONS

Chawla, R.C., **Doura, K.** and McKay, D. “*Solubility Enhancement of TCE using Alcohols as Cosolvents*,” Proceedings, 2001 Environmental Research Conference, Manhattan, KS

W. Zhou, E.I. Ross-Medgaarden, **K.F. Doura**, M. Watanabe, I.E. Wachs and C.J. Kiely “Revealing Structure-Activity Relationships in Model Double-Supported $\text{WO}_3/\text{TiO}_2/\text{SiO}_2$ Solid Acid Catalysts by Atomic Scale Characterization” *Microscopy and Microanalysis* 2010, 16, 1446-1447

Zhou, W., **Doura, K.F.**, Watanabe, M., Herzing, A.A., Okunishi, E., Ross-Medgaarden, E.I., Wachs, I.E., Kiely, C.J., “Abberation-corrected Analytical Microscopy Characterization of Double-Supported $\text{WO}_3/\text{TiO}_2/\text{SiO}_2$ Solid Acid Catalysts” *ChemCatChem*, n/a. doi:10.1002/cctc.201000273

Kevin F. Doura, Irène Malpartida, Marco Daturi, Israel E. Wachs “*Resolving the Contributions of Surface Lewis and Brønsted Acid Sites during NO_x/NH_3 SCR: An Operando TP-IR Spectroscopic Investigation*” (In Progress)

Kevin F. Doura, Israel E. Wachs “*Tuning the Selective Oxidation of CH_3OH to Dimethoxymethane Over Supported $\text{V}_2\text{O}_5/\text{TiO}_2/\text{SiO}_2$ with TiO_2 Nanoligands*” (In Progress)

Kevin F. Doura, Israel E. Wachs “*New Mechanistic Insights into the Selective Oxidation of CH_3OH to $\text{H}_2\text{C}(\text{OCH}_3)_2$* ” (In Progress)

Kevin F. Doura, Israel E. Wachs “*New Insights into Methanol Oxidation over Supported Vanadium Oxide Catalysts*” (In Progress)